JPL Publication 87-5

1982–1983 El Niño Atlas

Nimbus-7 Microwave Radiometer Data

W. Timothy Liu

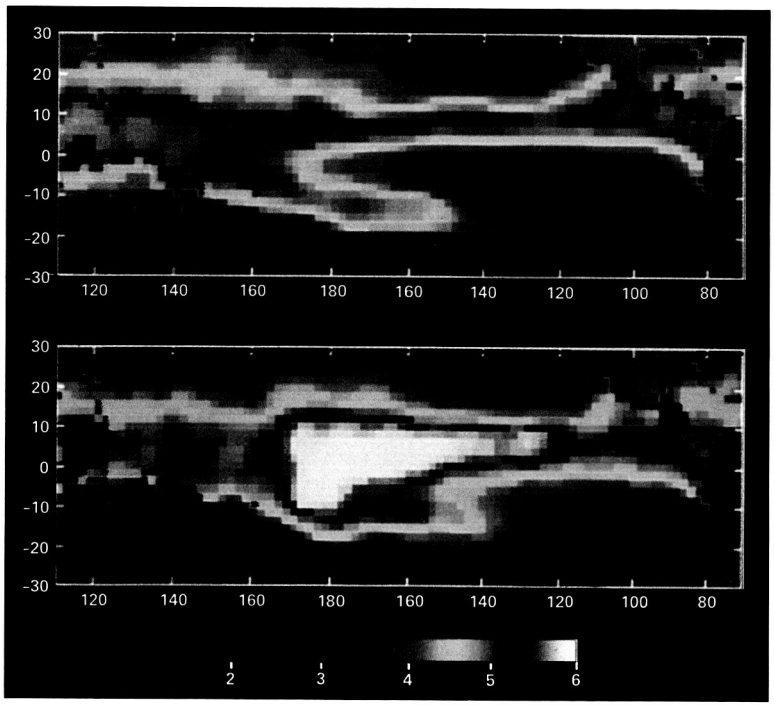

February 15, 1987

National Aeronautics and
Space Administration

Jet Propulsion Laboratory
California Institute of Technology
Pasadena, California

Cover: These two maps of the tropical Pacific Ocean show the atmospheric water vapor as measured by the Nimbus-7 microwave radiometer. The upper map is the average October distribution of 1980 and 1981, representing the normal state, while the lower one is the October distribution of 1982, during one of the most intense El Niño/Southern Oscillation (ENSO) episodes. High values of water vapor are located over regions of surface convergence or convective uplifting. In the upper map, a band of high values (red) in the eastern Pacific just north of the equator indicates the Intertropical Convergence Zone and another band running southeast from New Guinea marks the position of the South Pacific Convergence Zone. The area of highest intensity (white) is over Indonesia. Drastic changes have taken place in 1982 as shown in the lower map. A very intense area is centered on the date line at the equator with an eastward extension just north of the equator. The water vapor in the equatorial area west of the date line has been greatly diminished. During this episode, droughts were reported in Indonesia and floods in the Line Islands. The color bar at the bottom of the maps has units of g/cm^2.

JPL Publication 87-5

1982–1983 El Niño Atlas

Nimbus-7 Microwave Radiometer Data

W. Timothy Liu

February 15, 1987

National Aeronautics and
Space Administration

Jet Propulsion Laboratory
California Institute of Technology
Pasadena, California

The research described in this publication was carried out by the Jet Propulsion Laboratory, California Institute of Technology, under a contract with the National Aeronautics and Space Administration.

ACKNOWLEDGMENT

I am grateful to Dr. David Halpern, Dr. Richard Reynolds, and Dr. Jane Hsiung for making their data and analyses available for comparison. The untiring efforts by Donald Mock in perfecting the maps and by Harold Yamamoto in improving the publication quality of this report are appreciated. I would also like to thank Dr. Halpern and Dr. William Patzert for their comments on this study.

ABSTRACT

Monthly maps of sea surface temperature, atmospheric water vapor, and surface-level wind speed as measured by the Scanning Multichannel Microwave Radiometer (SMMR) on the Nimbus-7 satellite for the tropical Pacific from June 1982 to October 1983, during one of the most intense El Niño Southern Oscillation (ENSO) episodes, are presented. The non-ENSO annual cycle was compiled by averaging the 1980 and 1981 data for each calendar month and was removed from monthly fields of 1982 and 1983 to reveal the anomalous distributions. The anomaly fields and part of the non-ENSO annual cycle are also presented.

In the normal state, the distributions of these parameters are found to be closely related. High water vapor overlies warm water due to convective uplifting. Co-located with regions of high water vapor are areas of low wind speed due to surface convergence. The dominant features of the water vapor and wind speed distributions are the Doldrum over the warm water pool around New Guinea to the west of the date line, the Intertropical Convergence Zone located just north of the equator in the eastern Pacific, the South Pacific Convergence Zone running east-southeast from New Guinea, and the dry region over the cold tongue extending from the South American coast to the equatorial eastern Pacific. These features undergo coherent annual variation.

Water vapor anomalies generally indicate the potential for anomalous precipitation and anomalous heating of the atmosphere through latent heat release. The relative roles of surface wind and sea surface temperature in governing water vapor anomalies are found to be different in different regions and during different stages of the ENSO evolution. The convergence of equatorial Easterlies and the anomalous equatorial Westerlies causes an equatorial region of positive water vapor anomaly during the early stage of the 1982-83 ENSO. Convective uplifting due to anomalous warm sea surface temperature is the dominant cause of water vapor anomalies in the eastern Pacific during the later stages of development.

This study and earlier evaluations demonstrate that the Nimbus/SMMR can be used to monitor large-scale and low-frequency variabilities in the tropical ocean. The SMMR data support and extend conventional measurements. The variabilities of the three parameters are found to represent various aspects of ENSO related through ocean-atmosphere interaction. Their simultaneous and quantitative descriptions in this study pave the way for the derivation of ocean-atmospheric latent heat exchange and further our understanding of the coupled atmospheric and oceanic thermodynamics.

CONTENTS

Figures

1. INTRODUCTION

The Scanning Multichannel Microwave Radiometer (SMMR) was launched on board the Nimbus-7 satellite of the National Aeronautics and Space Administration (NASA) in October 1978. Among the geophysical parameters retrieved from SMMR observations are sea surface temperature (T), atmospheric columnar integrated water vapor (W), and surface-level wind speed (U) (Gloersen *et al.*, 1984). The observation period included the 1982-83 El Niño Southern Oscillation (ENSO) episode which was one of the most intense in the past century and had far reaching economical and ecological impacts. SMMR provided uniformly sampled measurements of T, W and U in the tropical and southern oceans where *in situ* measurements are scarce. Hwang *et al.* (1986) and Liu (1986a) demonstrated that SMMR data could be good atmospheric and oceanic indices for ENSO; Prabhakara *et al.* (1985) attempted to infer atmospheric dynamics from the patterns of W during the 1982-83 episode.

Since the successful flights of SMMR on Seasat and Nimbus-7, a number of algorithms to derive the geophysical parameters from SMMR measurements have been developed and different improvement schemes for the data have been suggested. Recently SMMR geophysical parameters were released to general users through the National Space Science Data Center (NSSDC). Liu and Mock (1986) evaluated and corrected four years (1981-1983) of SMMR geophysical data distributed by NSSDC by comparing them with *in situ* meaurements from research buoys, operational meteorological stations, and voluntary ships. In their study, low frequency temporal variabilities at various locations in the tropical oceans were found to be adequately resolved and documented by SMMR data. The annual and interannual variabilities of T, W and U are related through coupled atmospheric and oceanic thermodynamics; the main goal of this report is to demonstrate the utility of SMMR data in furthering our understanding of atmosphere-ocean interaction.

The non-ENSO annual cycle was derived by averaging the monthly fields of 1980 and 1981. In this report, monthly maps of T, W, and U in the tropical Pacific between June 1982 and October 1983 are included with their deviations from the non-ENSO annual cycle.

2. SATELLITE DATA AND THEIR VALIDATION

The geophysical parameters from Nimbus-7 SMMR were acquired from NSSDC. Corrections derived by the SMMR project (for errors due to calibration shifts and due to solar heating of the antenna feed horn) were applied to the data. Then 2° latitude by 2° longitude monthly averages of U and T in global tropical oceans were compared with coincident averages from voluntary ship reports where there were more than 10 ship reports per month. Ship data for four months of each year were used to derive additional annual correction formulae when necessary. Correction formulae for W were also derived by comparison with values derived from radiosonde reports at 28 selected mid-ocean stations. There was a large increase in W bias starting in June 1983; these errors were removed by adjusting SMMR data to radiosonde data each month.

The time series of co-located W, derived from SMMR and radiosonde data, at Majuro (7.1°N, 171.4°E) and Atuona (9.8°S, 139°W) are shown in Fig. 1. The SMMR data are coherent with radiosonde measurements. The 1982-83 ENSO is revealed by both the radiosonde and SMMR data as a W deficit at Majuro and a W surplus at

Atuona. The time series of co-located T, from SMMR and equatorial buoys, are compared in Fig. 2. Only buoy measurements collected within the hour of each satellite overpass are used. Binned 2°x2° averages centered at both 1°N and 1°S are shown because of the large meridional gradients in T in the region of the buoy. The SMMR and buoy measurements are coherent, and both show the ENSO warming starting in July 1982 superimposed on the regular annual cycle. The time series of co-located U from SMMR and equatorial buoys are shown in Fig. 3. Only SMMR measurements falling within 1° of the buoy location are used. Buoy measurements during the hour of satellite overpass were scaler averaged. The SMMR data track the annual cycle and the ENSO shows up as anomalously low wind speeds in October 1982 at 110°W. The moored buoys are part of the Equatorial Pacific Ocean Climate Studies and the data were provided by D. Halpern.

Only nighttime measurements of T were released by NSSDC, and U and T data within 600 km of land were excluded. The data, the correction procedures, and the comparison with ship, buoy, and radiosonde data were detailed in Liu and Mock (1986). The maps shown in this report were based on 2° x 2° averages. Data gaps over atolls in Polynesia and parts of Micronesia were spatially interpolated. A 3x3 average filter was applied twice in succession to smooth the isolines.

3. THE NON-ENSO ANNUAL CYCLE

The non-ENSO annual cycles of T, W, and U are compiled by averaging the monthly fields of 1980 and 1981. The average distributions for January, April, July, and October, representing the major seasons, are shown in Figs. 4-9. From the figures, it is obvious that the distributions of these three parameters are closely related. The warm water belt in the tropical Pacific is interrupted by a cold tongue extending from the South American coast to the eastern equatorial Pacific. High W overlies warm water due to convective uplifting. The area with highest W (over 5.5 g/cm^2) is over the warm water pool in the New Guinea region to the west of the date line. A narrow belt of high W is found in the eastern Pacific just north of the equator marking the position of the Intertropical Convergence Zone (ITCZ) and another one is found running east-southeast from New Guinea indicating the South Pacific Convergence Zone (SPCZ). Wedged in between these two convergence zones is a region of low W over the cold tongue. Co-located with regions of high W are areas of low U due to surface convergence. However, areas of low U are not necessarily areas of high W. The distributions of these three parameters exhibit coherent annual variabilities.

The cold tongue is weakest in April and strongest in October, with a range of approximately 5°C at its equatorial position. The warm water pool west of the date line, on the other hand, undergoes comparatively small annual change. When the cold tongue is strong, there is more than 8°C of zonal gradient of T across the equatorial Pacific. Two sets of long term monthly mean fields (hereafter referred to as climatology) of T in digital data were acquired and put in a similar form for comparison. These fields were derived mainly from ship reports and are described by Reynolds (1982) and Hsiung (1986). Both sets of climatological distributions show steeper gradients than the 1980-81 averages off the coast of Baja California and the northern coast of Chile. This results in approximately 1° higher T at the northeast and southeast corners of the 1980-81 average maps when compared with the climatological fields. Off the coast of

Central America, the 1980-81 averages show higher T than Hsiung's climatology, but show closer agreement with the Reynolds analysis. The annual cycle of W is very similar to that of T except that the annual minimum of W at the equator is located further to the west of the T minimum. The annual range of W at the equator east of the date line is approximately 1.5 g/cm^2 while the range is much smaller west of the date line. Unfortunately, there is no credible climatology for comparison.

Over the tropical oceans, low U regions generally indicate atmospheric convergence or divergence and high U regions are occupied by the Trade Winds. Climatological wind vector fields such as those by Wyrtki and Meyers (1975) and Weare *et al.* (1980) are vector averages and can not be quantitatively compared with the 1980-81 fields which are scaler averaged. But, as demonstrated below, the directional information of the climatological vector fields helps in the interpretation of the 1980-81 U fields. The area of high U at 30°N in the January map (Fig. 8) corresponds to an area of high westerly winds in the climatologies, while the high U area centered on 10°N corresponds to an area occupied by the Northeast Trades. In between these two areas is a region of low U corresponding to surface divergence. Wedged between the low U areas at the ITCZ and the SPCZ (as discussed before) is a broad area of the Southeast Trades. From January, the area of Northeast Trades expands north and intensifies until April when it covers the entire tropical Pacific north of the equator. In April, the high U area between the ITCZ and SPCZ is diminished. The low U belt in the eastern Pacific, corresponding the the ITCZ, moves north, and by July, it is positioned at the Central American coast at the eastern end. The Asian Monsoon pushes the western front of the Northeast Trades eastward, while the Southeast Trades grow in strength. The two convergence zones are very prominent in October. Digital data of the climatological fields of scaler averaged winds compiled from ship data by Hsiung (1986) were acquired and mapped in a similar way for comparison. While Hsiung's climatological fields agree in the annual variation of the large scale features, they are not as coherent as the 1980-81 average fields, particularly in the southern ocean due to coarser resolution and lack of data. The 1980-81 averages show more organized and stronger (by 1 to 2 m/s) Southeast Trades through the year. During April and October, the Northeast Trades are also stronger in the 1980-81 averages.

4. THE 1982-83 EL NIÑO SOUTHERN OSCILLATION

A. Sea Surface Temperature

The monthly distribution of T, from June 1982 to October 1983, and their deviation from the 1980-81 averages (hereafter referred to as anomaly) are shown in Figs. 10-26. In the first half of the year, there is no coherent anomaly. Starting in June 1982, an organized region of warm anomaly appears on the equator and intensifies very quickly. By August 1982, warm anomalies of more than 1°C appear on the equator from the American coast to the date line, surrounded by cold anomalies. The area of equatorial warm anomaly persists through January 1983 with its magnitude increasing to above 3°C. The cold anomalies surrounding this area reach -1°C in the north and the west. In January 1983, the area of warm anomaly starts to extend southward at 110°W. The intensity of the equatorial warm anomaly starts to decrease in March 1983. A region of warm anomaly in the eastern Pacific centered just south of the equator starts to intensify in April 1983, reaching above 4°C in June 1983, and persists until

September 1983. Unfortunately, coastal data are not available to gauge its full magnitude. Cold water from upwelling, marked by the 26°C isotherm, appears in the central equatorial Pacific in July 1983, returning the equatorial region to normal temperature.

The Climate Analysis Center (CAC) of the National Oceanic and Atmospheric Administration produced operational analyses of sea surface temperature during this period. The difficulty of getting accurate T fields from sparse ship and buoy measurements in the tropical and the southern Pacific is well known (Reynolds and Gemmill, 1984). During this time, measurements by the operational Advanced Very High Resolution Radiometer (AVHRR) were handicapped by cloud cover and aerosols introduced by the eruptions of El Chichon (McClain *et al.*, 1985). Interpolation and filtering schemes also made significant differences. Digital data of two sets of improved T anomaly fields (not shown) from CAC were mapped and compared with the SMMR fields; the first one is derived from ship measurements (Reynolds and Gemmill, 1984) and the other from blended ship and AVHRR data (Reynolds and Gemmill, 1985). The CAC anomaly fields agree with SMMR fields in most large-scale features although different annual cycles have been used to derive them. Slight differences in range of T between SMMR and CAC fields showed up in some months; for example, the anomaly ranged from -1°C to 4°C for CAC fields and -1.5°C to 3.5°C for the SMMR fields in the equatorial Pacific during January 1983. This difference is considered to be within the uncertainty of sensor accuracy and the difference between the 1980-81 averages and Reynold's climatology.

B. Atmospheric Water Vapor

The monthly distributions of W and their deviations from the 1980-81 averages are shown in Figs. 27-43. In the first half of 1982, the distributions are normal, with high values of W located at the ITCZ, the SPCZ, and the area over New Guinea; there are no strong, organized anomaly in the region. In July, a small region with more than a 1 g/cm^2 anomaly on the equator at the date line has started to intensify and extend eastward. The area to the west is occupied by a negative anomaly. The center of the positive anomaly moves eastward slowly and by October, the center is at 160°W on the equator and has a magnitude of more than 2 g/cm^2. The reported catastrophic droughts in Indonesia and floods in the Line Islands are dramatic confirmation of these anomalies. By November, the area of positive anomaly is surrounded on three sides by negative anomalies. The center of the positive anomaly reaches 140°W in January 1983 with a magnitude of 3 g/cm^2. While the center of the anomaly continues to move eastward, its magnitude stops increasing after February 1983. The high W ridge in the eastern Pacific, which is normally located at the ITCZ, starts to move south in the fall of 1982 and reaches the equator in January 1983. Until April 1983, it occupies a position to the south of its climatological mean, causing a broad region of positive anomaly just south of the equator in the central and eastern Pacific. The excess rainfall reported in Ecuador during this time is evidence of this anomaly. Starting in February 1983, negative anomalies develop at the normal position of ITCZ and SPCZ. In March, a belt of negative anomaly runs from 160°E at the equator to the coast of Central America and another runs southeast from New Guinea. These areas of negative anomaly are obvious in April. By July, the intensities of both positive and negative anomalies have weakened but there is still an area of 1.5 g/cm^2 positive anomaly centered at 100°W. The distribution returns to normal by October 1983.

C. Surface-Level Wind Speed

The monthly distributions of U and their deviations shown in Figs. 44-60 are difficult to interpret without directional information. An anomaly in U may be due to the change in the strength of the Trade Winds, or the change in position of the surface convergence. Wind-stress vector maps, such as those constructed by Inoue and O'Brien (1984), provide qualitative comparison and help in the following interpretaton of the SMMR U maps. In July, an small region of negative U anomaly appears on the equator at the date line with another area of positive anomaly to the west of it. The location of the negative anomaly coincides with the leading front of the westerly winds; both progress eastward at the same speed. By October, the negative anomaly reaches 160°W. Between October 1982 and January 1983, the Southeast Trades are weaker than usual and negative anomalies appear in the eastern South Pacific, but the Northeast Trades are stronger, causing positive anomalies in the central and western North Pacific. By January 1983, the negative equatorial anomaly is centered at 140°W with a magnitude over 3 m/s and continues to extend eastward. A positive anomaly of 2 m/s is located to the west of the date line. The Southeast Trades have collapsed and there is a negative anomaly across the entire tropical South Pacific. In April 1983, there is a belt of strong convergence represented by low wind speeds and negative anomaly running from the date line along the equator to 120°W and then northeastward to the Central American coast. This negative anomaly belt persists through June 1983 and the distribution starts to return to normal in July.

D. Interrelation

Water vapor anomalies generally indicate the potential for anomalous precipitation and anomalous heating of the atmosphere through latent heat release. During the early phase of the ENSO in 1982, the equatorial high W anomaly is co-located with the low wind speed anomaly and moves eastward at approximately the same speed. Both appear as small regions at the date line in July, 1982. During this time, the sea surface temperature anomaly appears as an equatorial belt extending from the date line to the American coast. The location of the W anomaly, therefore, depends more on the anomalous position of surface wind convergence than the distribution of T anomaly. But as the ENSO develops, the area of positive W anomaly expands and occupies almost the same area as the positive T anomaly by February 1983. In spring 1983, the position of the surface convergence belt (low wind speed) in the eastern Pacific is to the north of the high W ridge. During this time, the W anomaly appears to be mainly driven by the convective uplifting due to warm T anomaly. There is no U anomaly associated with the reintensification of warm T anomaly in the eastern Pacific during the summer of 1983.

5. DISCUSSION

This study shows that the Nimbus/SMMR can be effectively used to study the large-scale and low-frequency variabilities in the tropical ocean. Some details might have been smoothed out in contouring but more accurate color images such as those shown on the cover are also available. SMMR provided simultaneous measurements of three parameters (T, W and U), each of which describes a certain aspect of the evolution of the 1982-83 ENSO. Since their variabilities are related through the interaction

between the ocean and the atmosphere, an understanding of the underlying physics requires the knowledge of the local and basin-wide ocean-atmosphere exchanges in heat and momentum.

With the relation of Liu (1986b), surface-level humidity can be derived from W, with good accuracy on monthly time scales, and the latent heat flux can be computed from SMMR data alone. The variability of latent heat flux and its relation with other parameters during the 1982-83 ENSO will be discussed in the next report. Together with radiative fluxes (Gautier, 1986) the major components of ocean-atmosphere heat exchanges can be monitored by spaceborne sensors. The Tropical Ocean and Global Atmosphere (TOGA) Heat Exchange Project (THEP) was established at the Jet Propulsion Laboratory (JPL) in an attempt to demonstrate the feasibility of determining ocean-atmosphere heat exchange in the tropical ocean using a combination of spaceborne sensors (Liu and Niiler, 1985). The data described in this report will be disseminated through the NASA Ocean Data System at JPL under THEP.

SMMR can only measure the wind speed but not the direction; no spaceborne sensor during the 1982-83 episode were designed to measure surface-level wind vectors. But, in addition to latent heat flux computation, SMMR wind speeds could be used in the interpolation of conventional wind vector measurements. This study also serves as an example on how SMMR wind speed distribution can complement water vapor distribution in locating regions of surface convergence.

The fluctuations of atmospheric water vapor have often been related to atmospheric advection and circulation (e.g., Rasmusson, 1967). The water budget in the atmosphere also governs the diabatic heating due to the release of latent heat. Given the sparsity of upper air measurements over oceans, only spaceborne sensors can provide the data to study the temporal and spatial variability of atmospheric water content. Spaceborne microwave radiometers will be indispensable in future studies of atmospheric water and heat budgets. The Outgoing Longwave Radiation (OLR) derived as part of the Earth Radiation Budget (ERB) experiment on board Nimbus-7 has recently received much attention as an index of precipitation and corresponding diabatic heating over the tropical ocean. Since there are some similarities between the W maps in this report and the OLR patterns of Kyle *et al.* (1986) as related to the 1982-83 ENSO episode, the two data sets may complement each other in understanding atmospheric thermodynamics.

Microwave radiometers do not have the resolution of infrared radiometers (Advanced Very High Resolution Radiometer AVHRR) in measuring sea surface temperature but microwave radiometers do have all-weather capability. This is very important in monitoring sea surface temperature in the tropics where the atmosphere contains large amounts of moisture and the convergence zones are covered by clouds. The Special Sensing Microwave Imager (SSMI) to be launched on the operational Defense Meteorological Space Program (DMSP) spacecraft can measure atmospheric water vapor and surface-level wind speed, but it lacks the low frequencies for sea surface temperature retrieval. With the deterioration of the Nimbus/SMMR, there will be no spaceborne microwave sensor to measure sea surface temperature in the near future.

REFERENCES

Gautier, C., 1986: Evolution of the net surface shortwave radiation over the Indian Ocean during summer MONEX. *Mon. Wea. Rev., 114*, 525-533.

Gloersen, P., D.J. Cavalieri, A.T.C. Chang, T.T. Wilheit, W.J. Campbell, O.M. Johannessen, K.B. Katsaros, K.F. Kunzi, D.B. Ross, D. Staelin, E.P.L. Windsor, F.T. Barath, P. Gudmandsen, E. Langham, and R.O. Ramseier, 1984: A summary of results from the first Nimbus 7 SMMR observations. *J. Geophys. Res., 89*, 5335-5344.

Hsiung, J., 1986: Mean surface energy fluxes over the global ocean. *J. Geophys. Res., 91*, 10585-10606.

Hwang, P.H., D.S. MacMillan, C.C. Fu, S.T. Kim, D. Han, and P. Gloersen, 1986: Observation of El Niño by the Nimbus-7 SMMR. *Second Conferenence on Satellite Meteorology/Remote Sensing and Application, Preprint Volume*, Amer. Meteor. Soc., Boston, MA, 333-337.

Inoue, M., and J.J. O'Brien, 1984: Analyzed pseudo wind stress data: January 1981 to December 1983. *El Nino Atlas 1982-83*, A. Leetmaa and J. Witte (Eds.), Nova University, Dania, FL, 1-16.

Kyle, H.L., P.E. Ardanuy, R.R. Hucek, and the Nimbus-7 Experiment Team, 1986: *El Nino and Outgoing Longwave Radiation: An Atlas of Nimbus-7 Earth Radiation Budget Observations.* NASA RP-1163, National Aeronautics and Space Administration, Washington, DC, 92 pp.

Liu, W.T., 1986a: Month-to-month varaibility of ocean-atmosphere latent heat flux as observed from the Nimbus Microwave Radiometer. *Second Conference on Satellite Meteorology/Remote Sensing and Application, Preprint Volume*, Amer. Meteor. Soc., Boston, MA, 328-332.

Liu, W.T., 1986b: Statistical relation between monthly mean precipitable water and surface-level humidity over global oceans. *Mon. Wea. Rev., 114*, 1591-1602.

Liu, W.T., and P.P. Niiler, 1985: *Tropical Ocean and Global Atmosphere (TOGA) Heat Exchange Project - A Summary Report.* JPL Publication 85-49, Jet Propulsion Laboratory, Pasadena, CA, 12 pp.

Liu, W.T., and D.R. Mock, 1986: *Evaluation of Geophysical Parameters Measured by the Nimbus-7 Microwave Radiometer for the TOGA Heat Exchange Project.* JPL Publication 86-50, Jet Propulsion Laboratory, Pasadena, CA, 19 pp.

McClain, E.P., W.G. Pichel and C.C. Walton, 1985: Comparative performance of AVHRR-based multichannel sea surface temperatures. *J. Geophys. Res., 90*, 11587-11601.

Prabhakara, C., D.A. Short, and B.E. Vollmer, 1985: El Niño and atmospheric water vapor: observations from Nimbus 7 SMMR. *Mon. Wea. Rev., 24,* 1311-1324.

Rasmusson, E.M., 1967: Atmospheric water vapor transport and the water balance of North America: Part I. Characteristics of the water vapor flux field. *Mon. Wea. Rev., 95,* 403-426.

Reynolds, R.W., 1982: *A Monthly Average Climatology of Sea Surface Temperatures.* NOAA Tech. Rep., NWS31, National Oceanic and Atmospheric Administration, Washington, DC, 35 pp.

Reynolds, R.W., and W.H. Gemmill, 1984: An objective global monthly mean sea surface temperature analysis. *Tropical Ocean-Atmosphere Newsletter, 23,* 4-5.

Reynolds, R.W., and W.H. Gemmill, 1985: A sea surface temperature analysis based on *in situ* and satellite data. *Proc. Ninth Annual Climate Diagnostics Workshop,* National Oceanic and Atmospheric Administration, Washington, DC, 408-416.

Weare, B.C., P.T. Strub, and M.D. Samuel, 1980: *Marine Climate Atlas of the Tropical Pacific Ocean.* Contribution to Atmospheric Science No. 20, University of California, Davis, CA, 147 pp.

Wyrtki, K., and G. Meyers, 1975: *The Trade Wind Field Over the Pacific Ocean Part I. The Mean Field and the Mean Annual Variation.* HIG-75-1, Hawaii Institute of Geosphysics, University of Hawaii, Honolulu, HI, 26 pp.

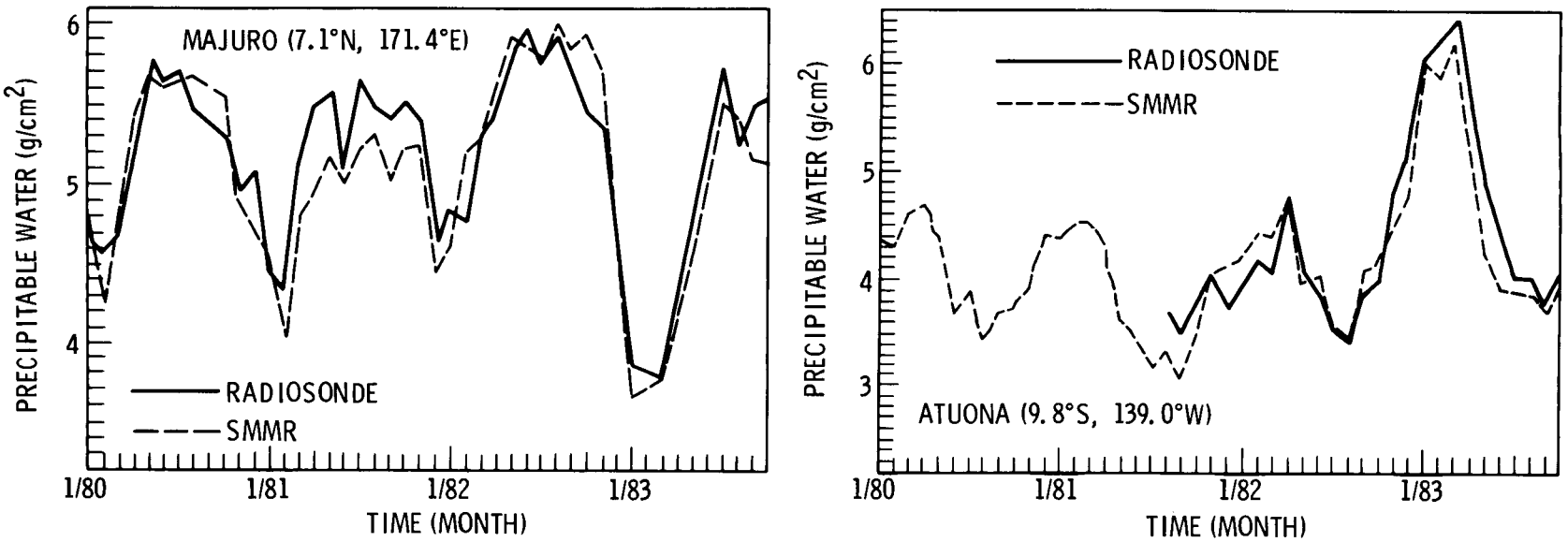

Fig. 1. Comparison of the temporal variation of atmospheric water vapor derived from radiosondes and from SMMR data at two stations in the tropical Pacific (from Liu and Mock, 1986)

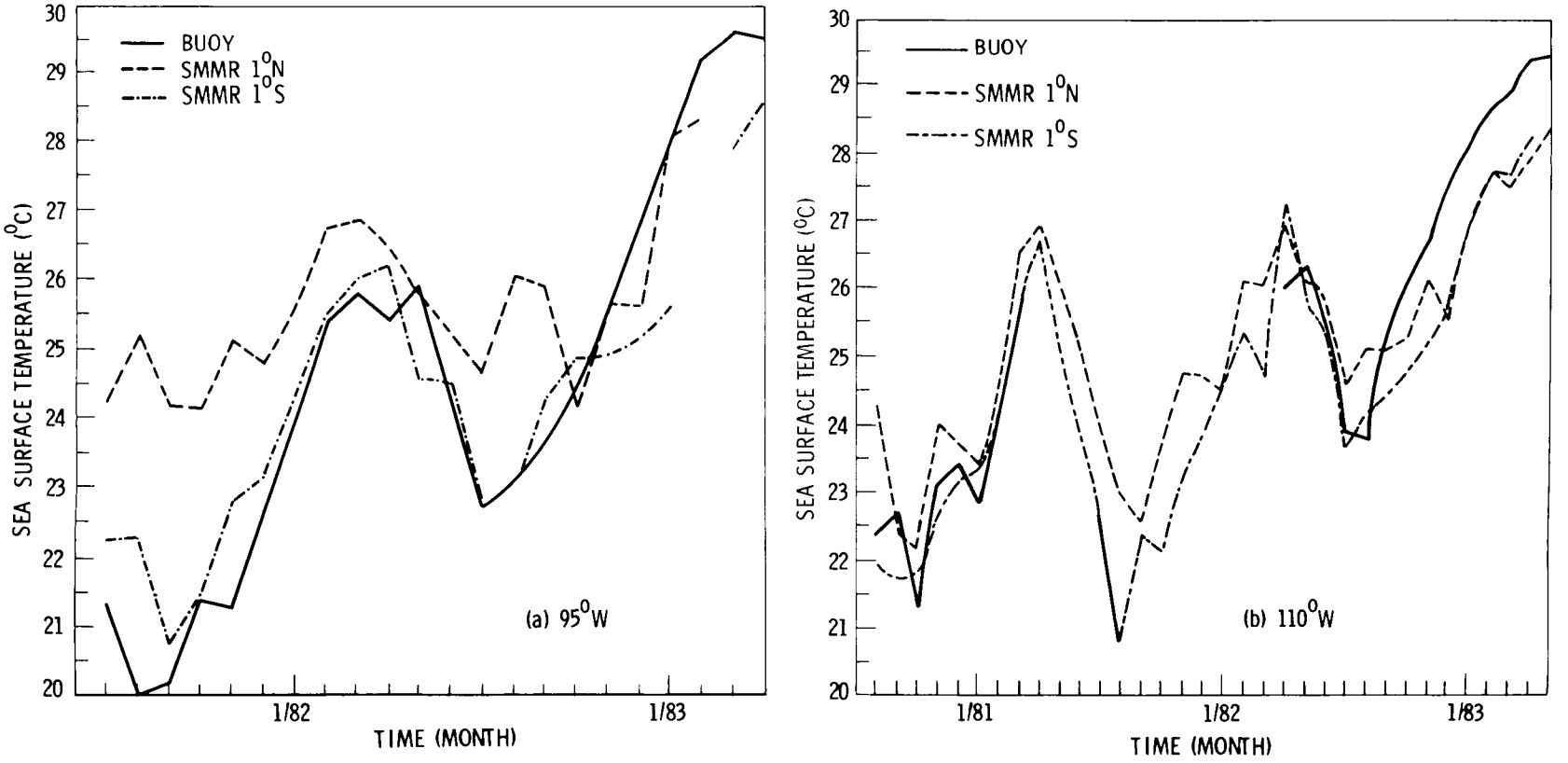

Fig. 2. Comparison of the temporal variation of sea surface temperature derived from binned SMMR data with averaged measurements at two equatorial buoys during satellite overpasses (from Liu and Mock, 1986)

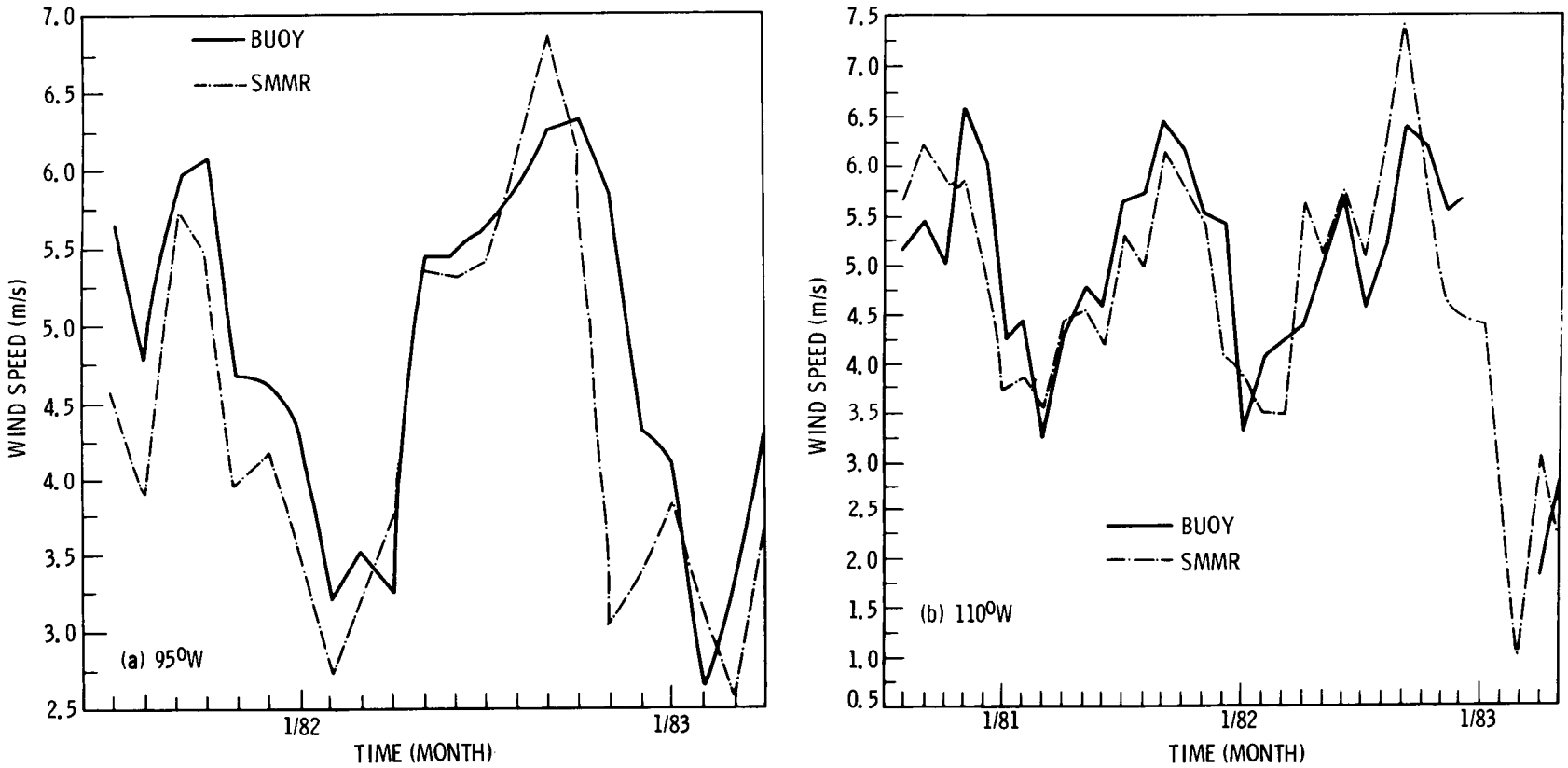

Fig. 3. Comparison of the temporal variation of surface-level wind speed derived from SMMR data with averaged measurements at two equatorial buoys during satellite overpasses (from Liu and Mock, 1986)

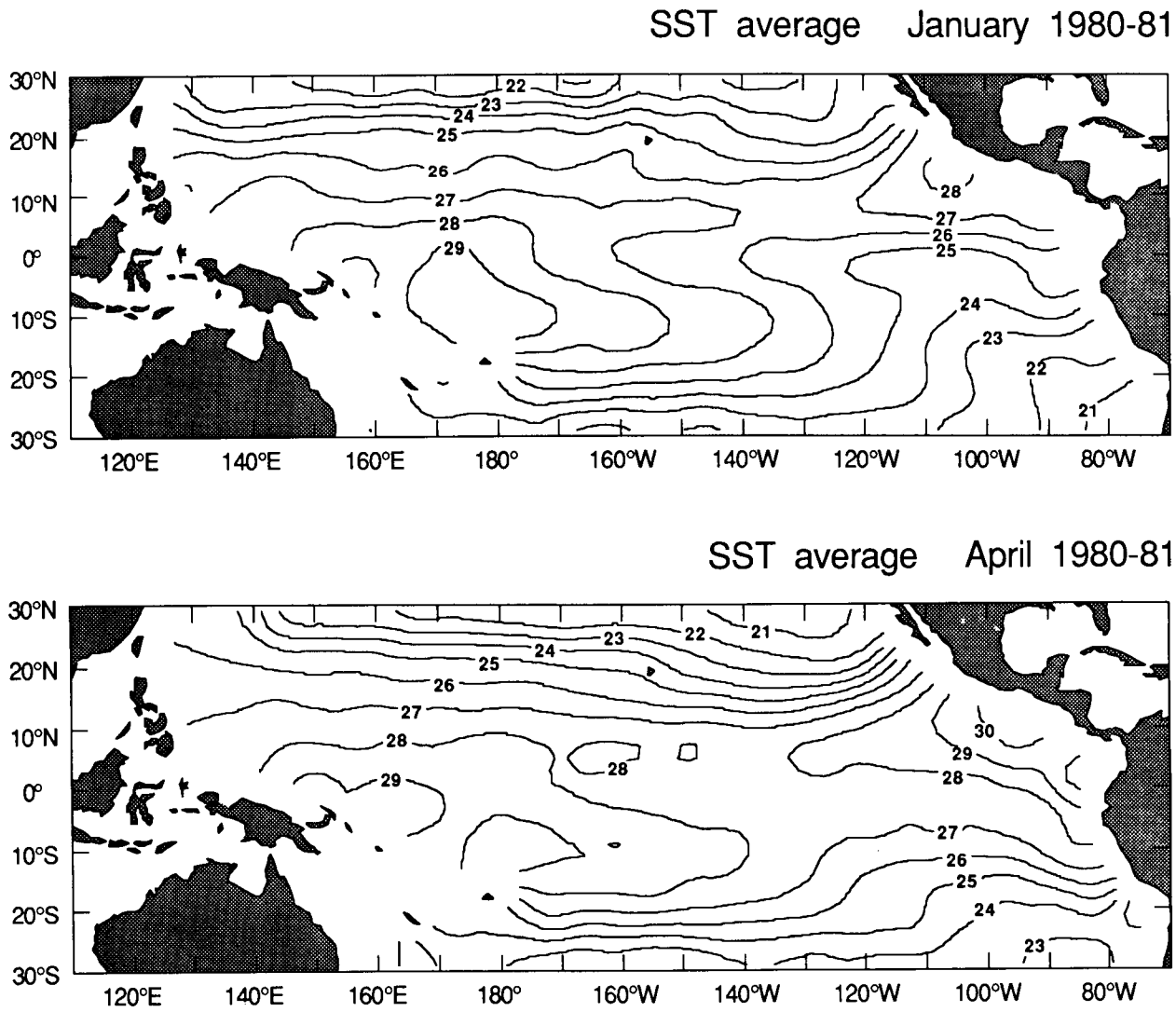

Fig. 4. Averaged January and April sea surface temperature measured by SMMR for 1980-1981

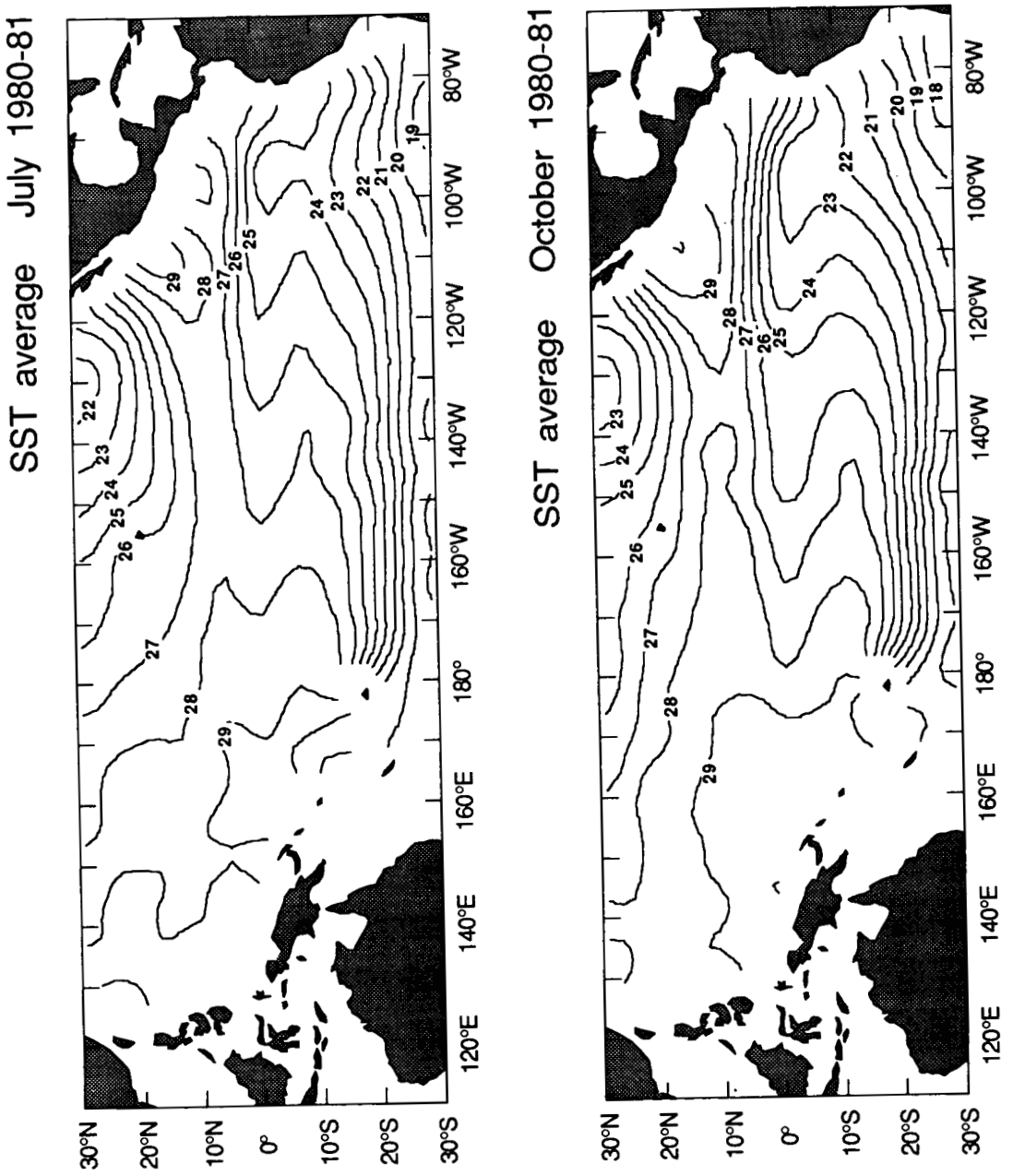

Fig. 5. Same as Fig. 4, except for July and October

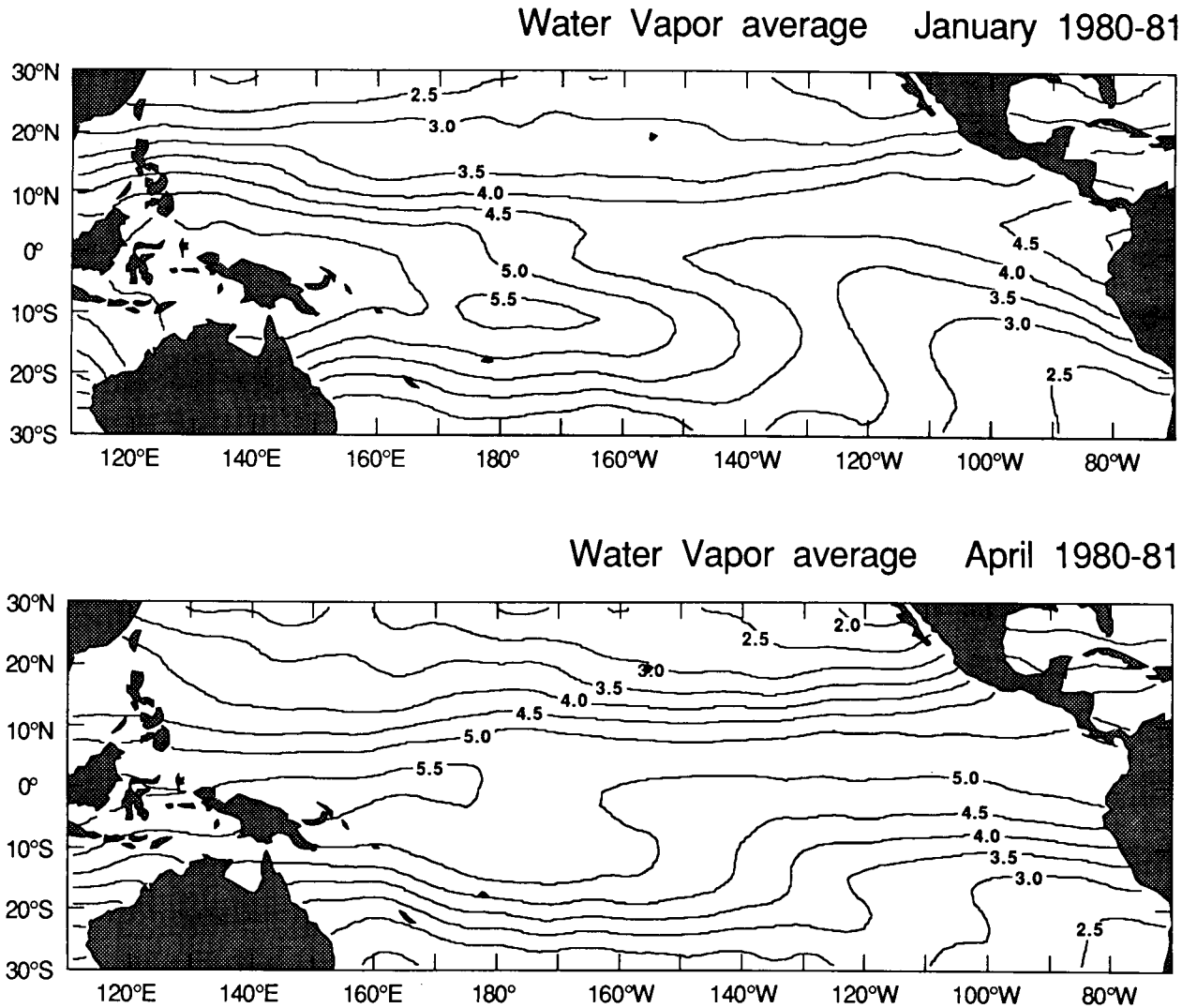

Fig. 6. Averaged January and April atmospheric water vapor measured by SMMR for 1980-81

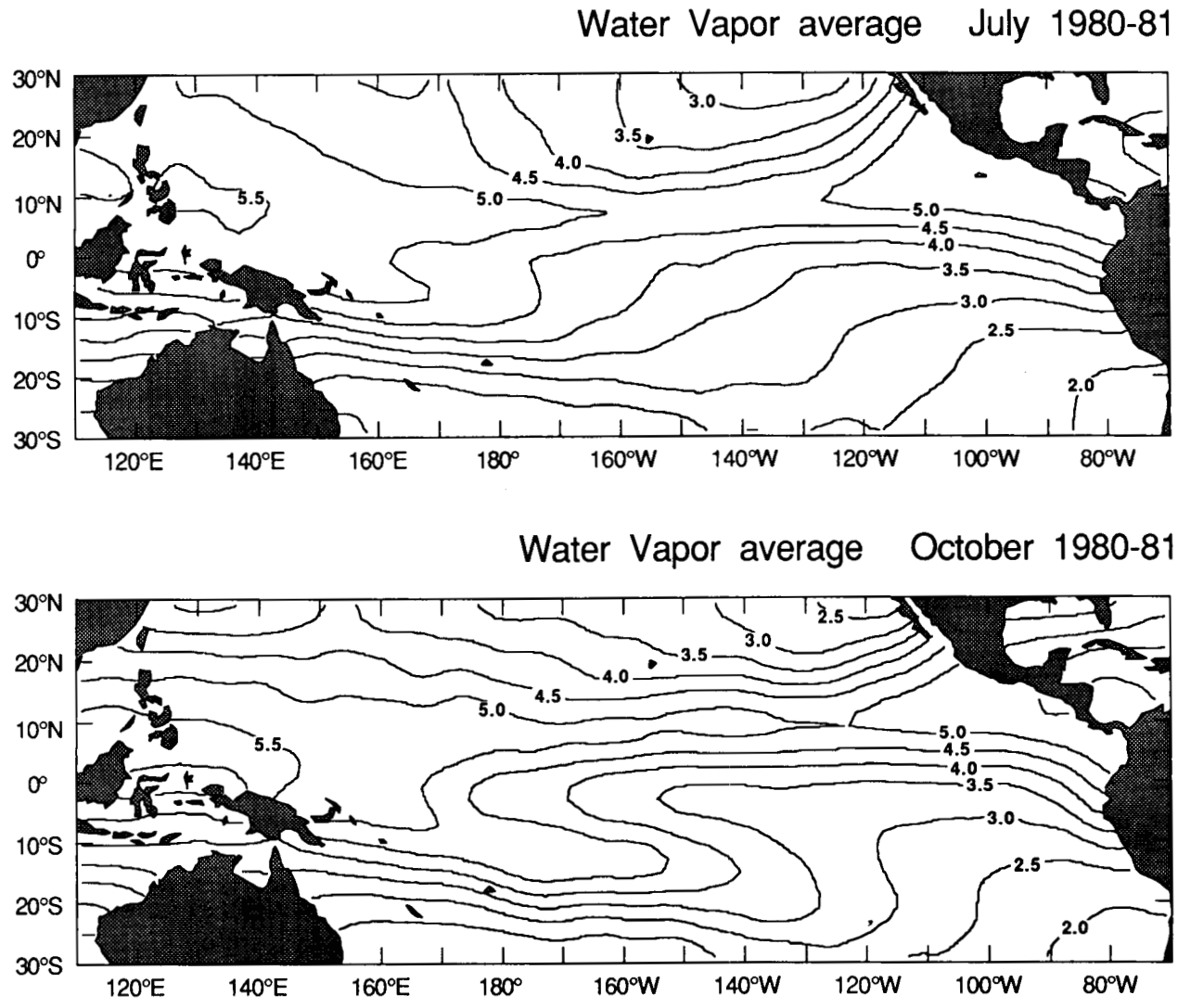

Fig. 7. Same as Fig. 6, except for July and October

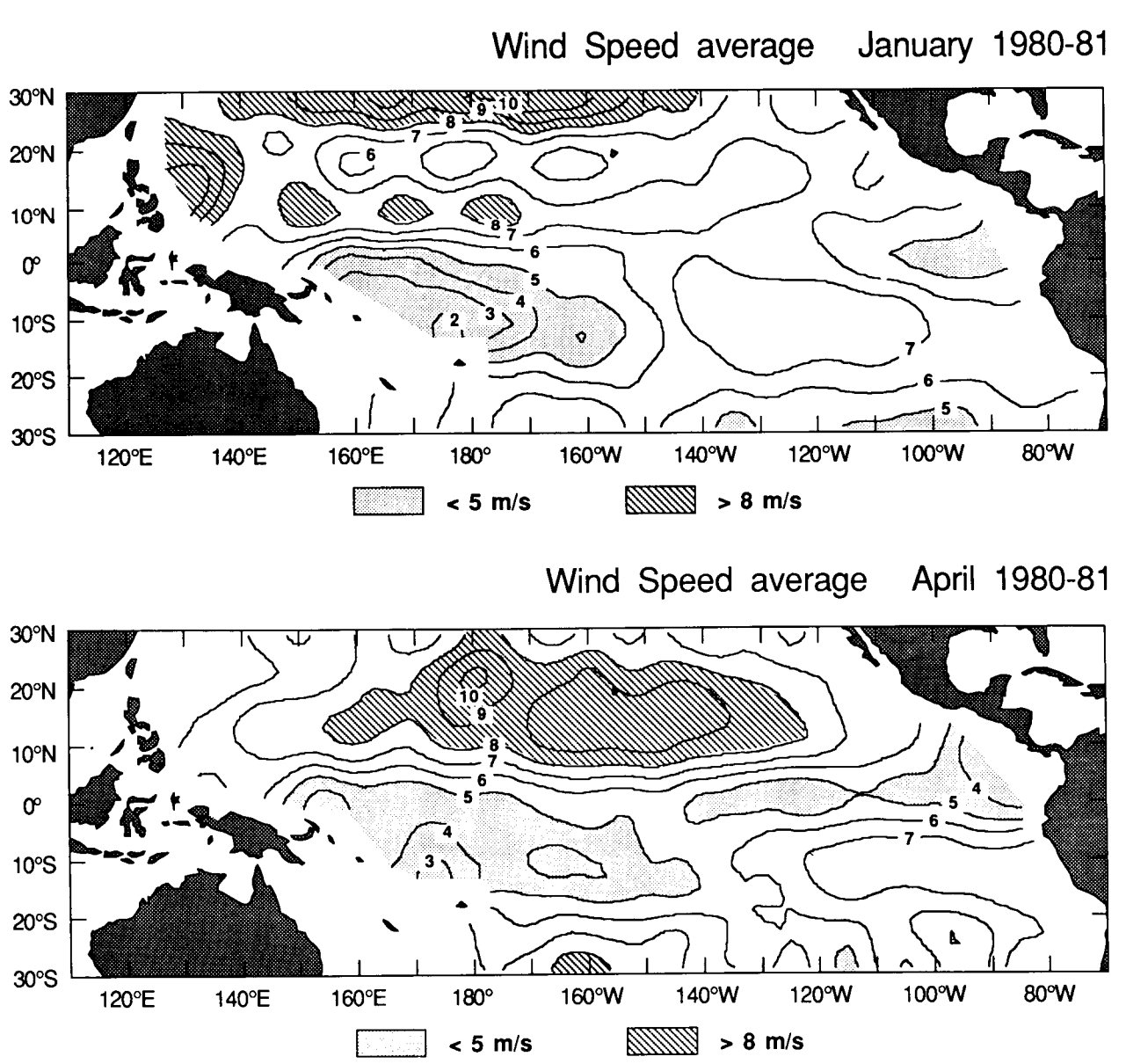

Fig. 8. Average January and April surface-level wind speed measured by SMMR for 1980-1981

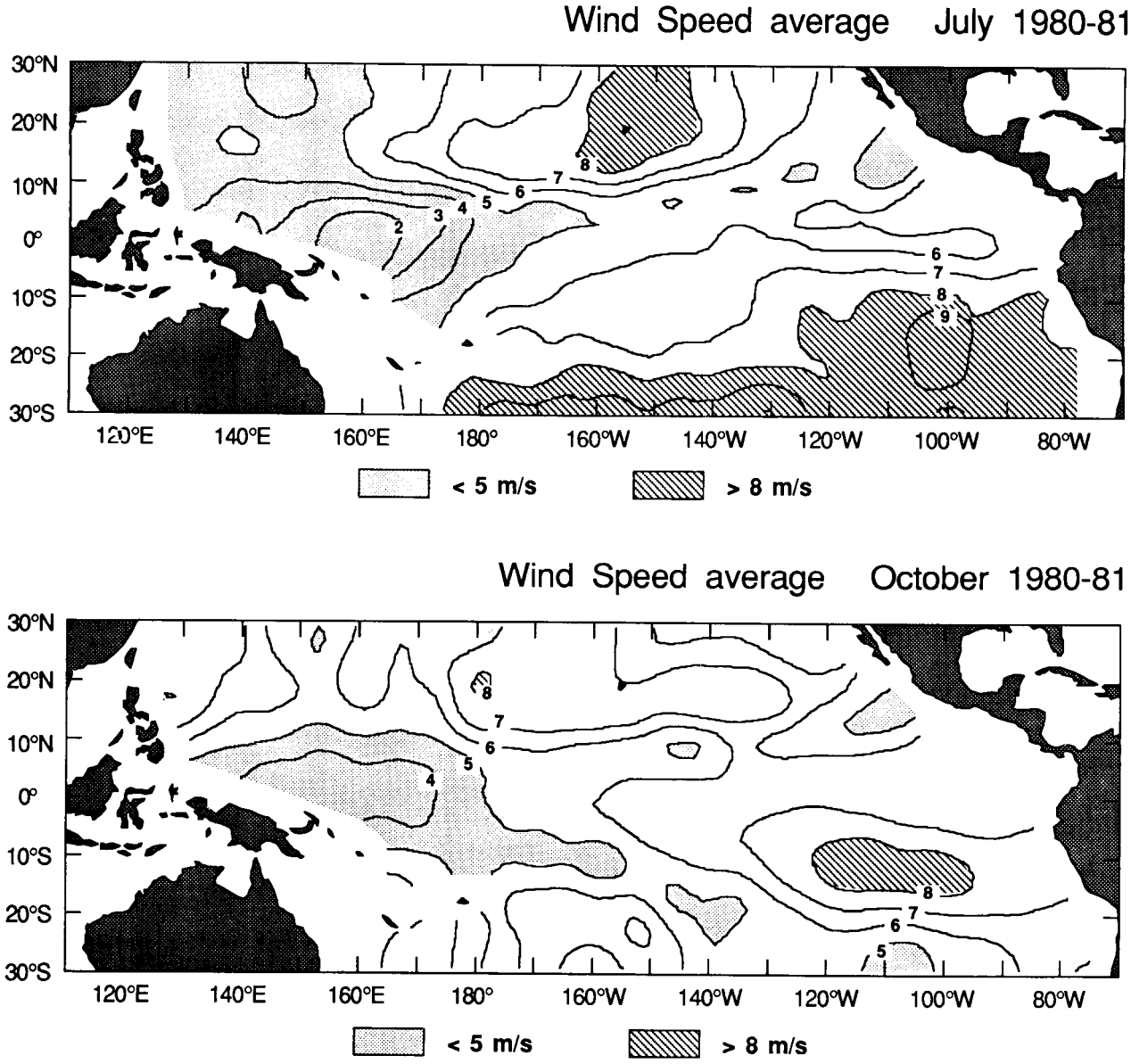

Fig. 9. Same as Fig. 8, except for July and October

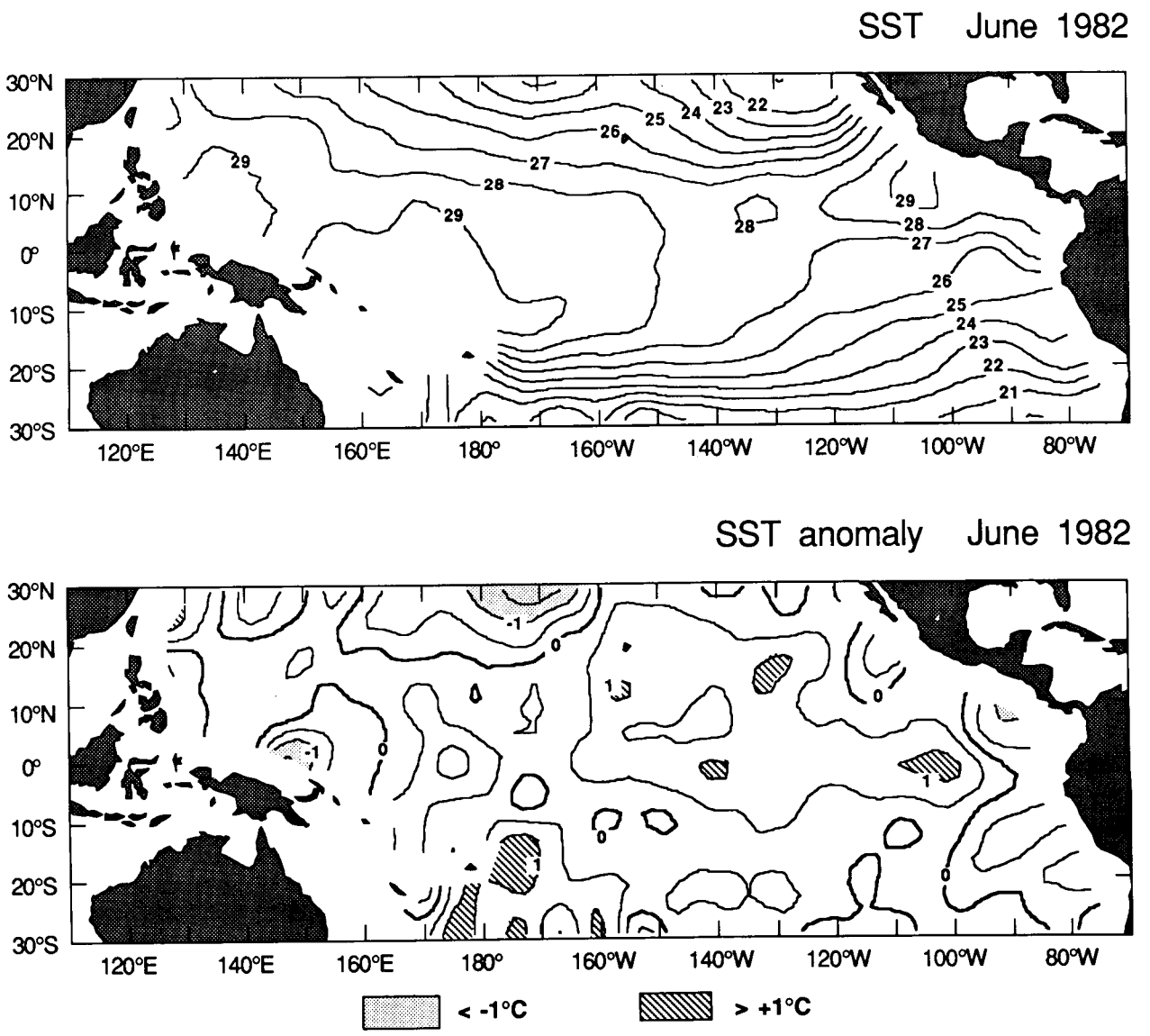

Fig. 10. Sea surface temperature measured by SMMR in June 1982 and its deviation (anomaly) from the corresponding 1980-81 mean

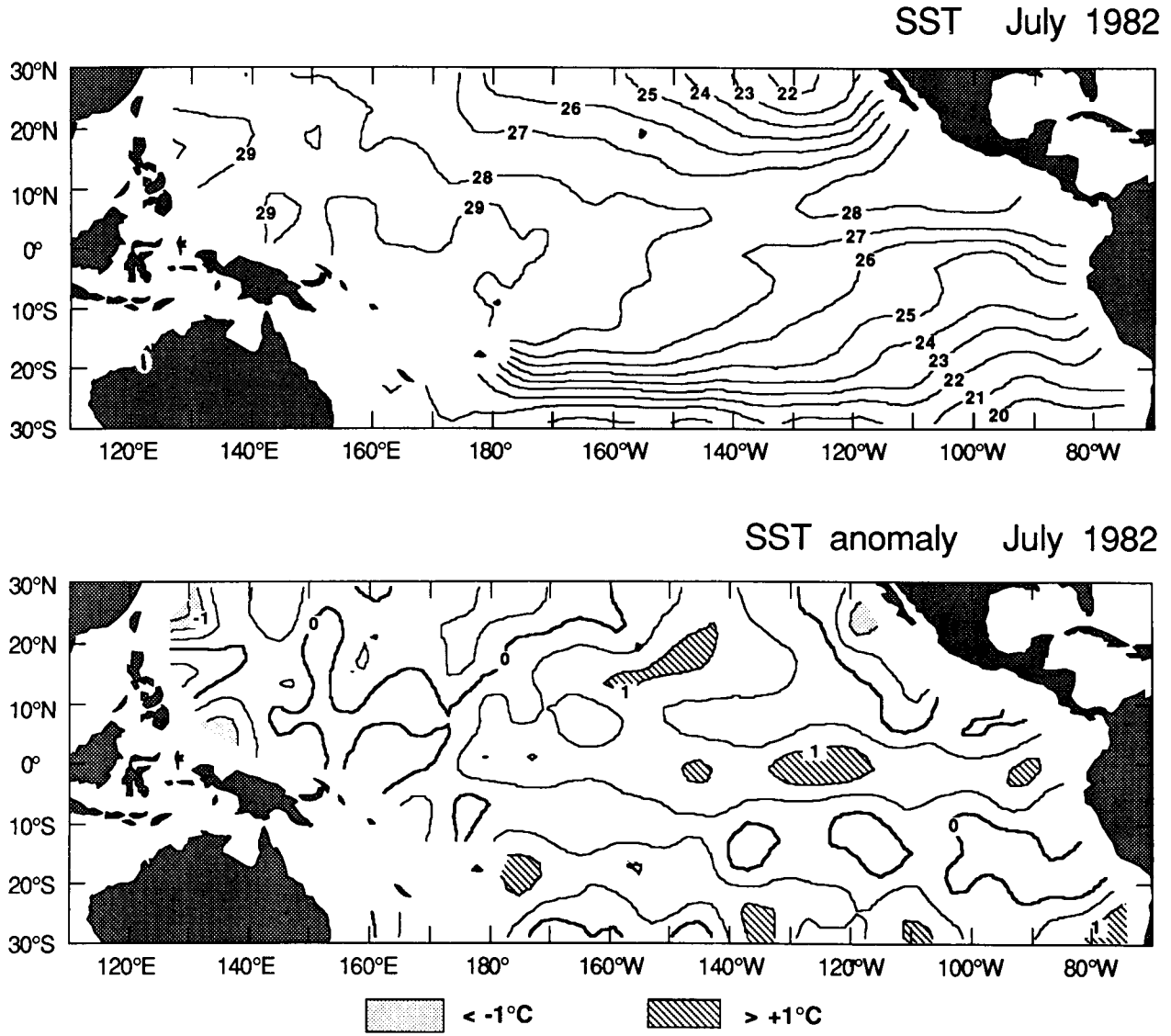

Fig. 11. Same as Fig. 10, except for July 1982

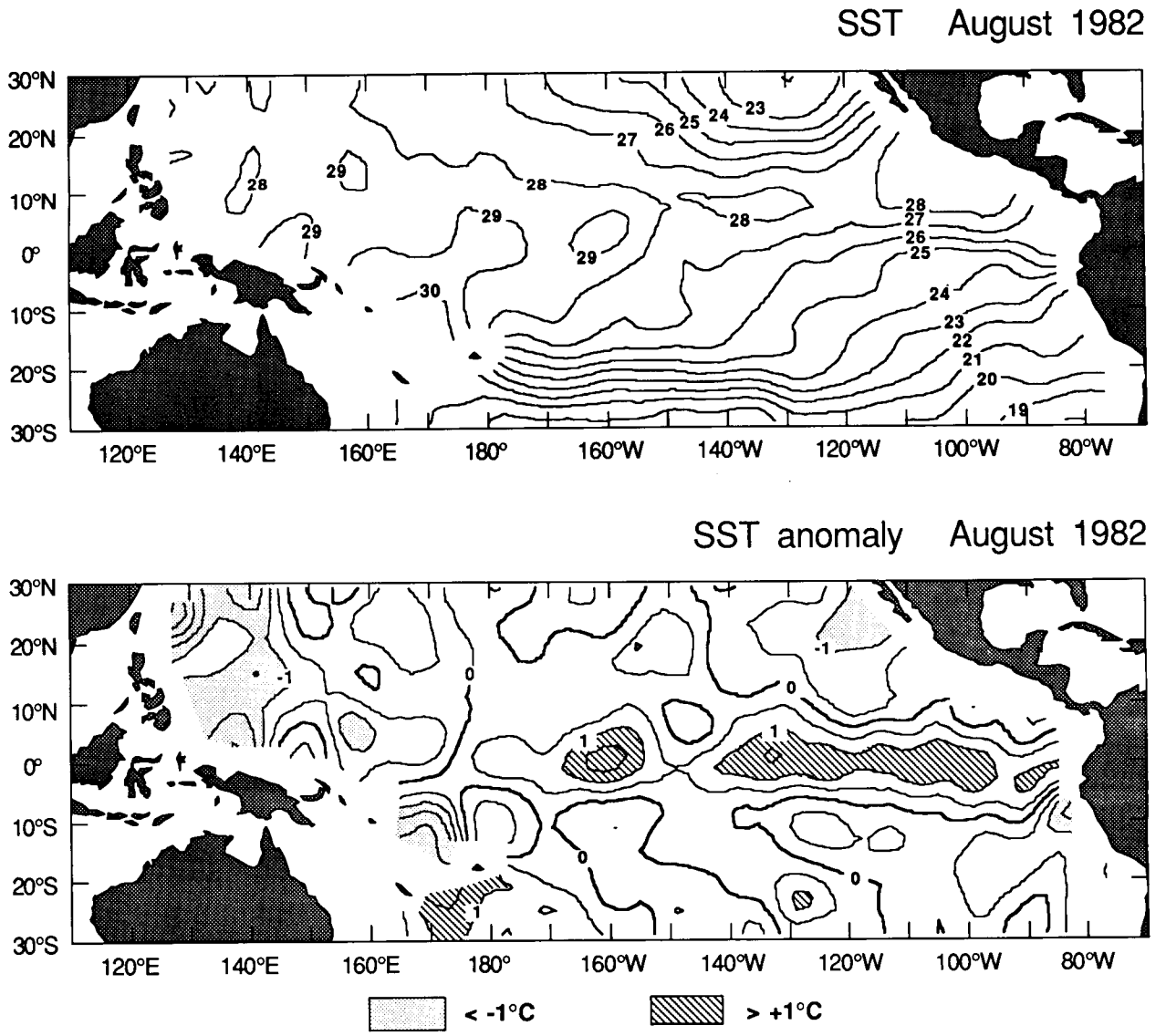

Fig. 12. Same as Fig. 10, except for August 1982

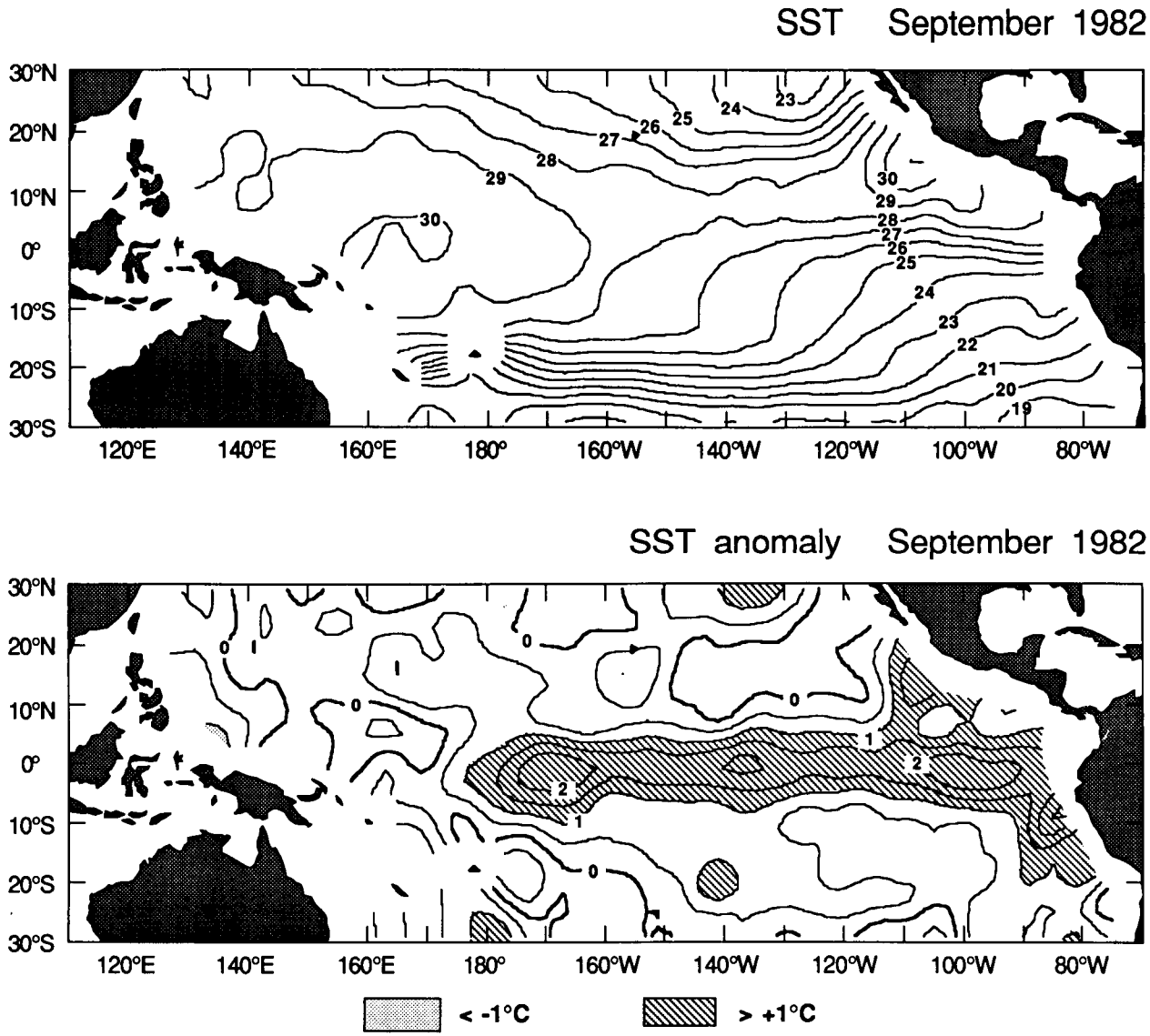

Fig. 13. Same as Fig. 10, except for September 1982

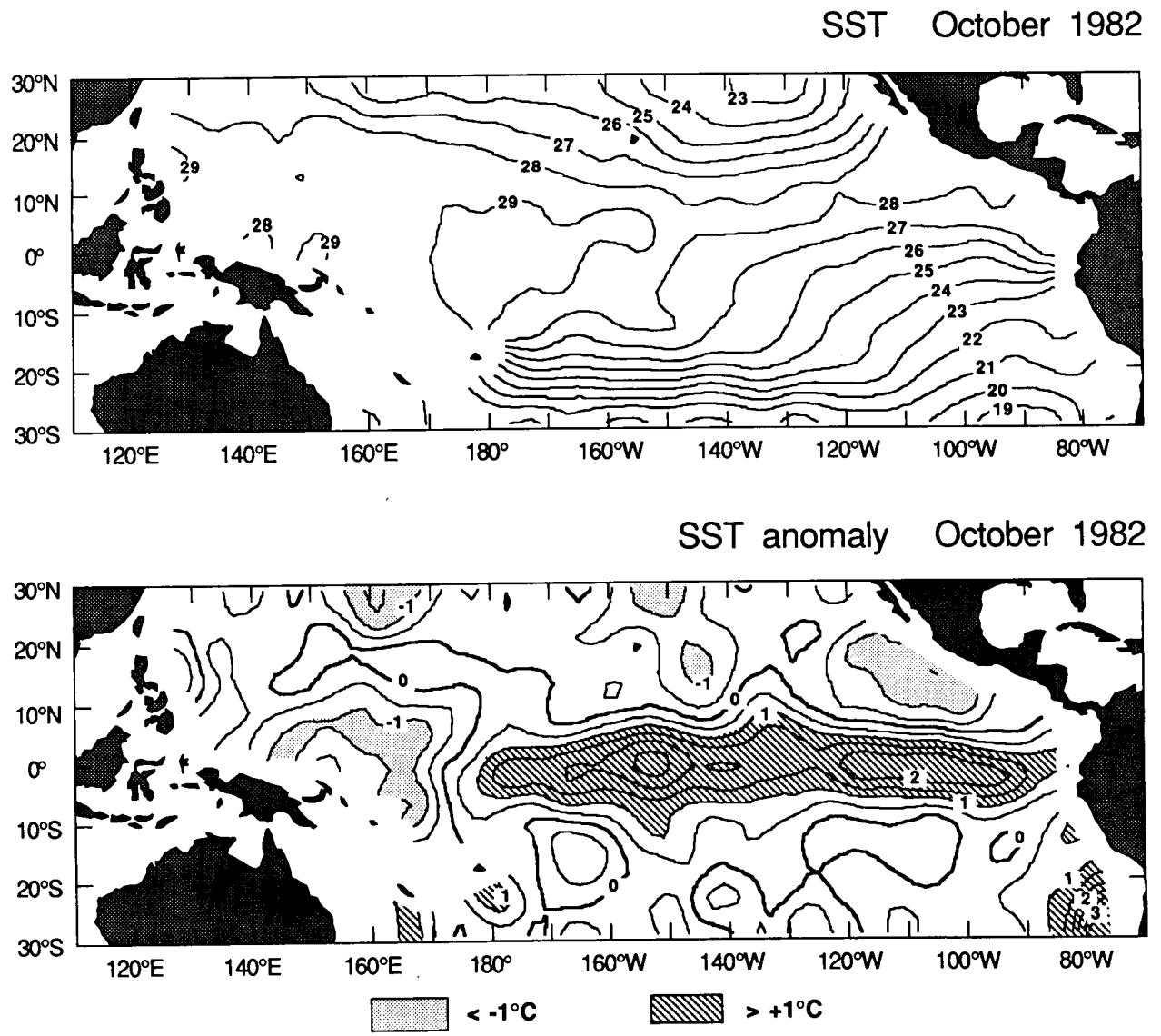

Fig. 14. Same as Fig. 10, except for October 1982

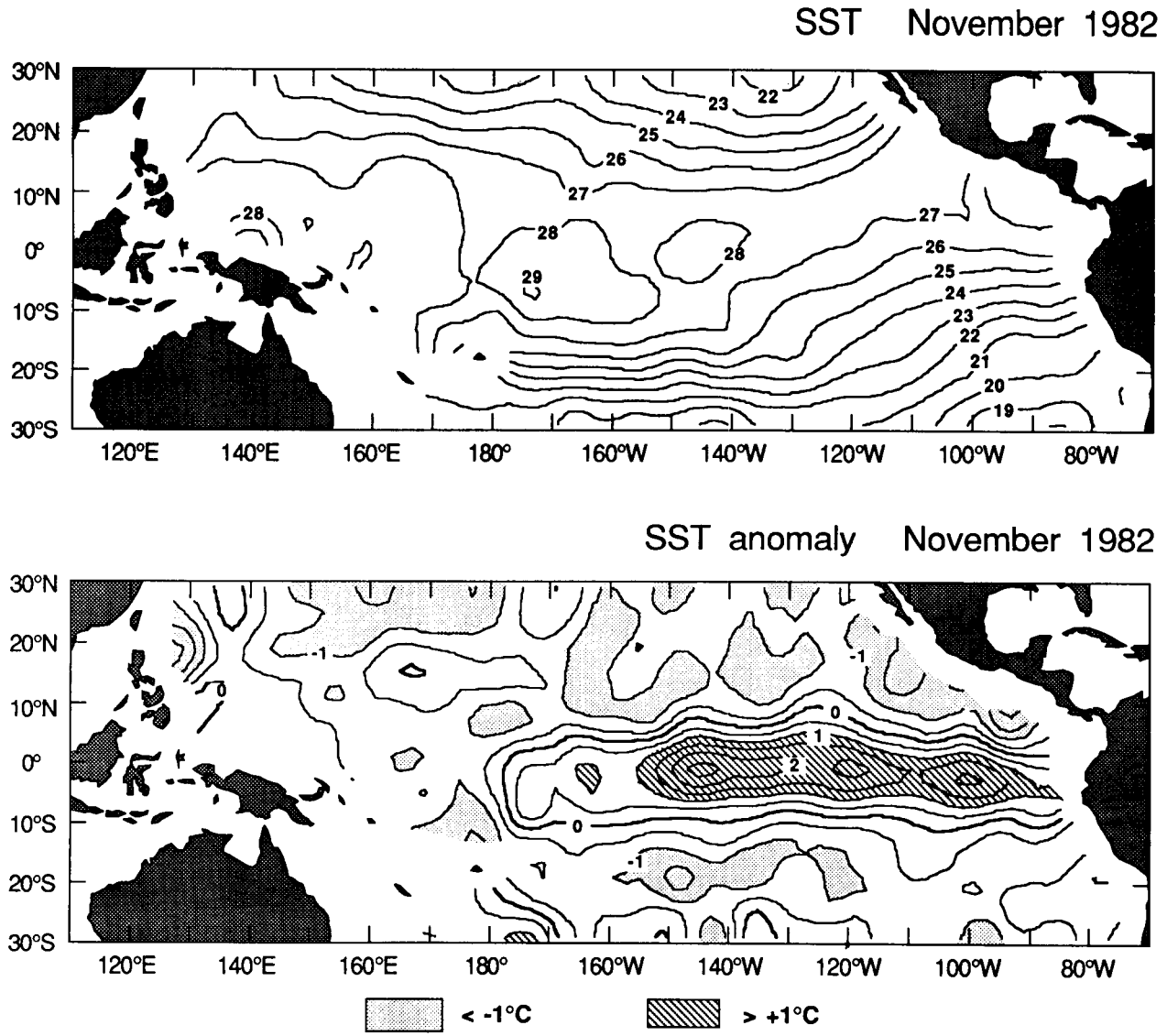

Fig. 15. Same as Fig. 10, except for November 1982

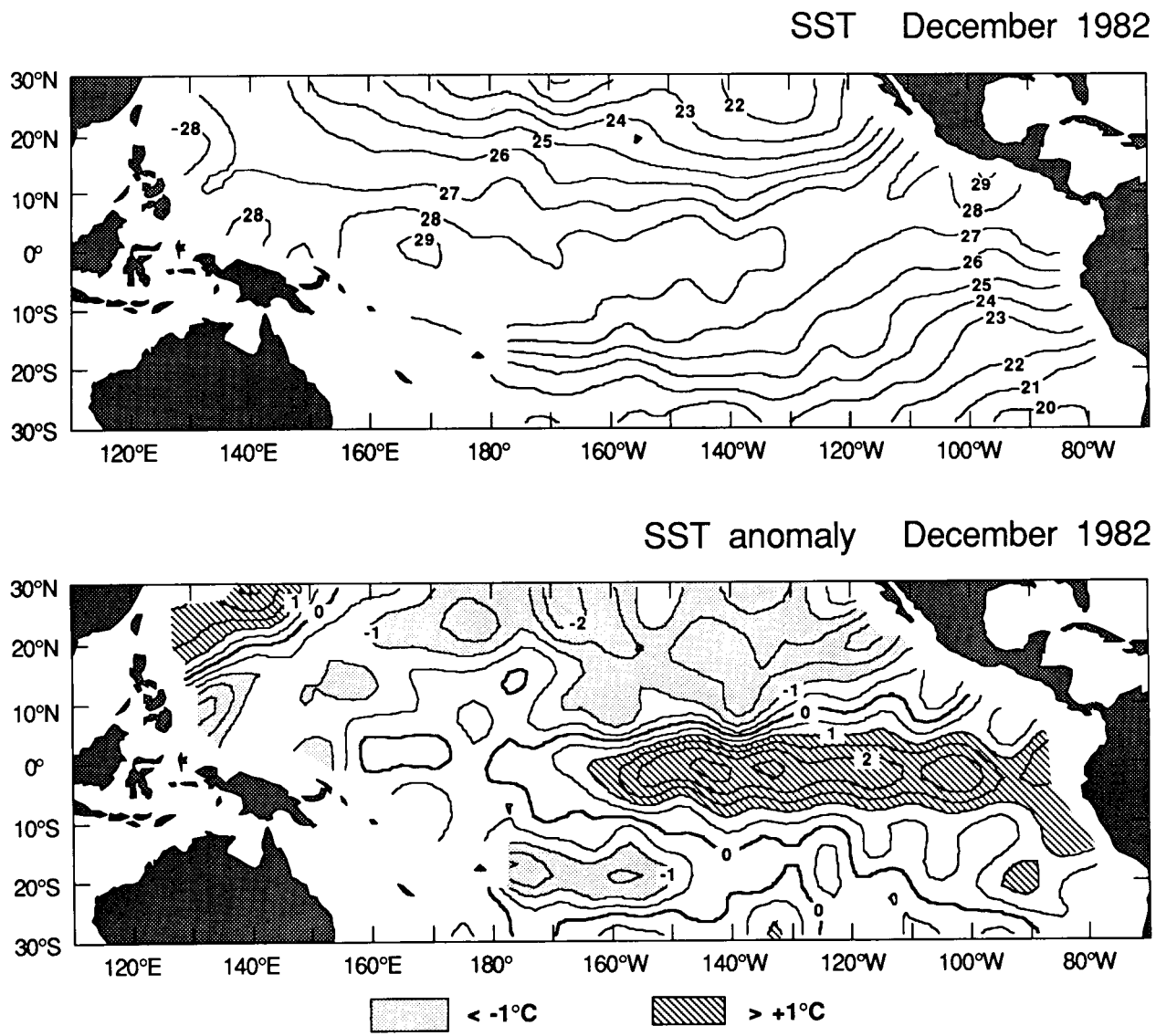

Fig. 16. Same as Fig. 10, except for December 1982

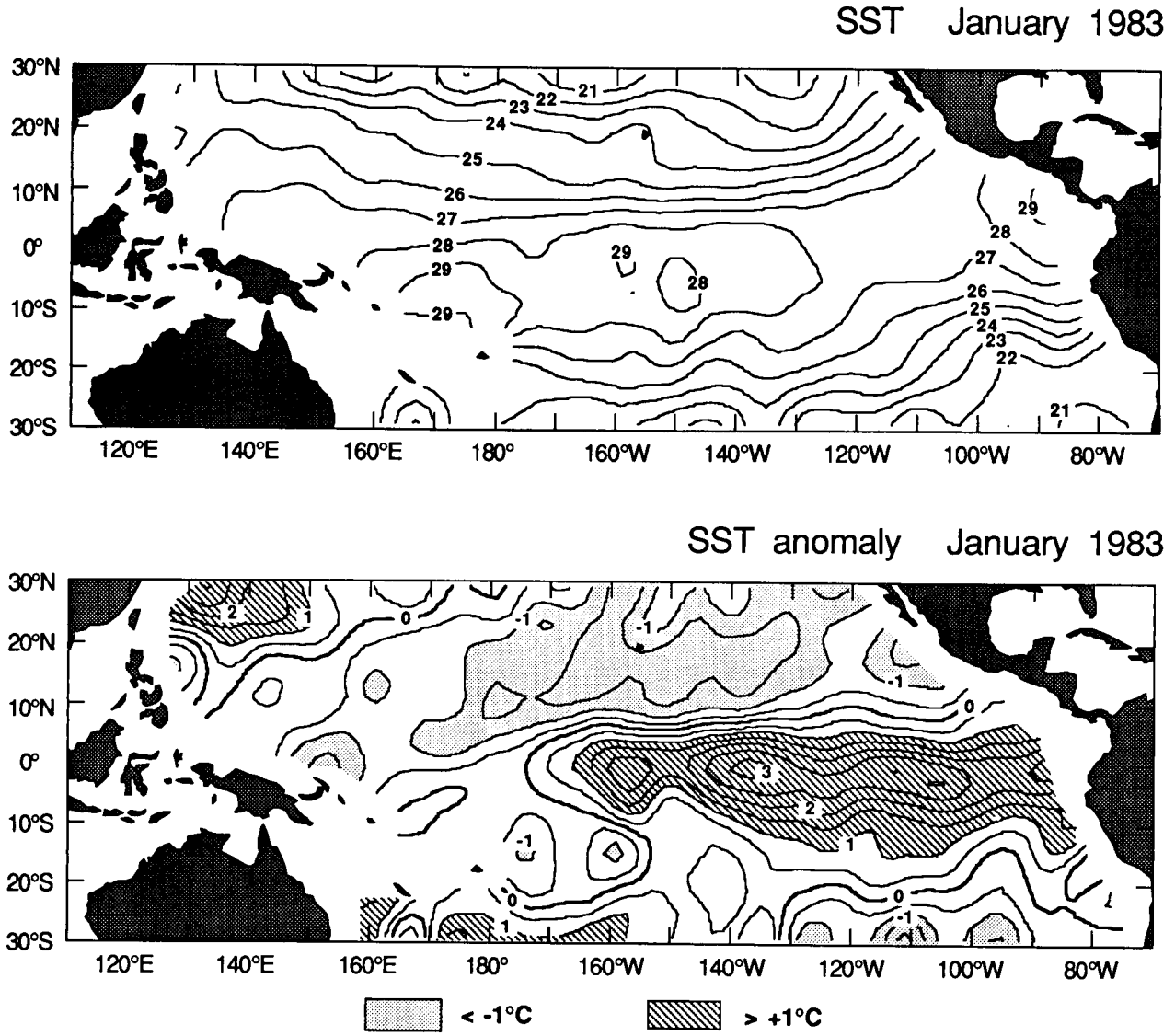

Fig. 17. Same as Fig. 10, except for January 1983

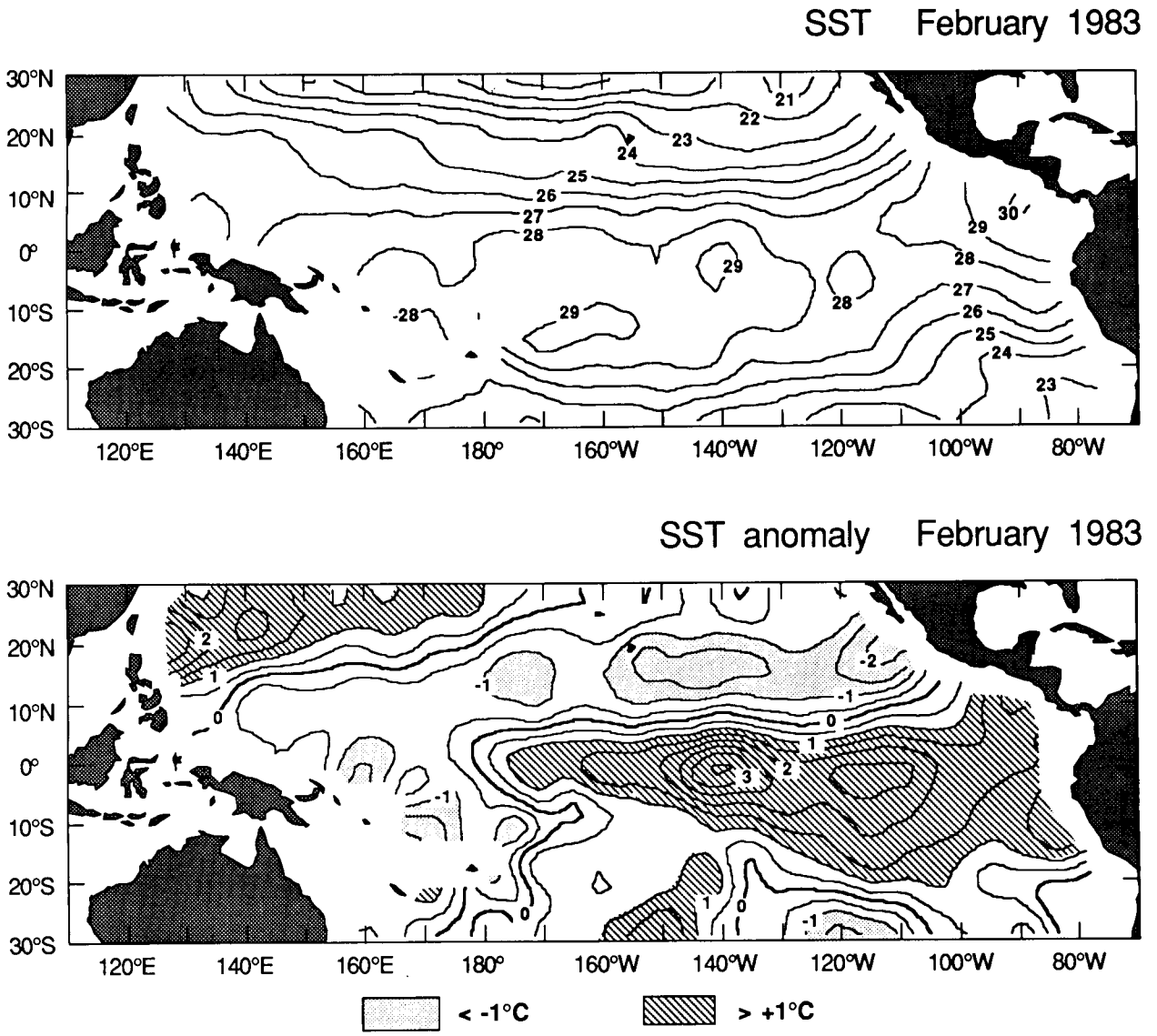

Fig. 18. Same as Fig. 10, except for February 1983

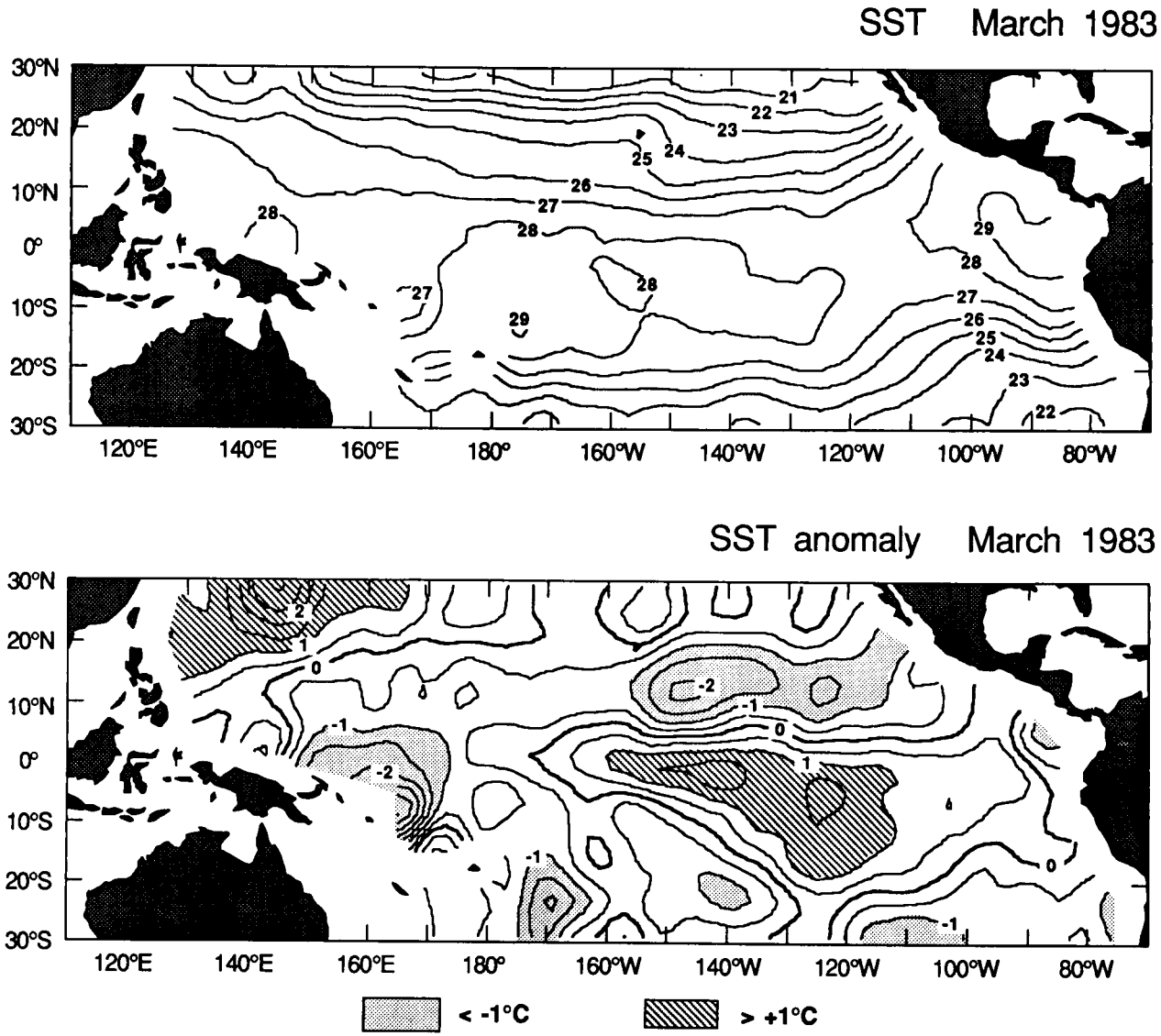

Fig. 19. Same as Fig. 10, except for March 1983

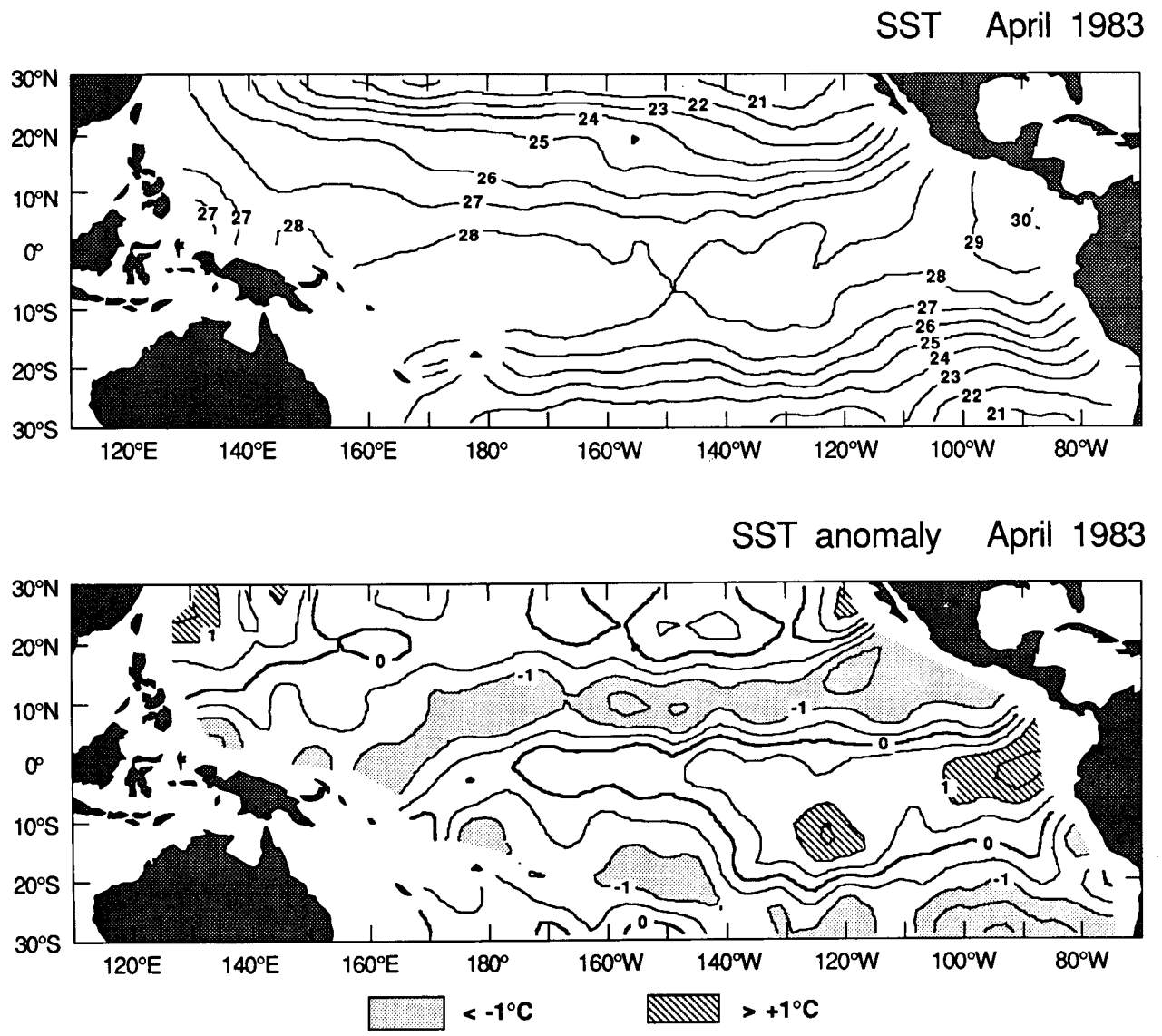

Fig. 20. Same as Fig. 10, except for April 1983

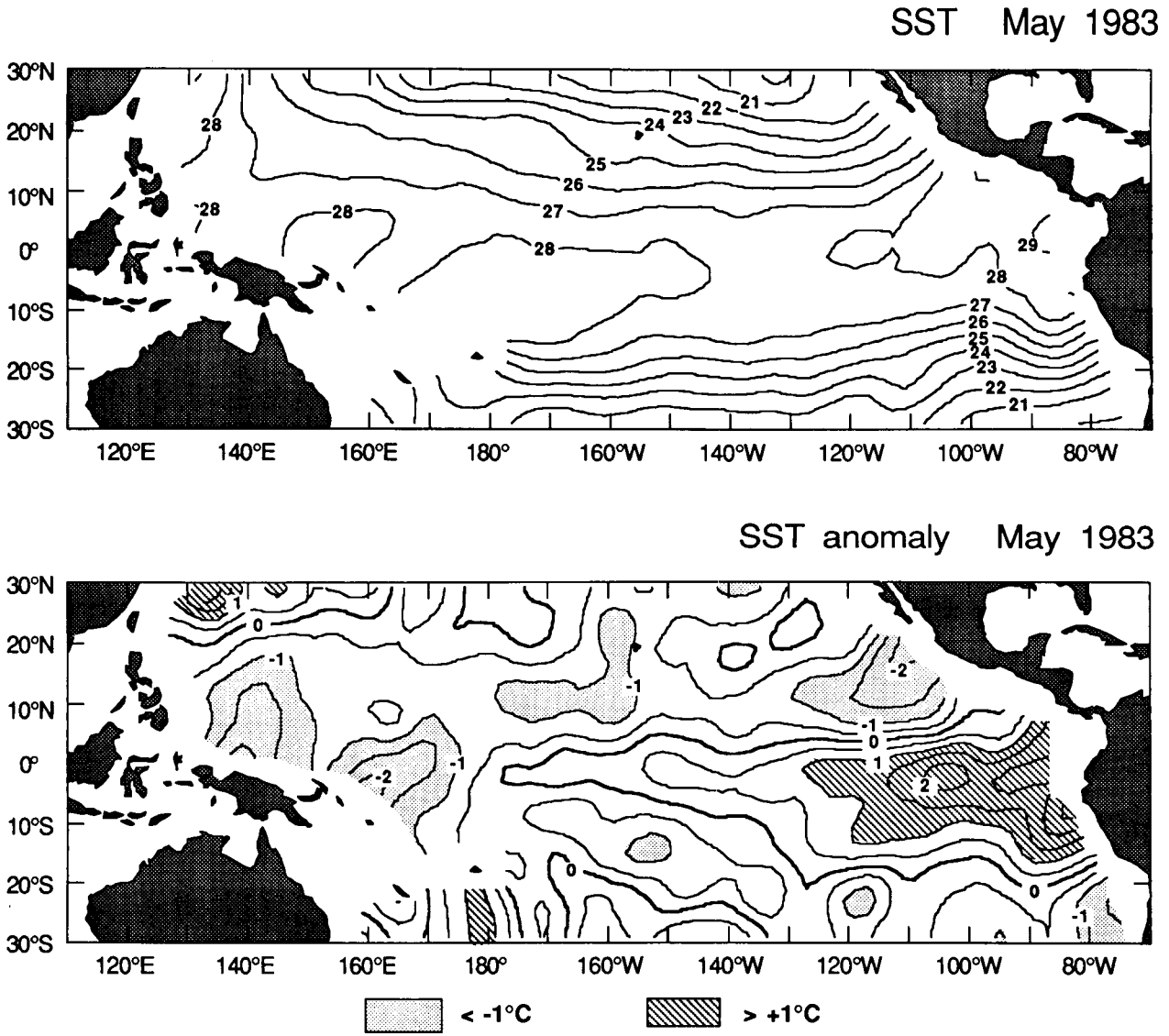

Fig. 21. Same as Fig. 10, except for May 1983

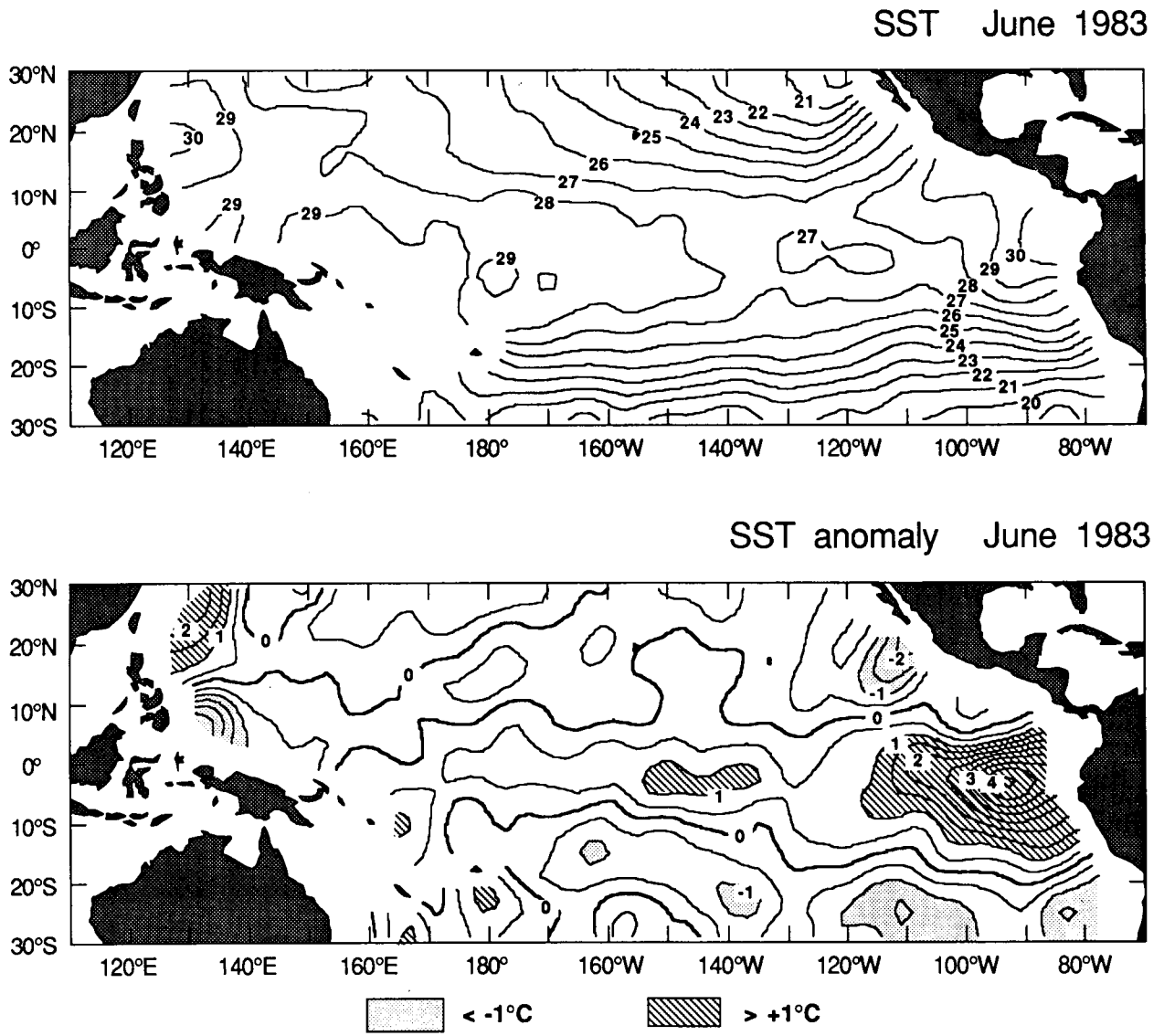

Fig. 22. Same as Fig. 10, except for June 1983

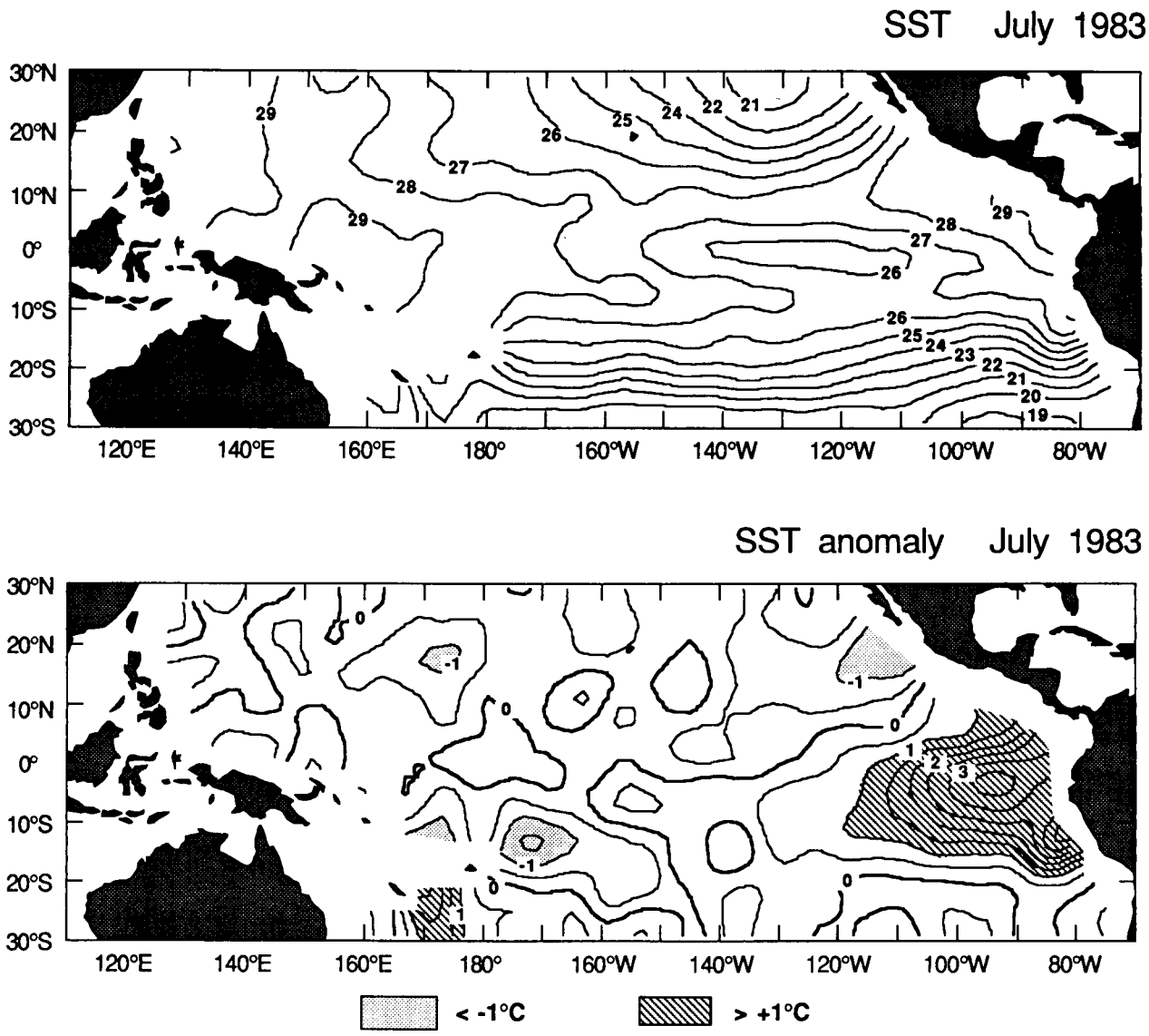

Fig. 23. Same as Fig. 10, except for July 1983

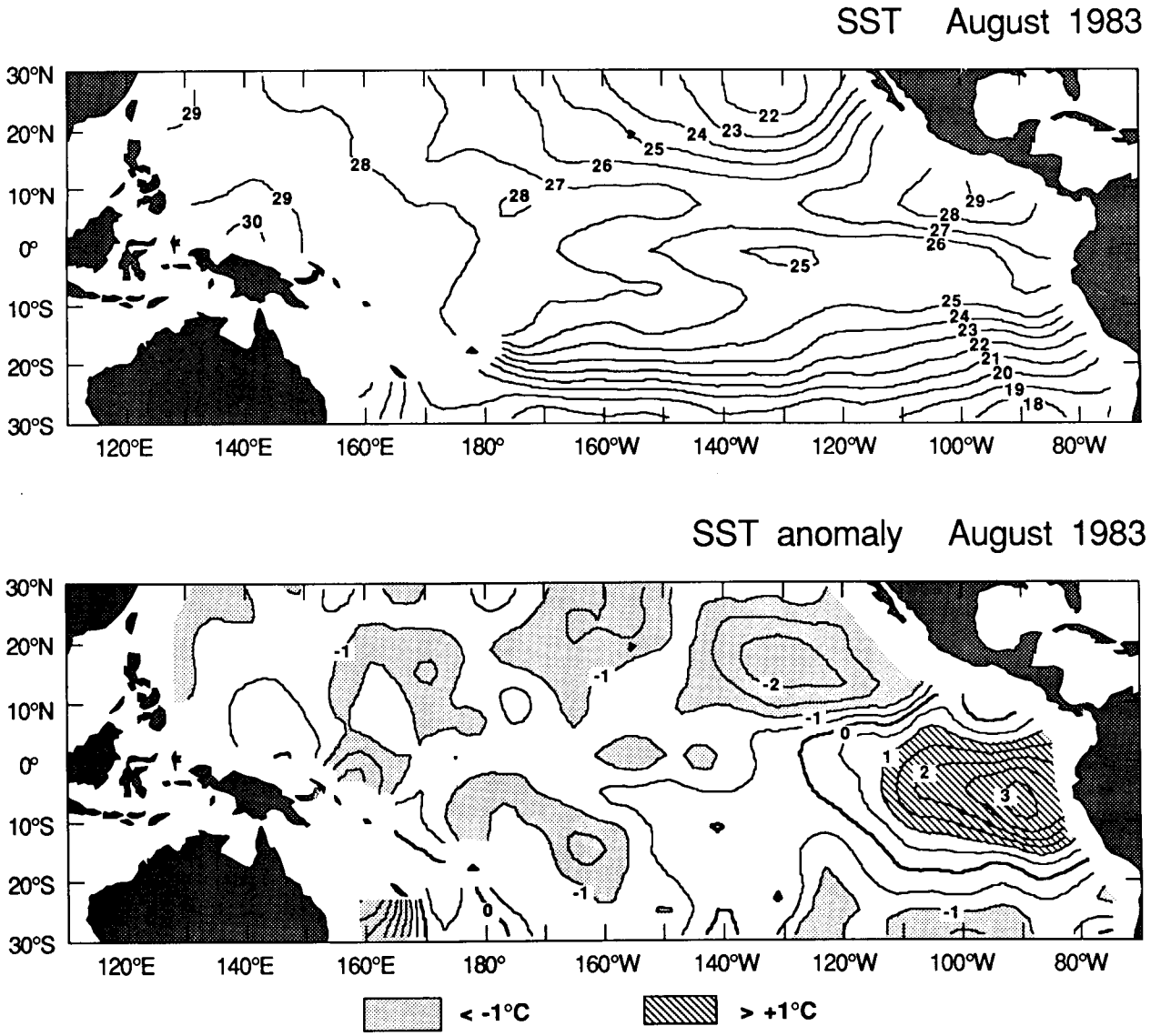

Fig. 24. Same as Fig. 10, except for August 1983

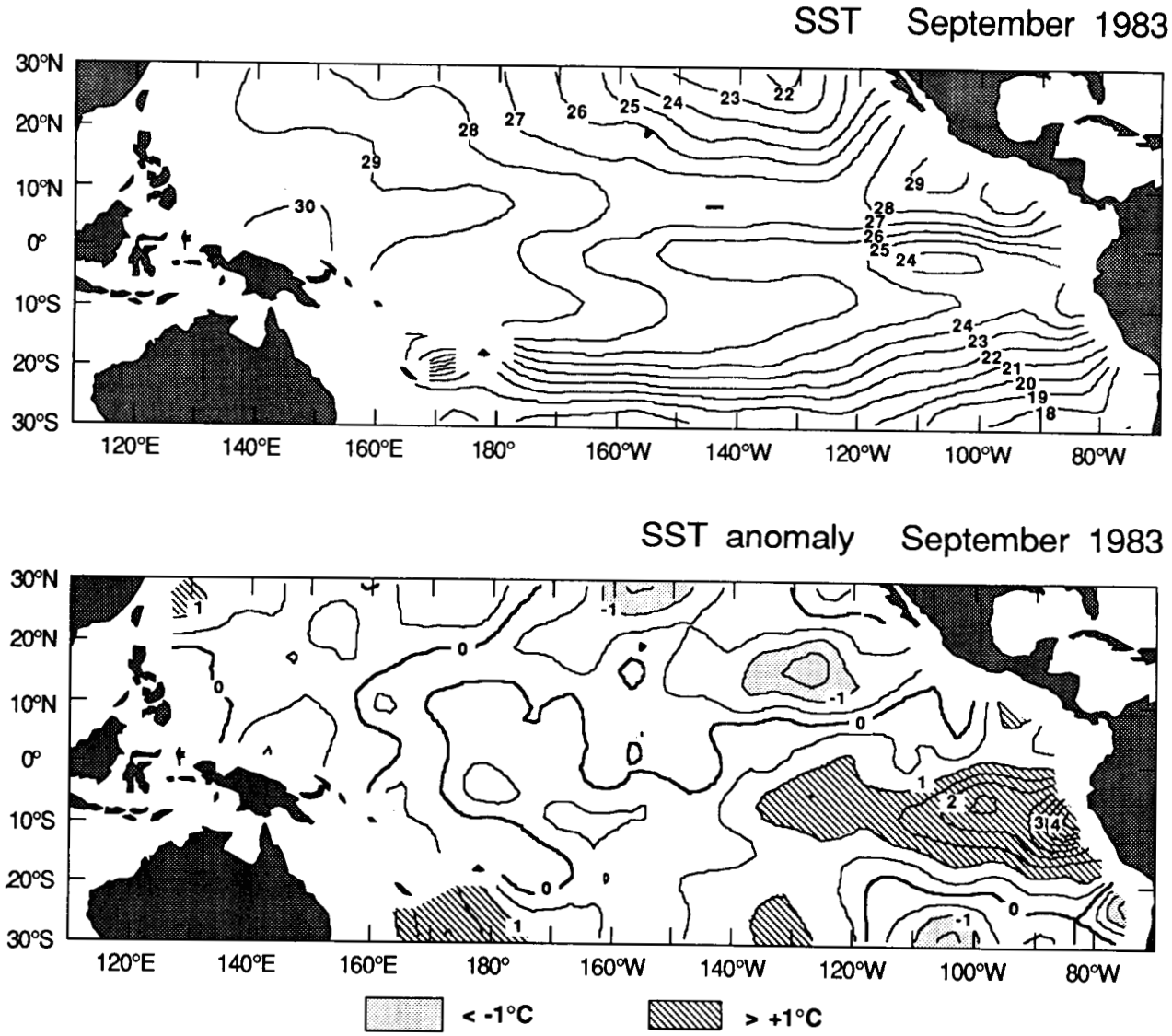

Fig. 25. Same as Fig. 10, except for September 1983

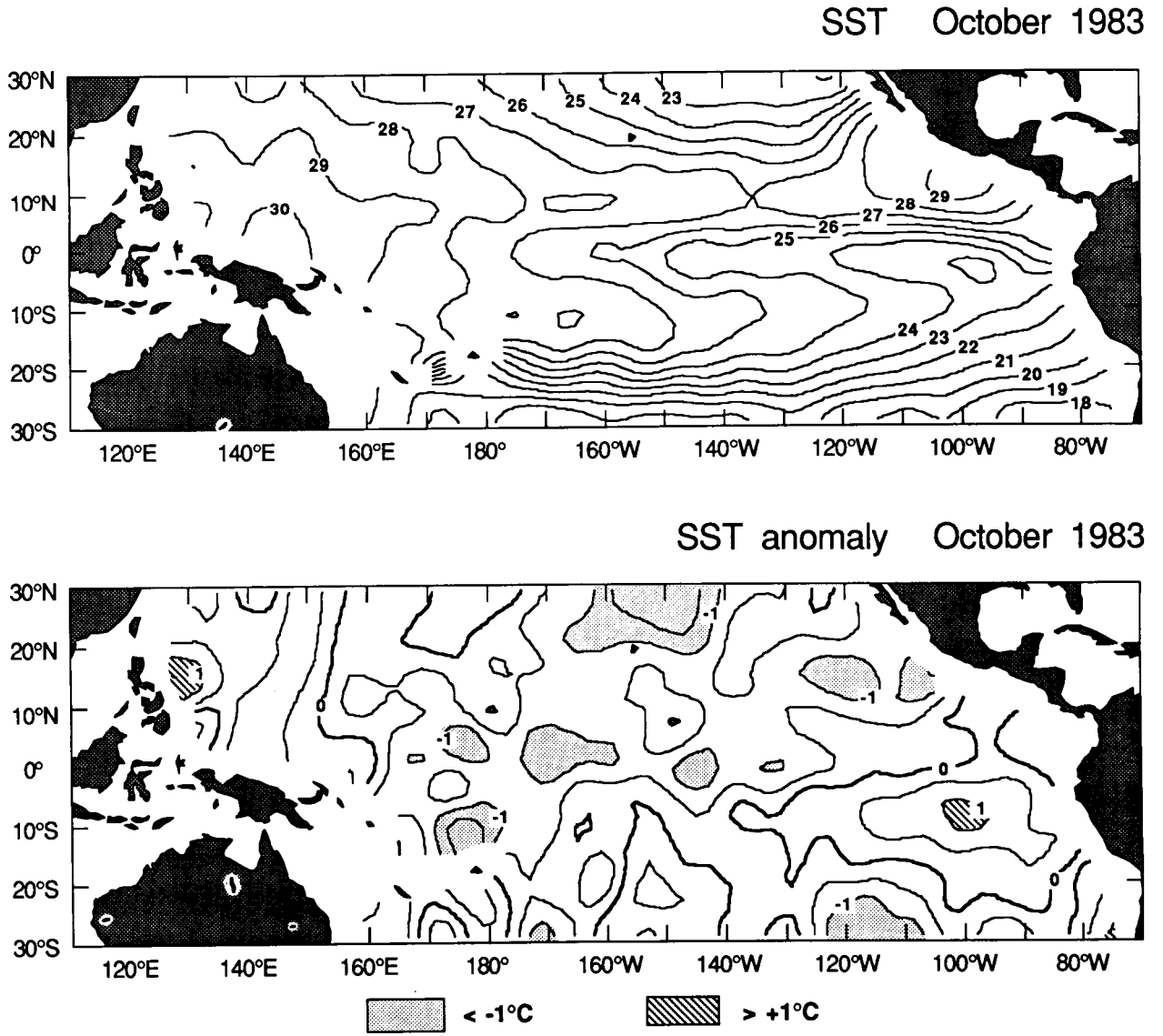

Fig. 26. Same as Fig. 10, except for October 1983

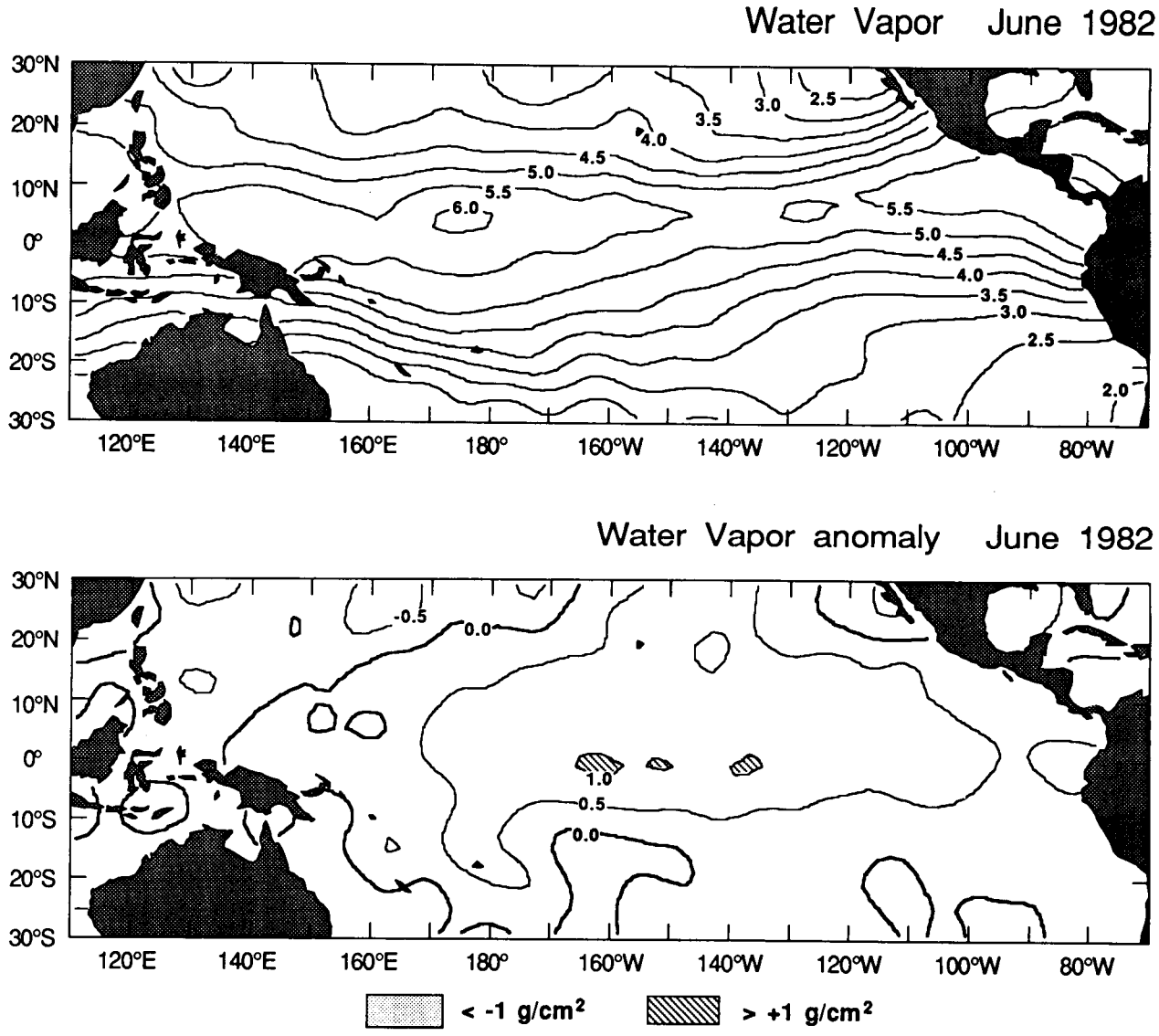

Fig. 27. Atmospheric water vapor measured by SMMR in June 1982 and its deviation (anomaly) from the corresponding 1980-81 mean

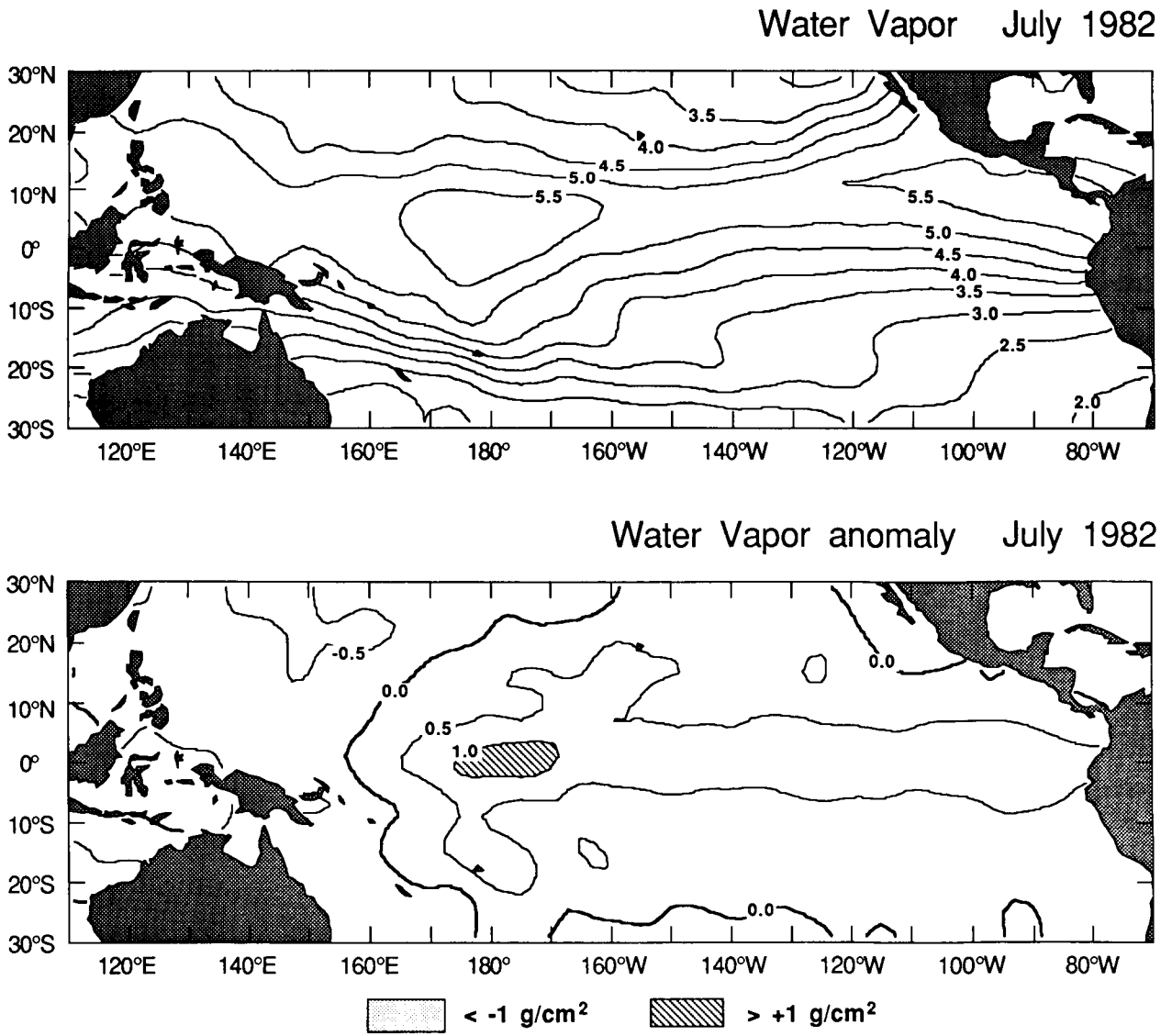

Fig. 28. Same as Fig. 27, except for July 1982

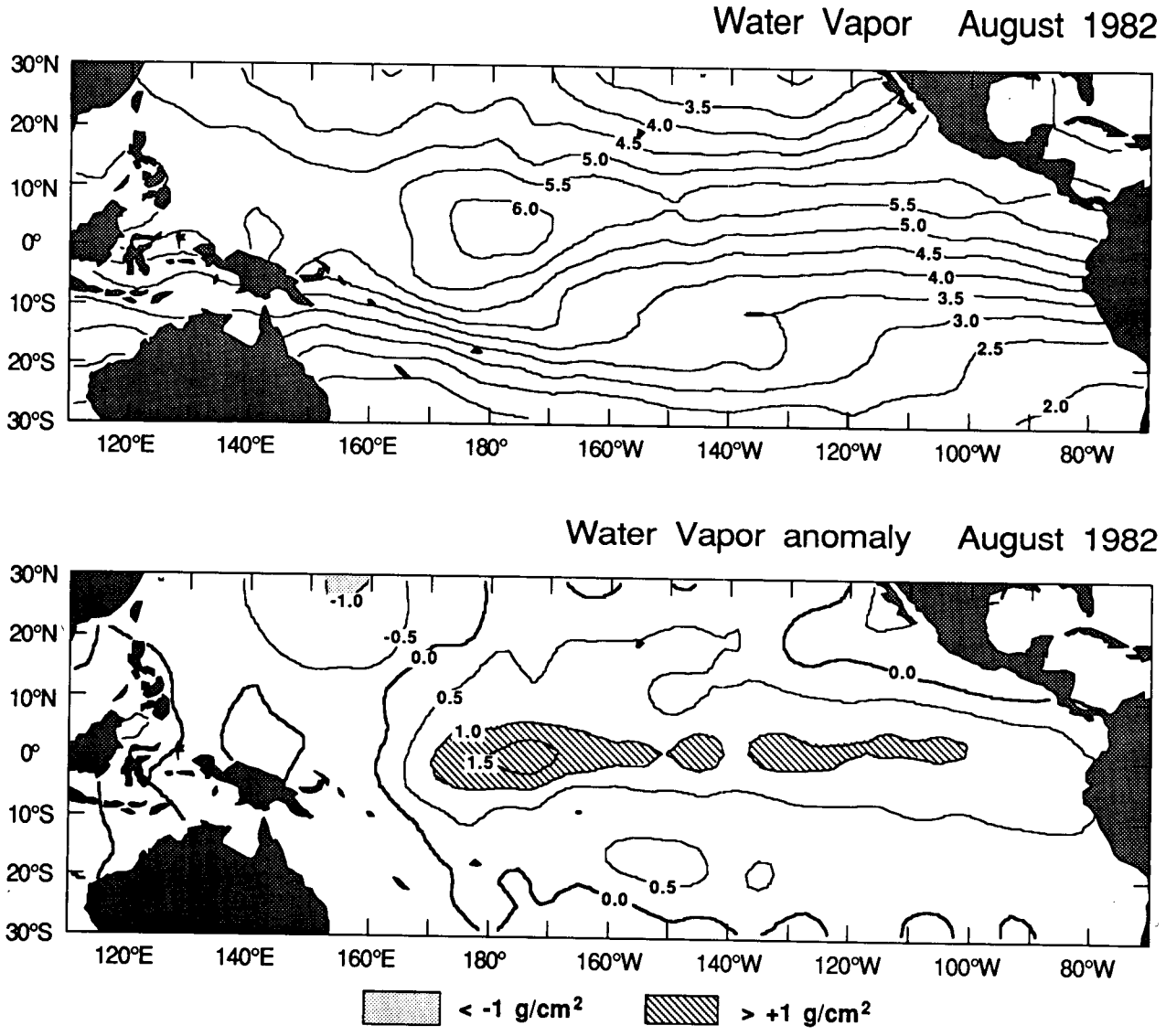

Fig. 29. Same as Fig. 27, except for August 1982

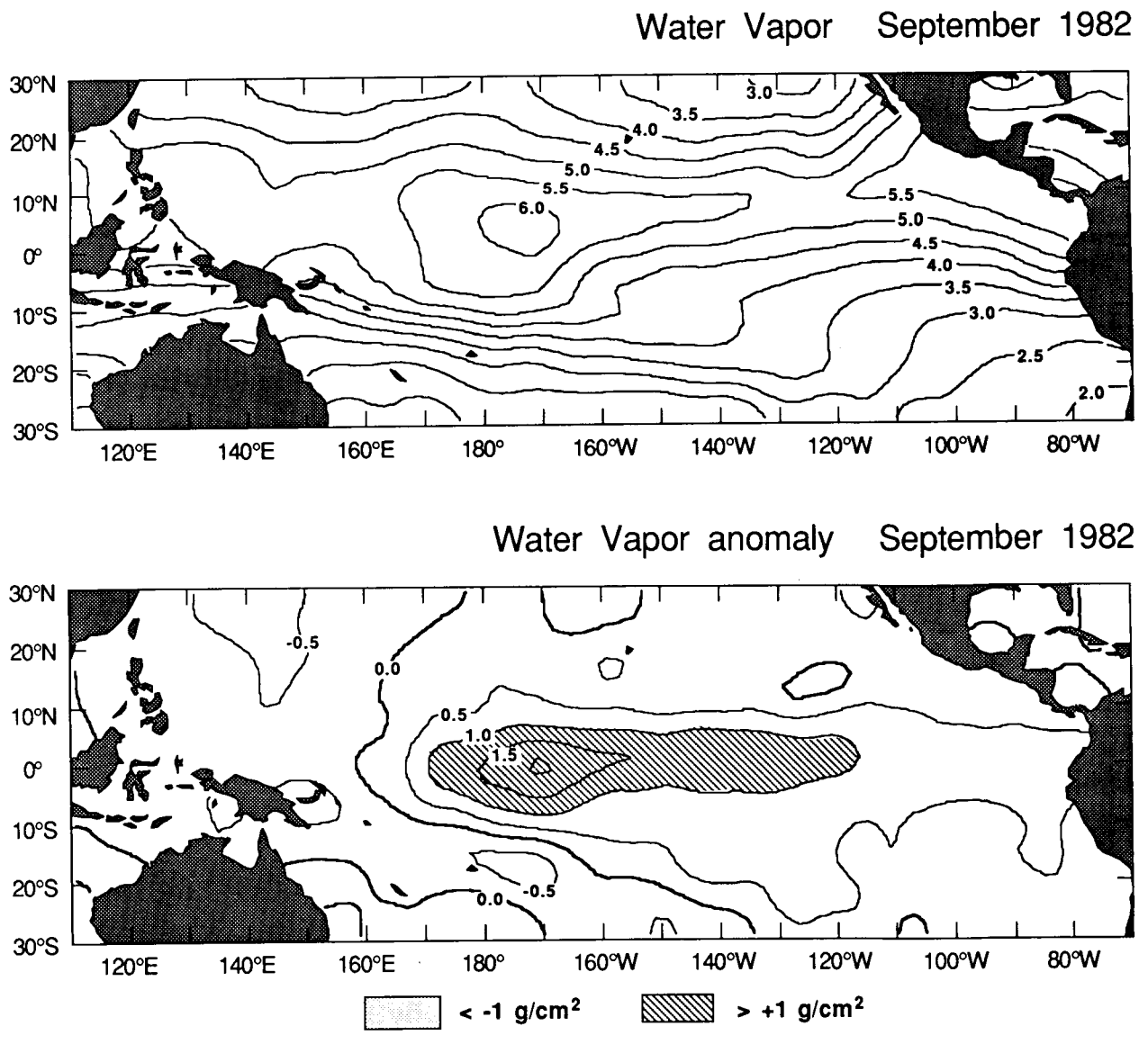

Fig. 30. Same as Fig. 27, except for September 1982

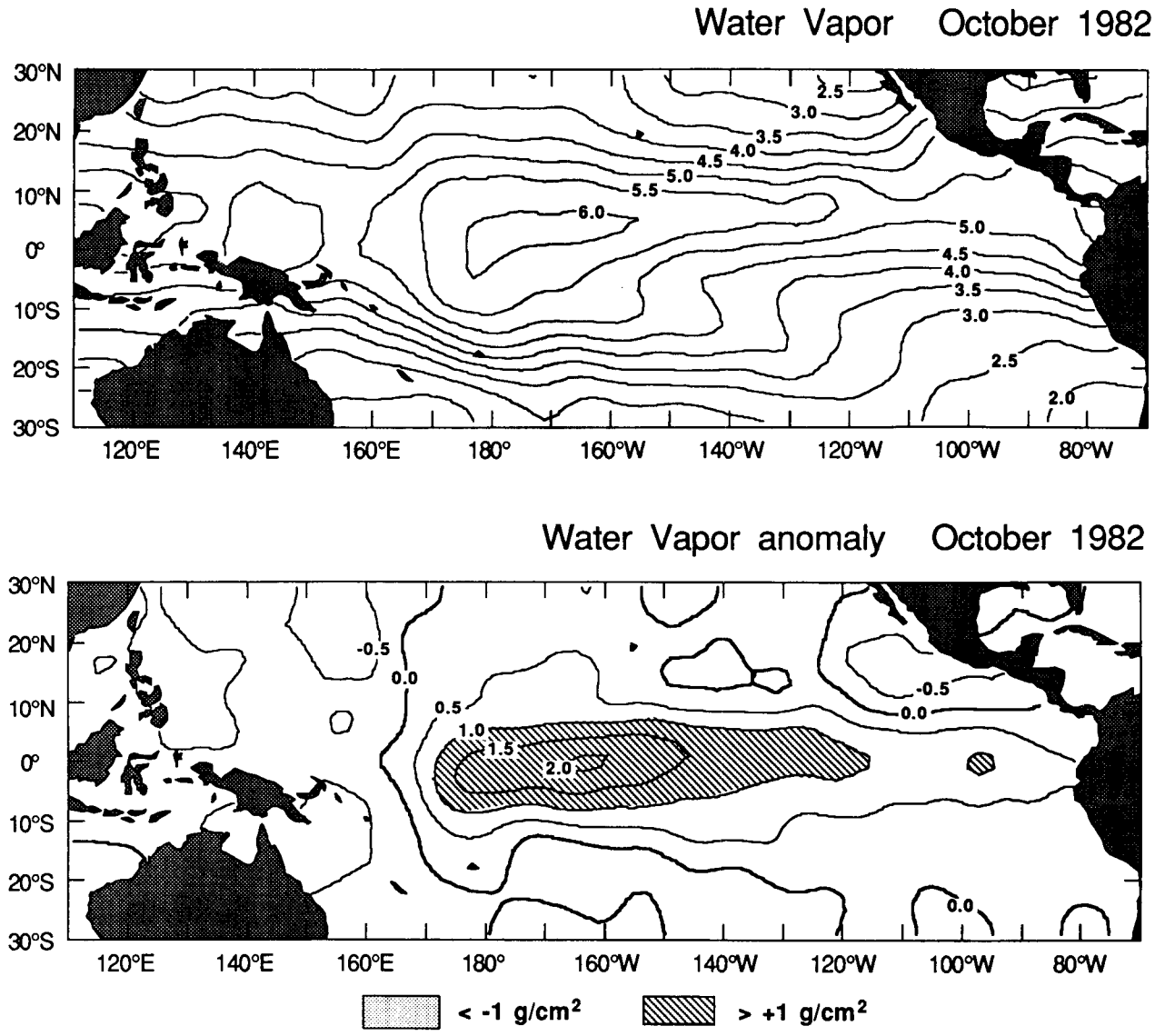

Fig. 31. Same as Fig. 27, except for October 1982

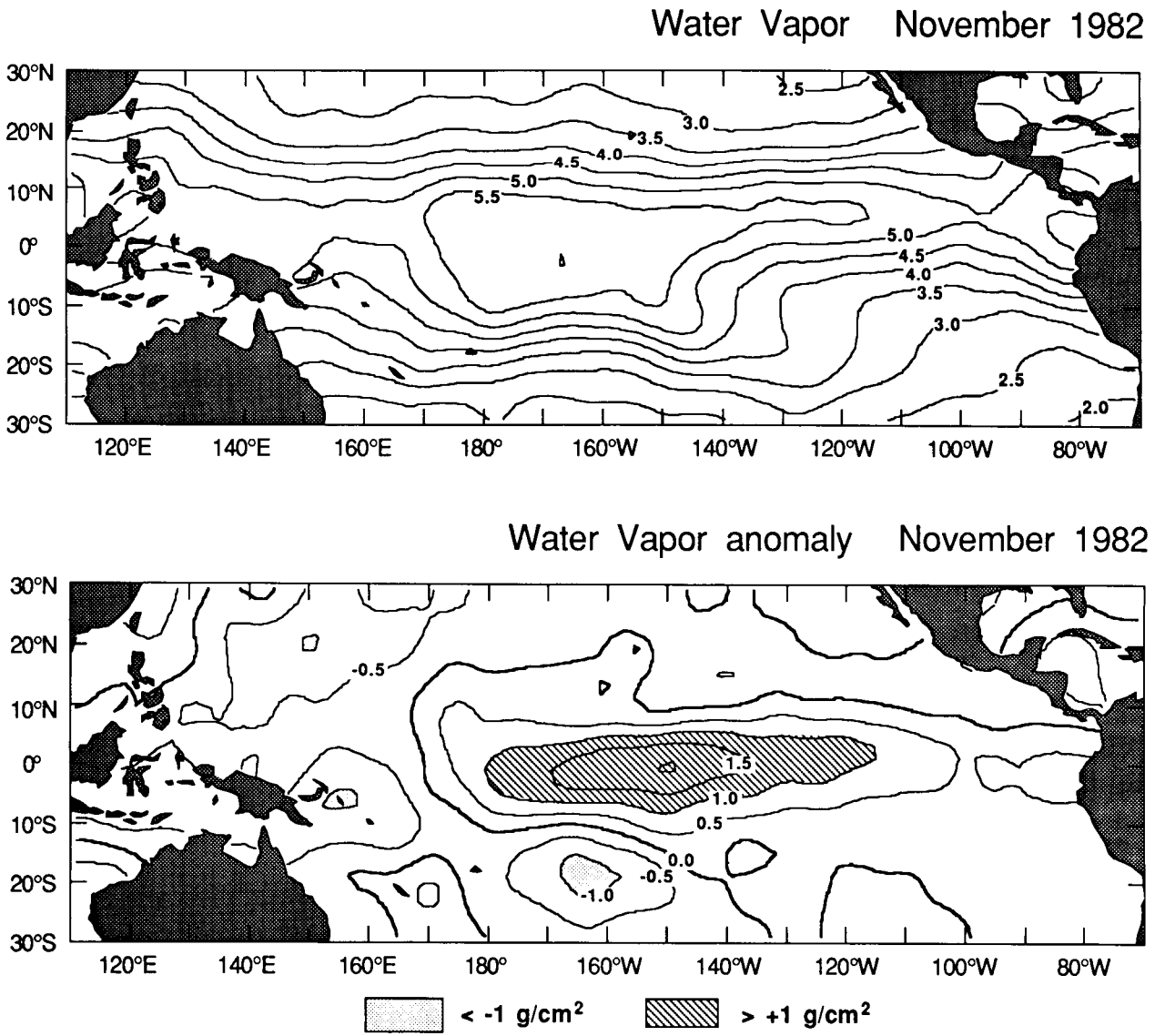

Fig. 32. Same as Fig. 27, except for November 1982

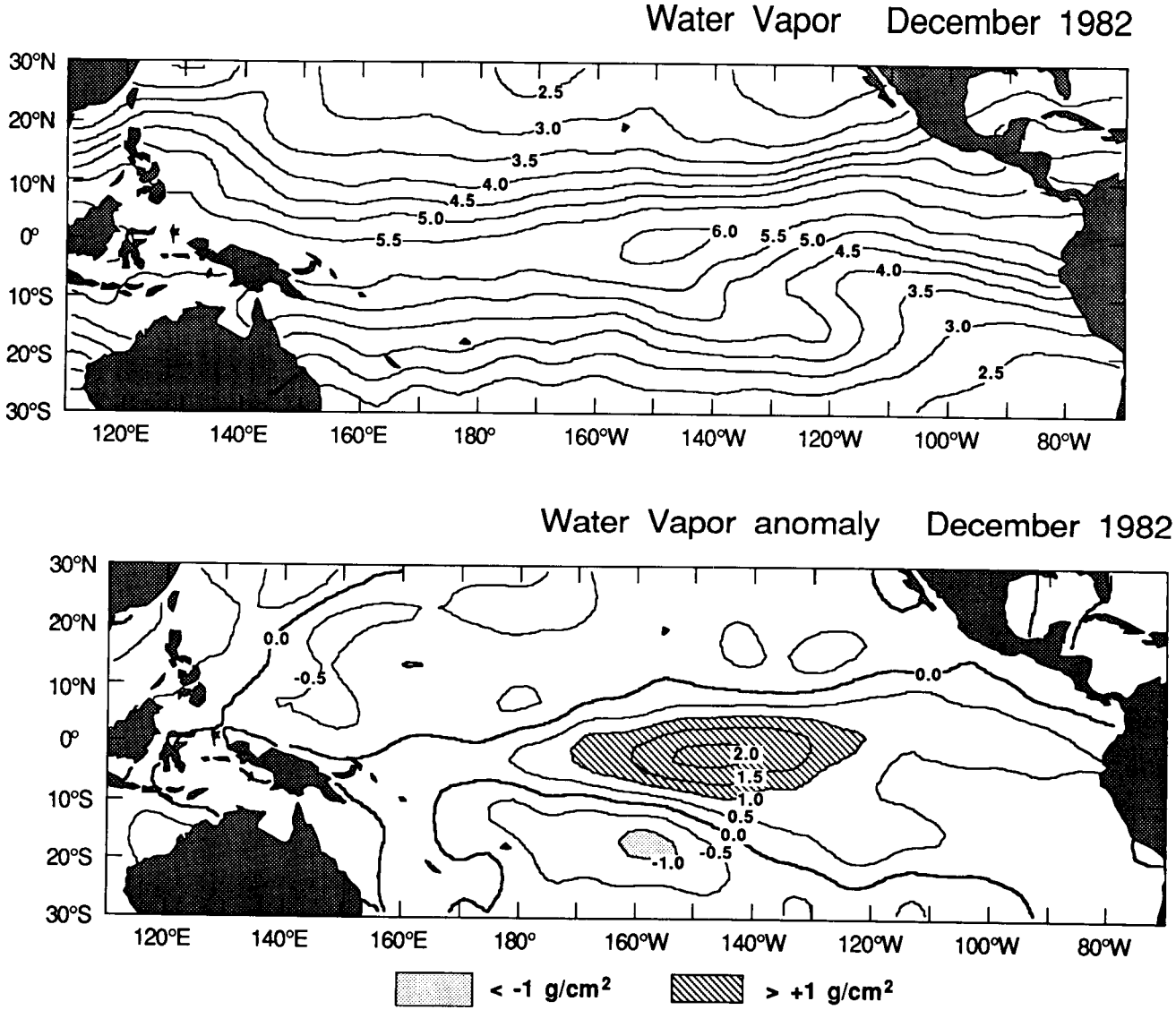

Fig. 33. Same as Fig. 27, except for December 1982

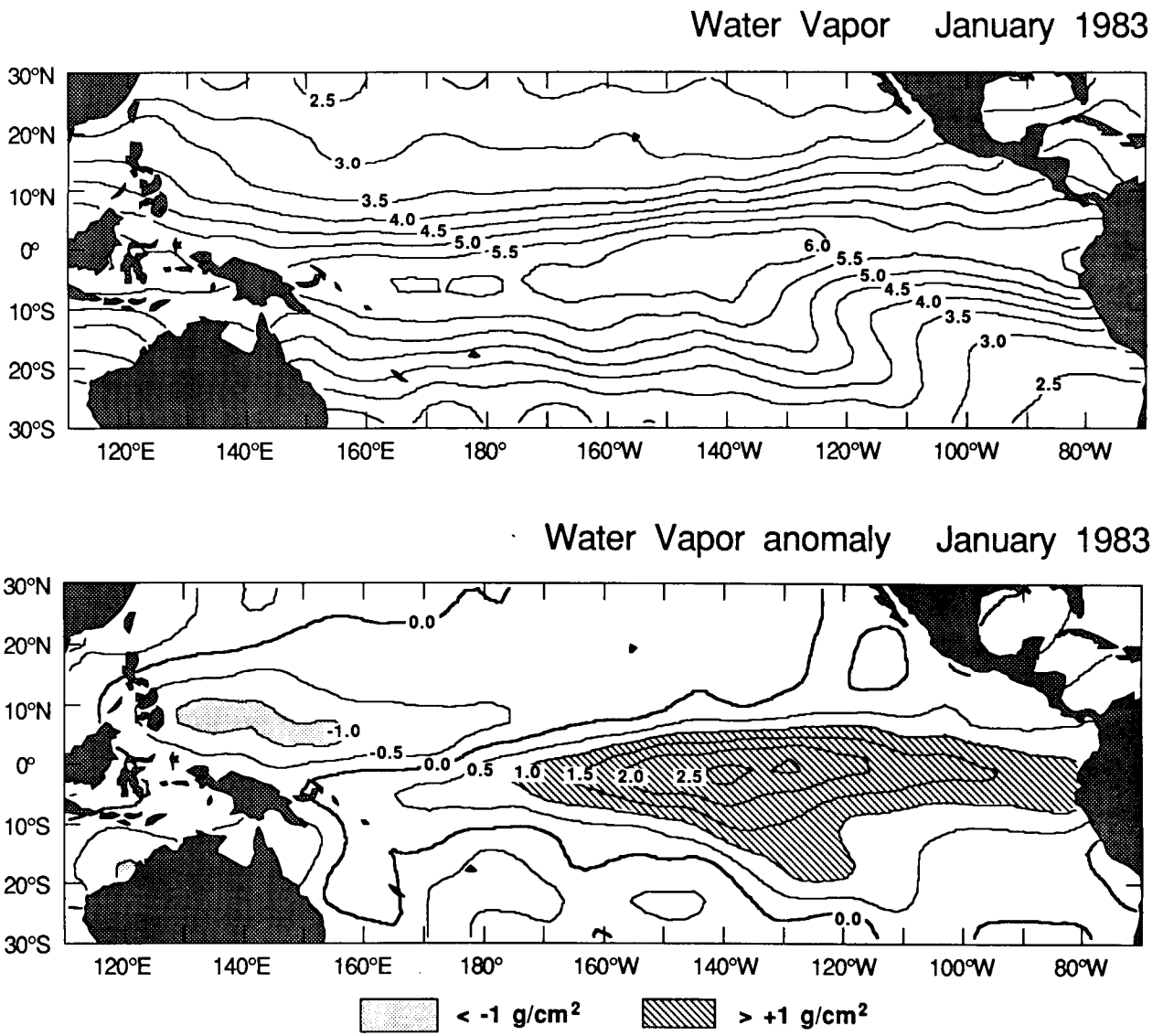

Fig. 34. Same as Fig. 27, except for January 1983

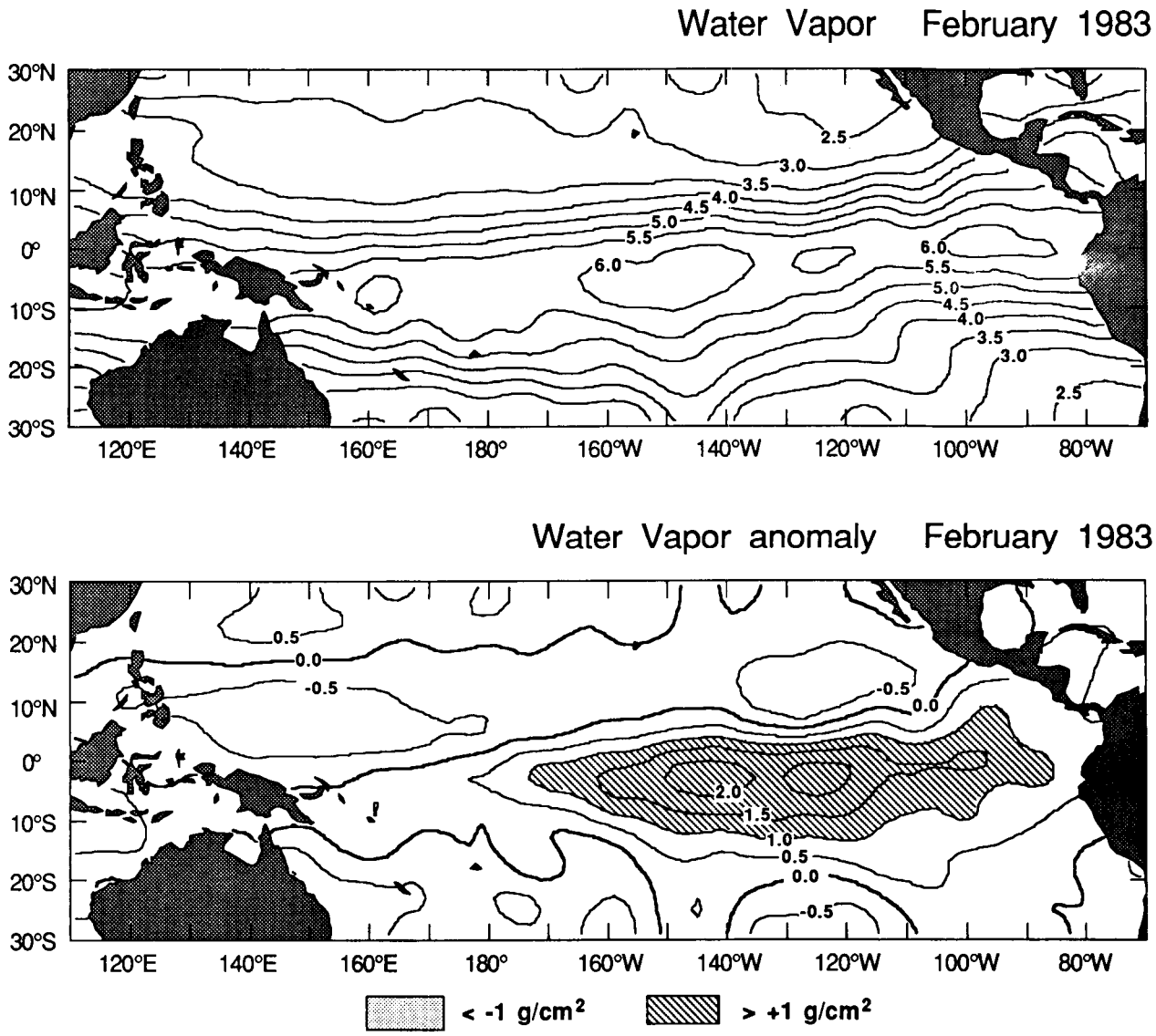

Fig. 35. Same as Fig. 27, except for February 1983

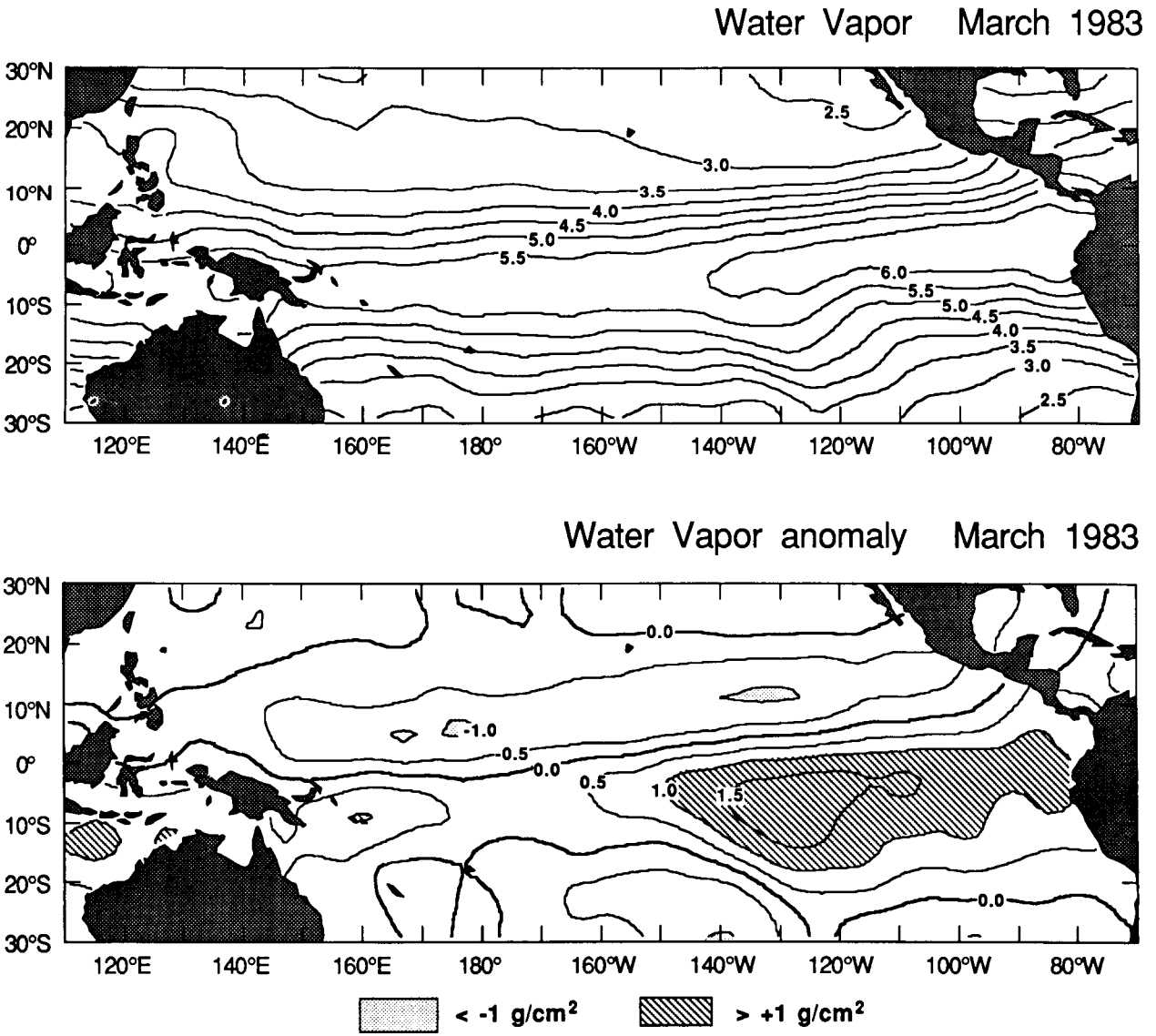

Fig. 36. Same as Fig. 27, except for March 1983

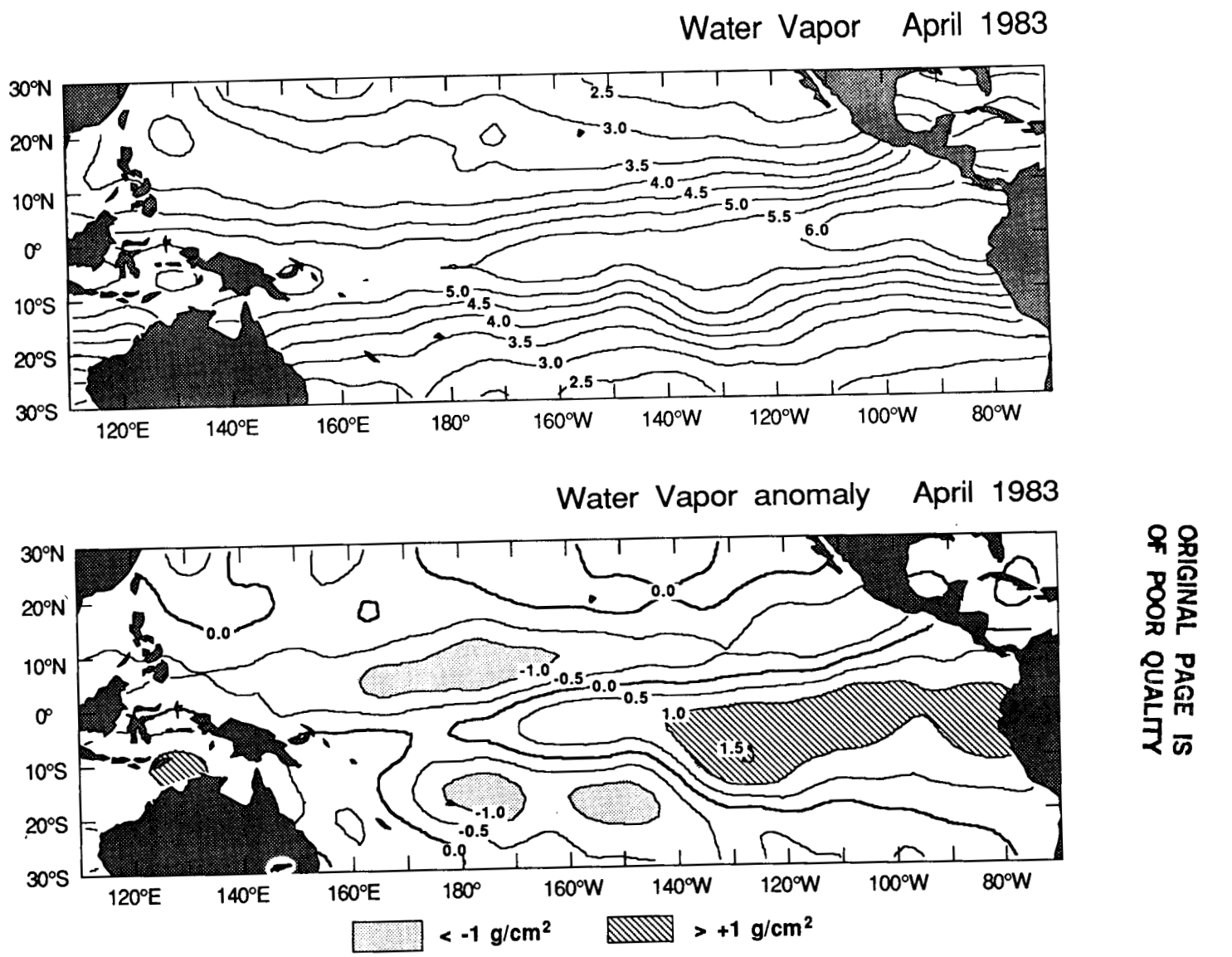

Fig. 37. Same as Fig. 27, except for April 1983

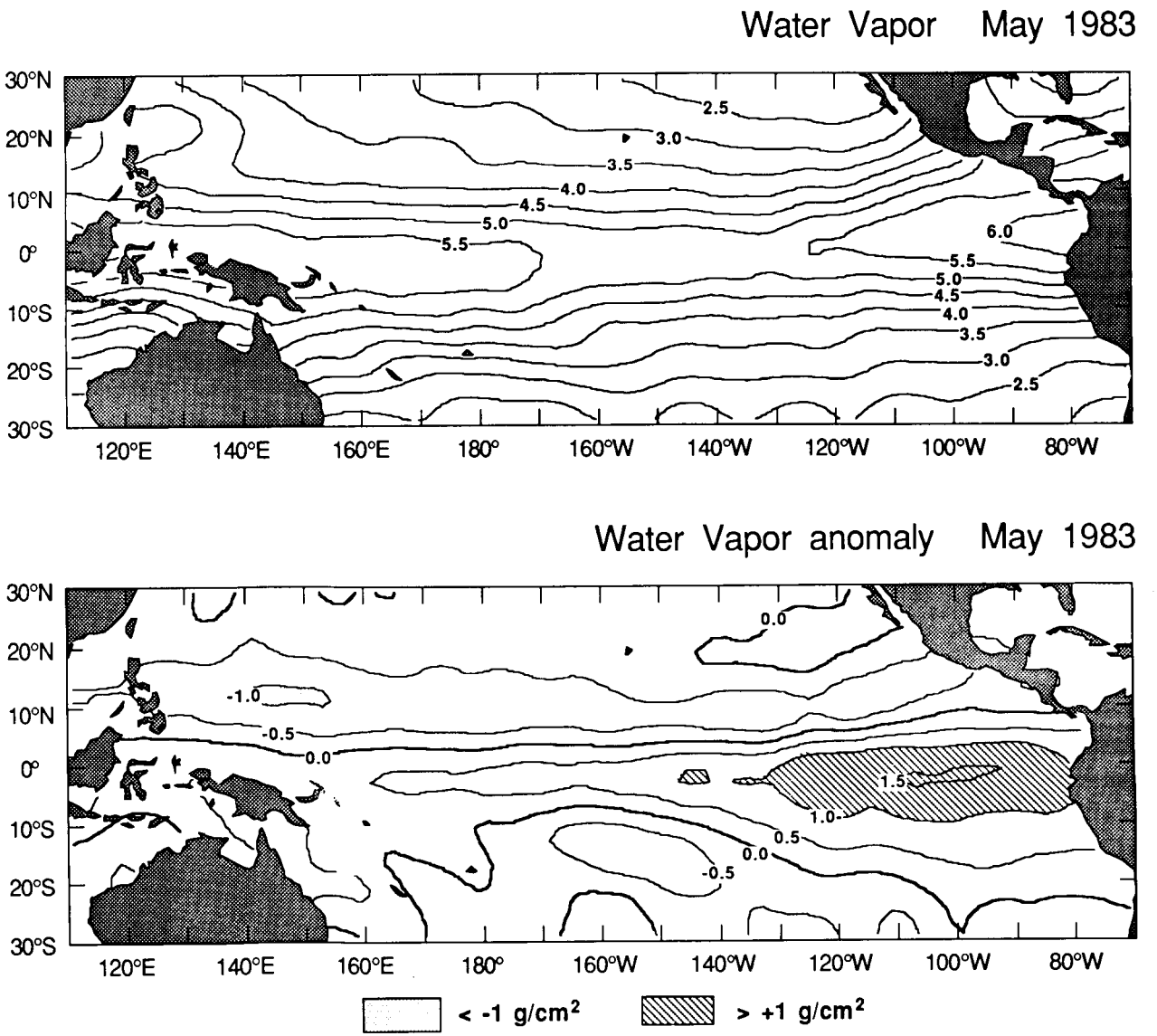

Fig. 38. Same as Fig. 27, except for May 1983

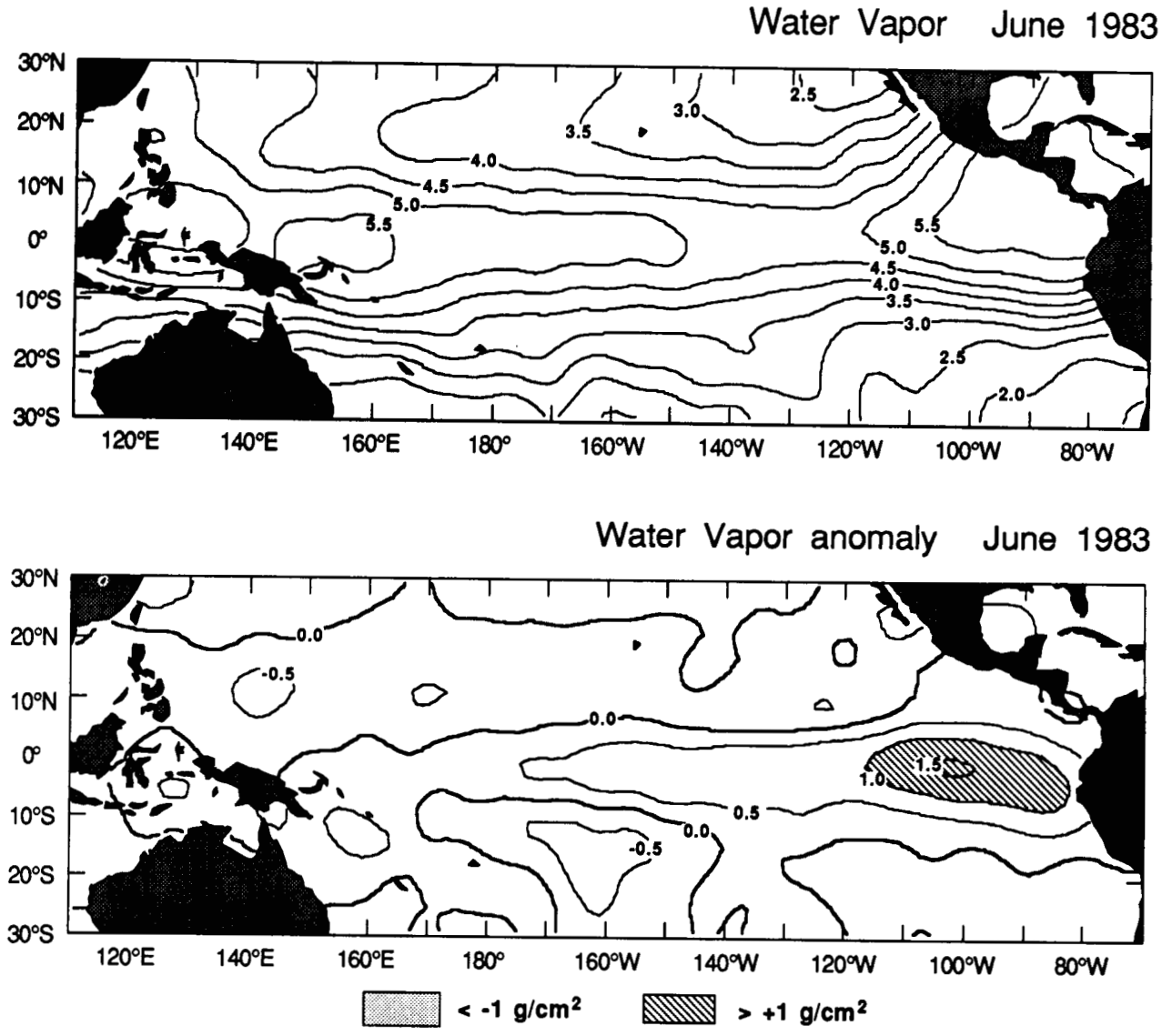

Fig. 39. Same as Fig. 27, except for June 1983

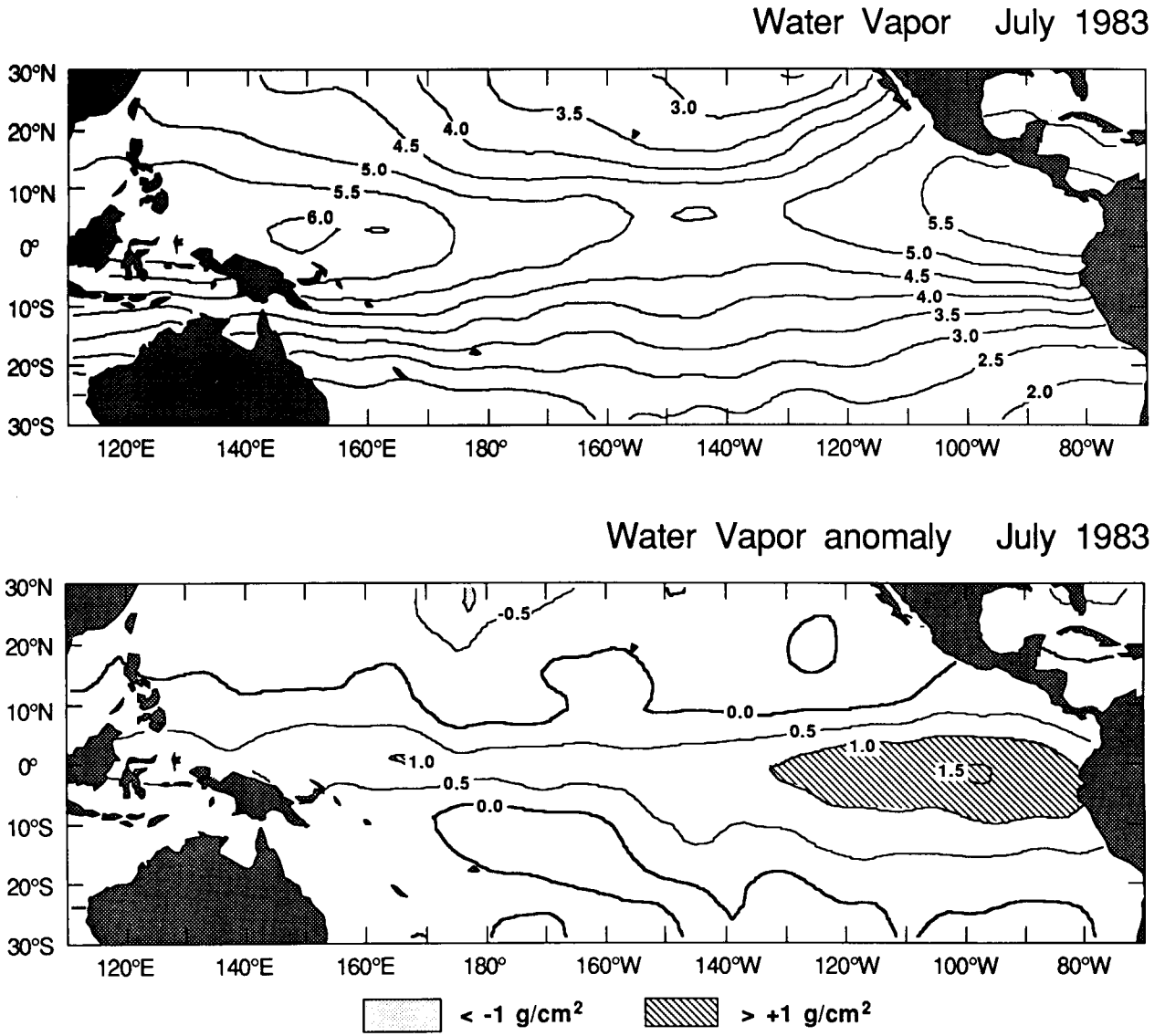

Fig. 40. Same as Fig. 27, except for July 1983

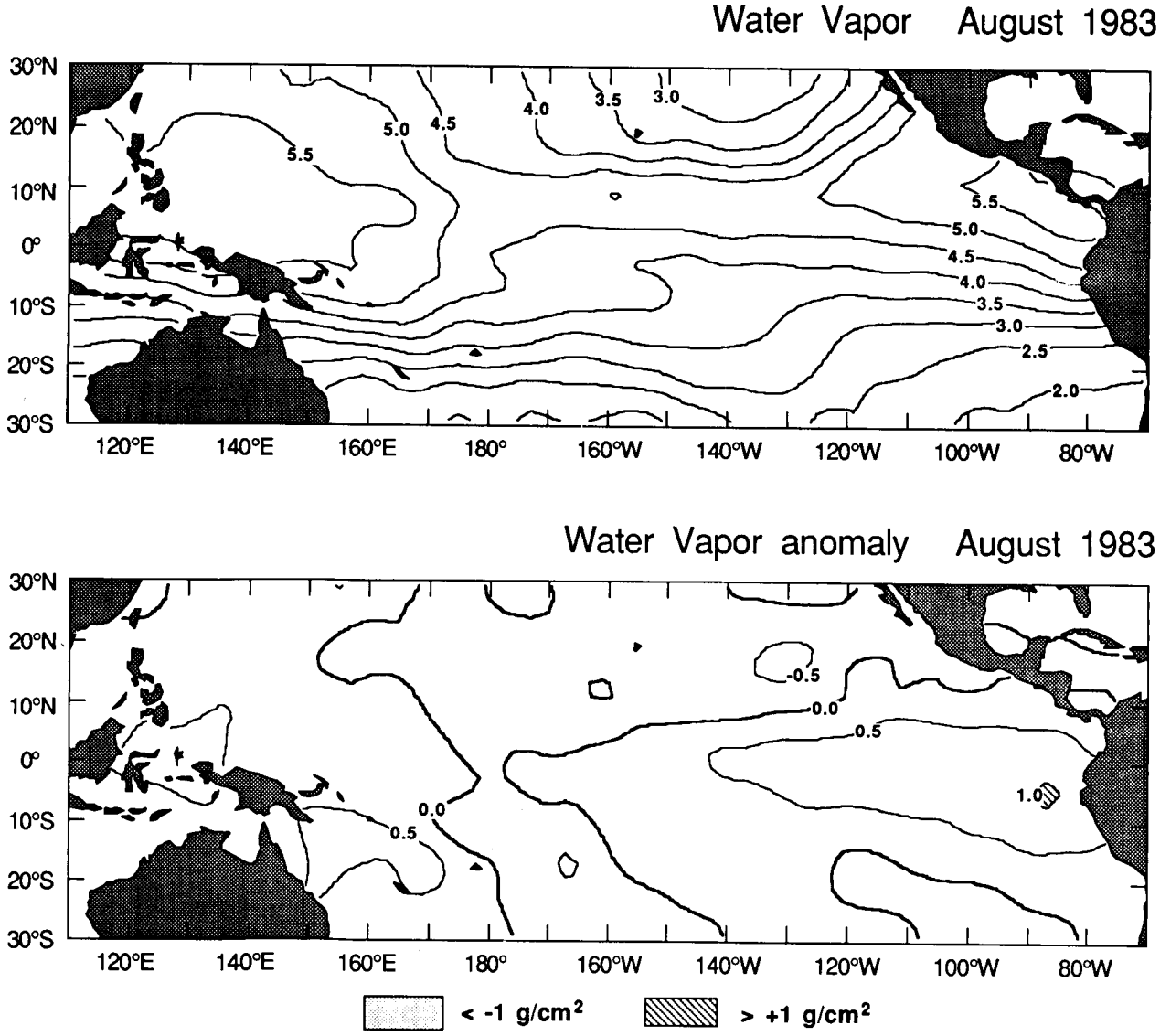

Fig. 41. Same as Fig. 27, except for August 1983

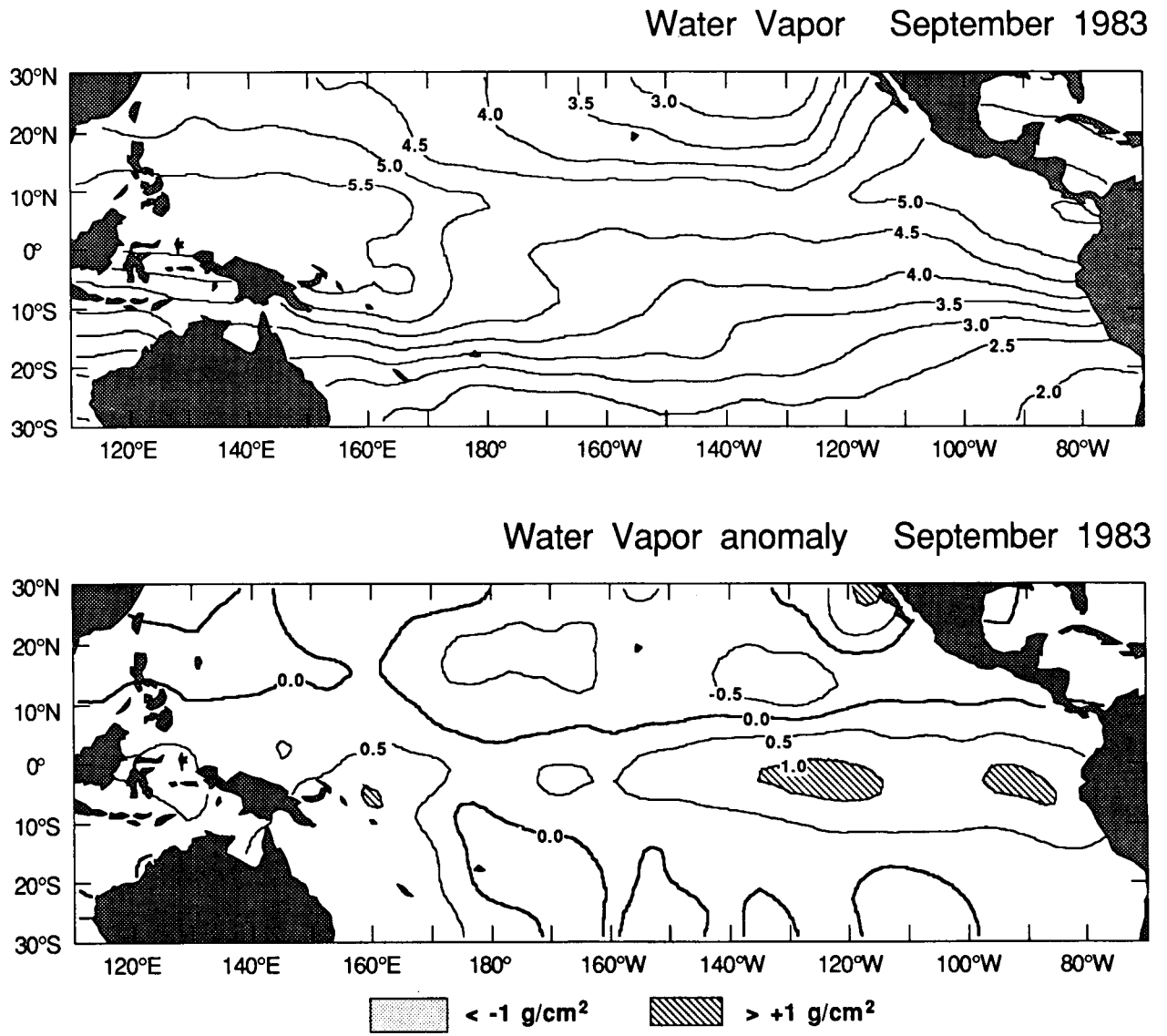

Fig. 42. Same as Fig. 27, except for September 1983

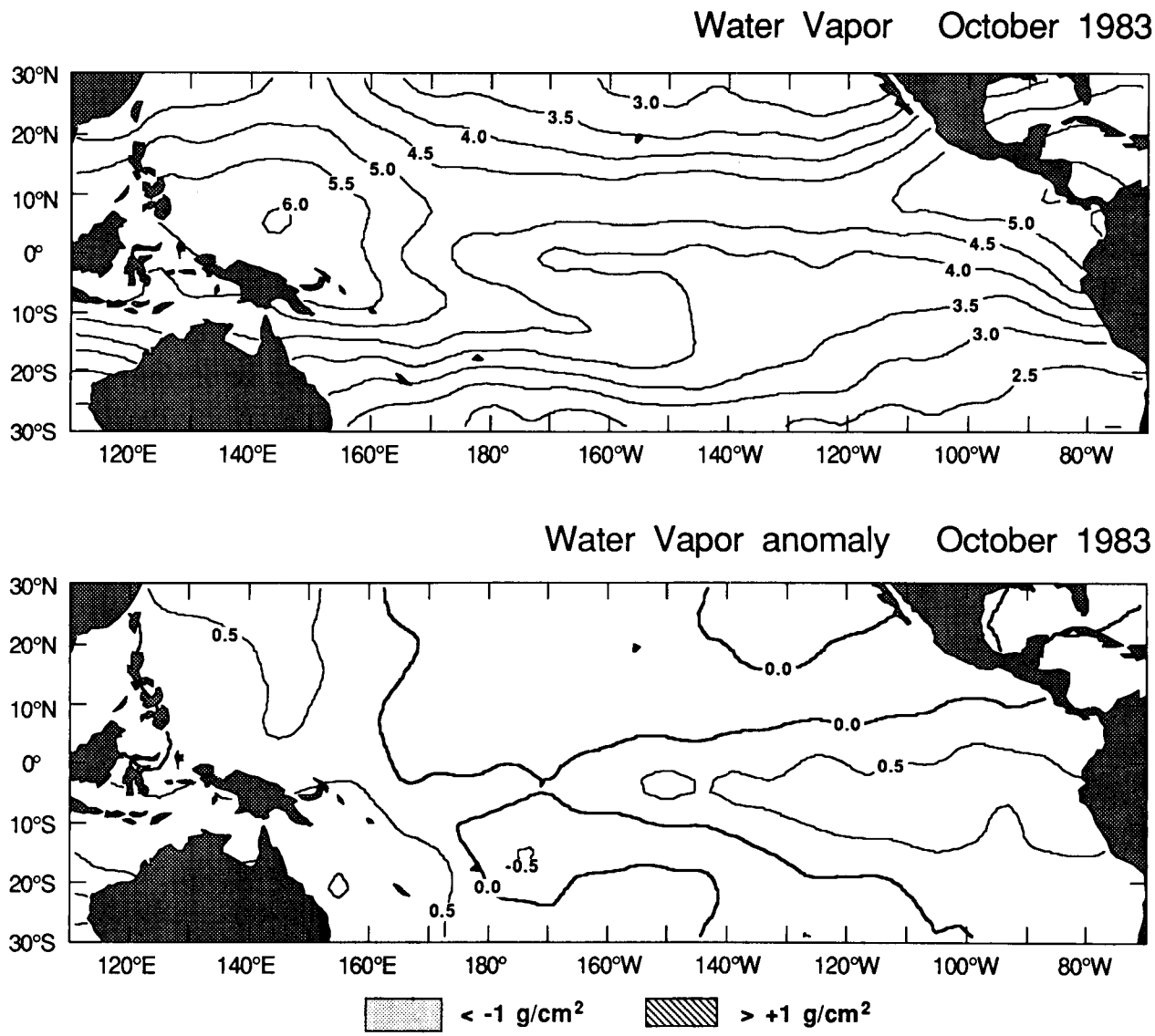

Fig. 43. Same as Fig. 27, except for October 1983

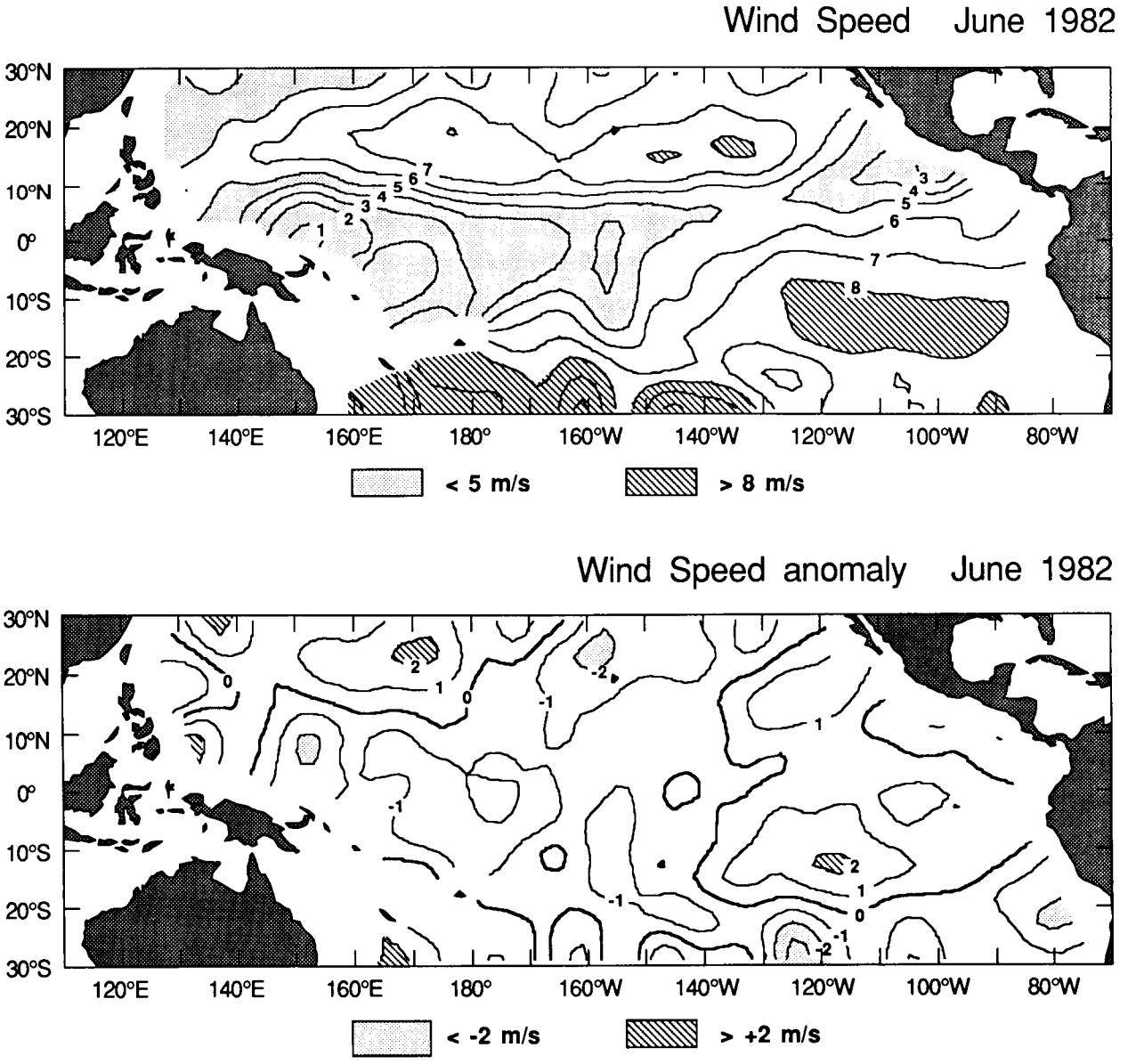

Fig. 44. Surface-level wind speed measured by SMMR in June 1982 and its deviation (anomaly) from the corresponding 1980-81 mean

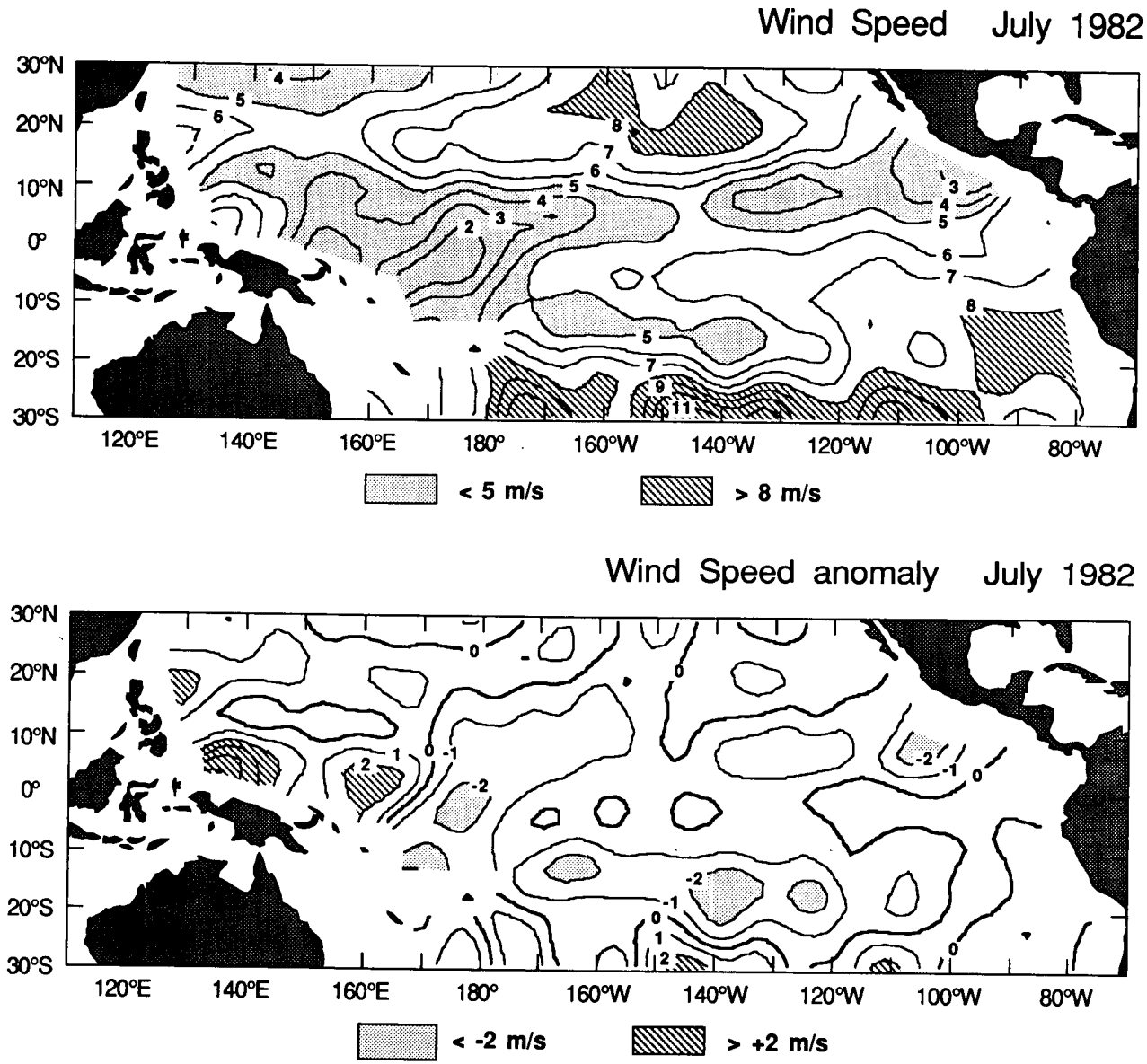

Fig. 45. Same as Fig. 44, except for July 1982

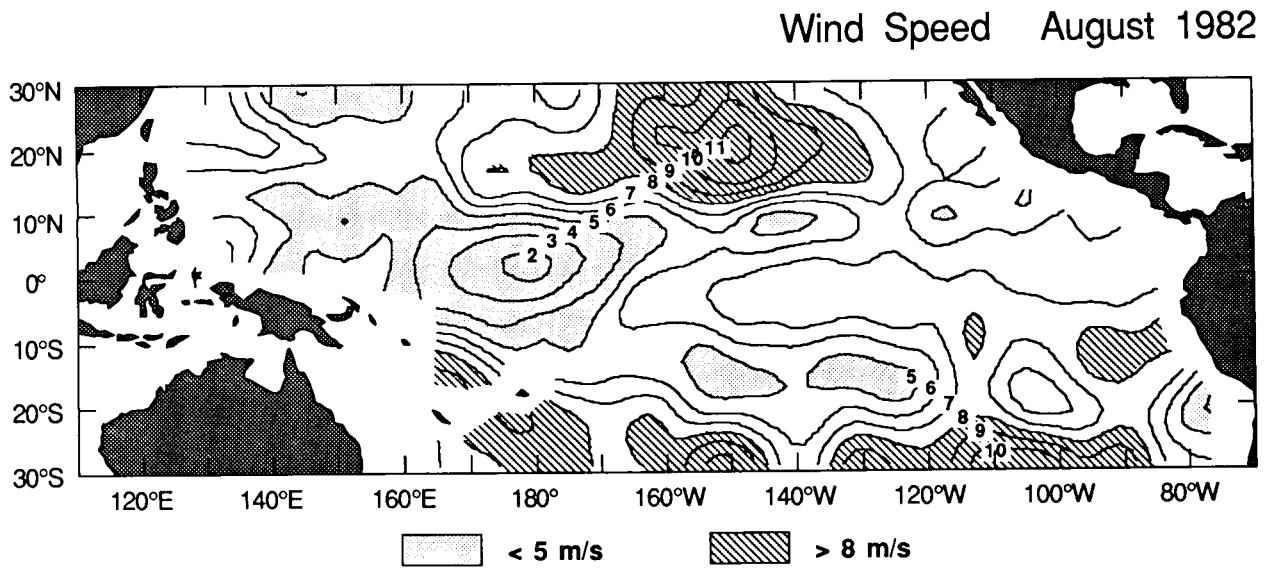

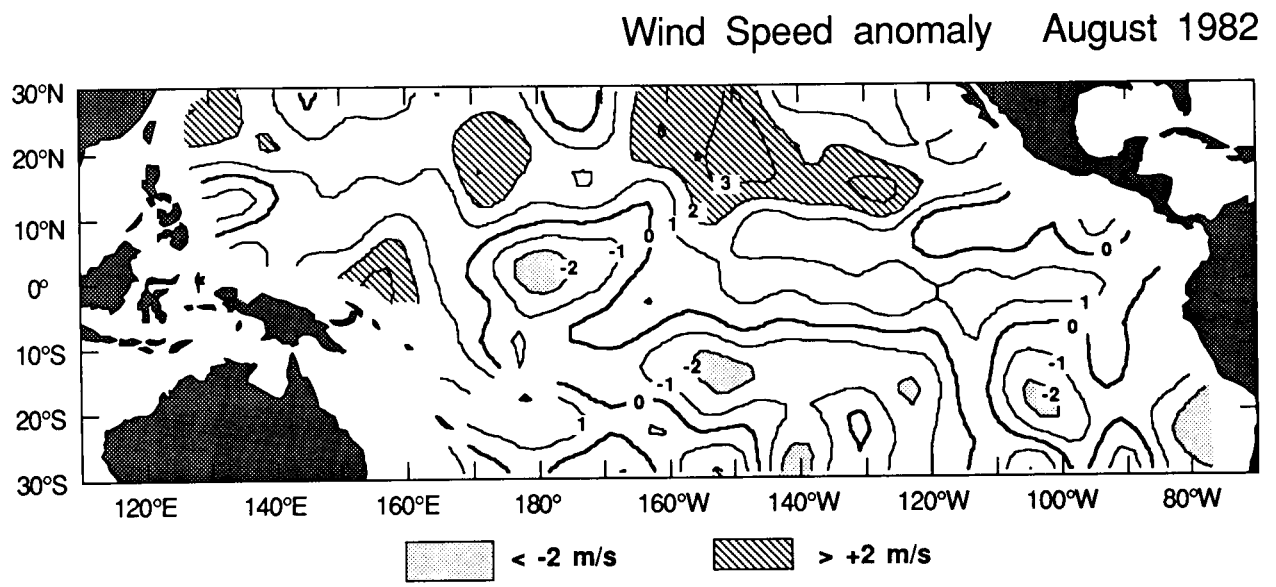

Fig. 46. Same as Fig. 44, except for August 1982

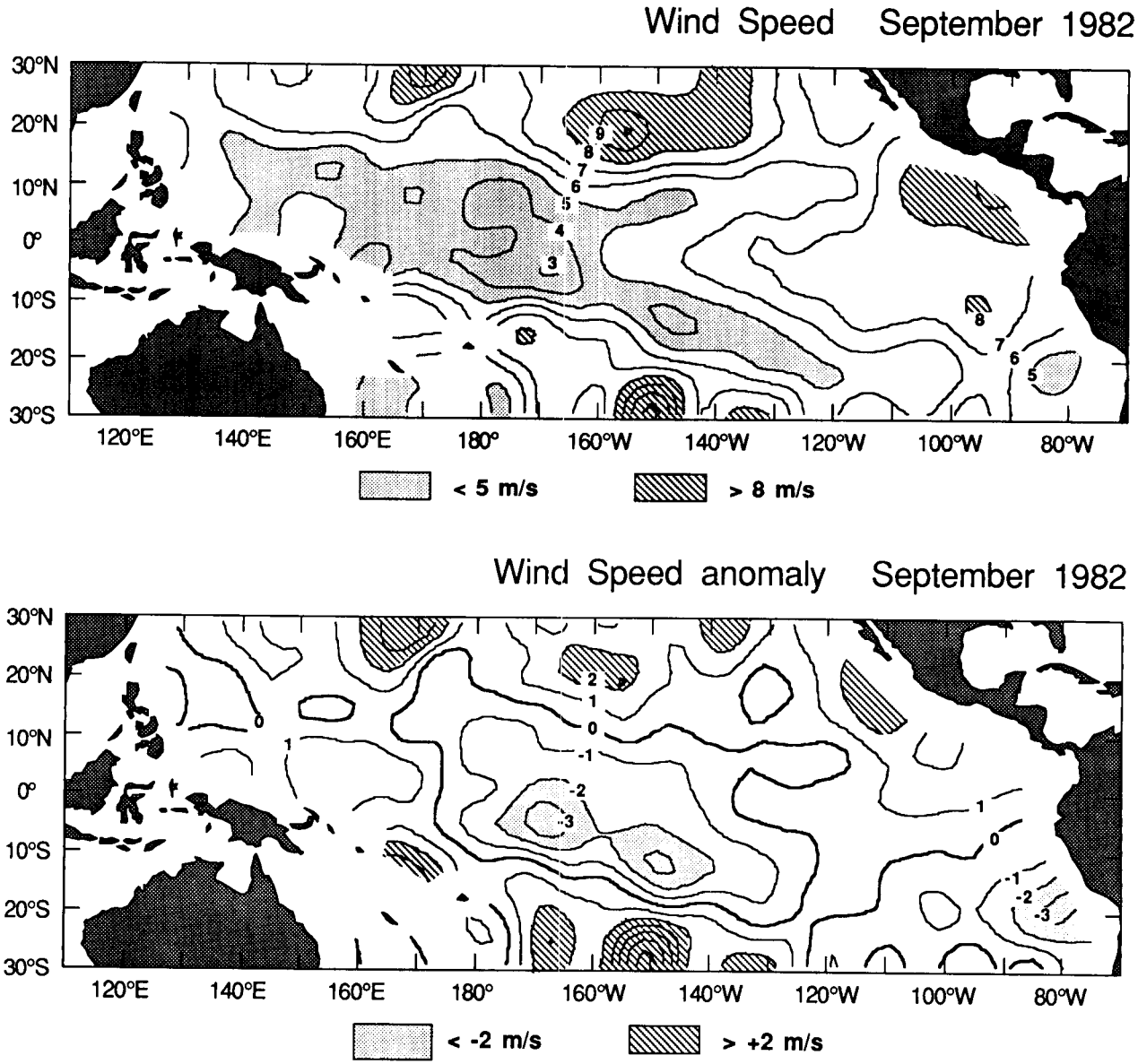

Fig. 47. Same as Fig. 44, except for September 1982

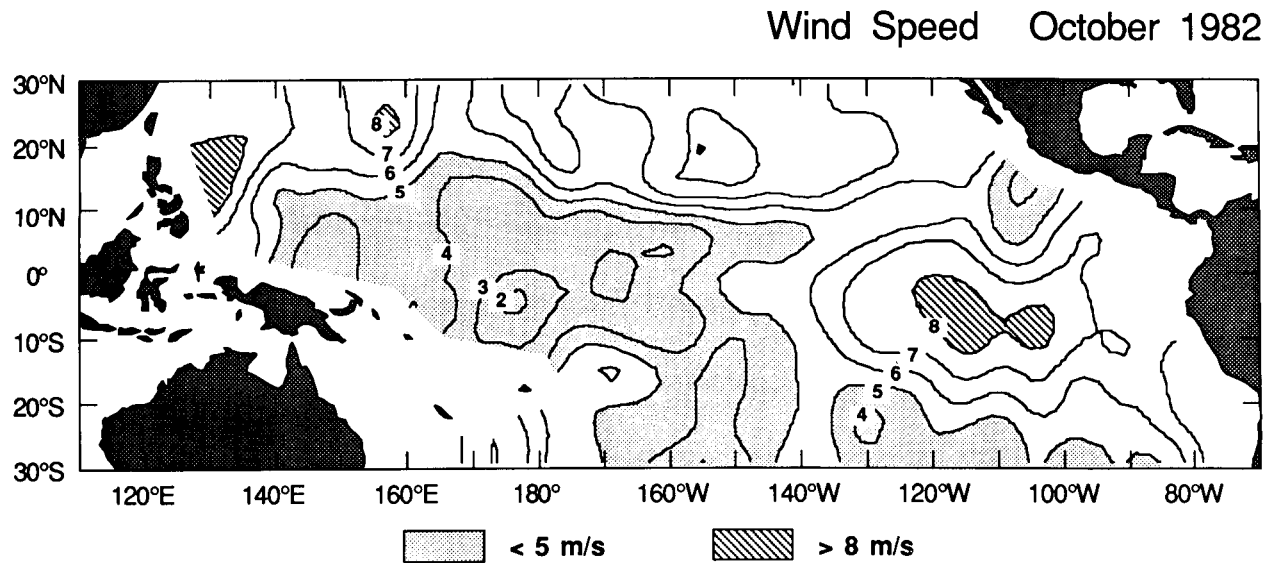

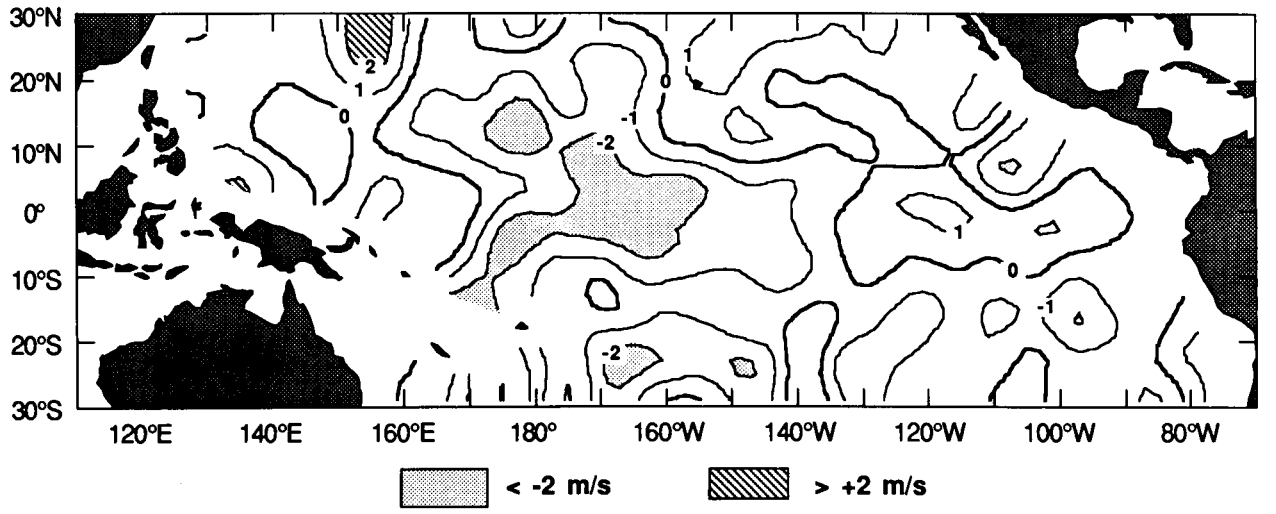

Fig. 48. Same as Fig. 44, except for October 1982

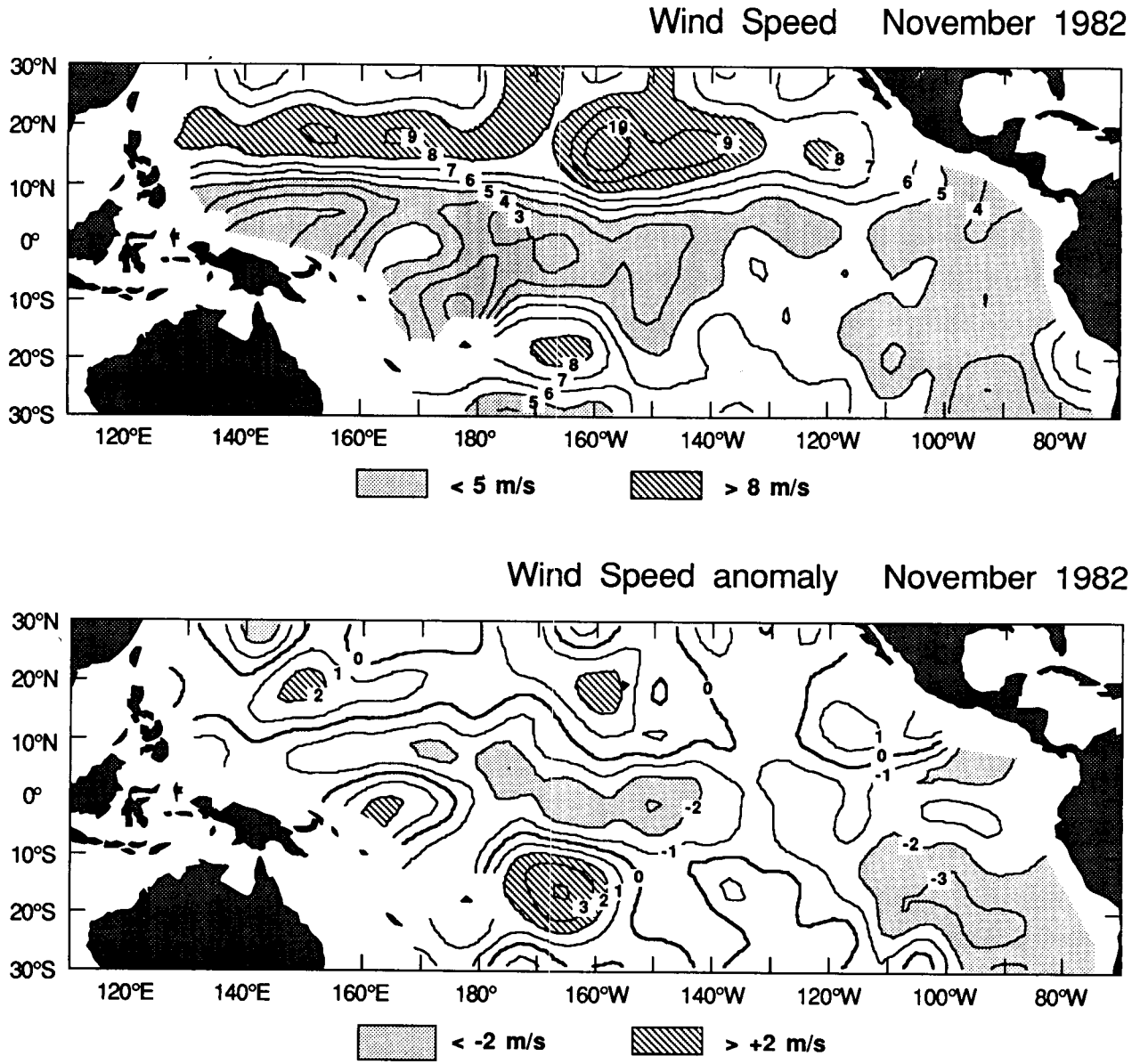

Fig. 49. Same as Fig. 44, except for November 1982

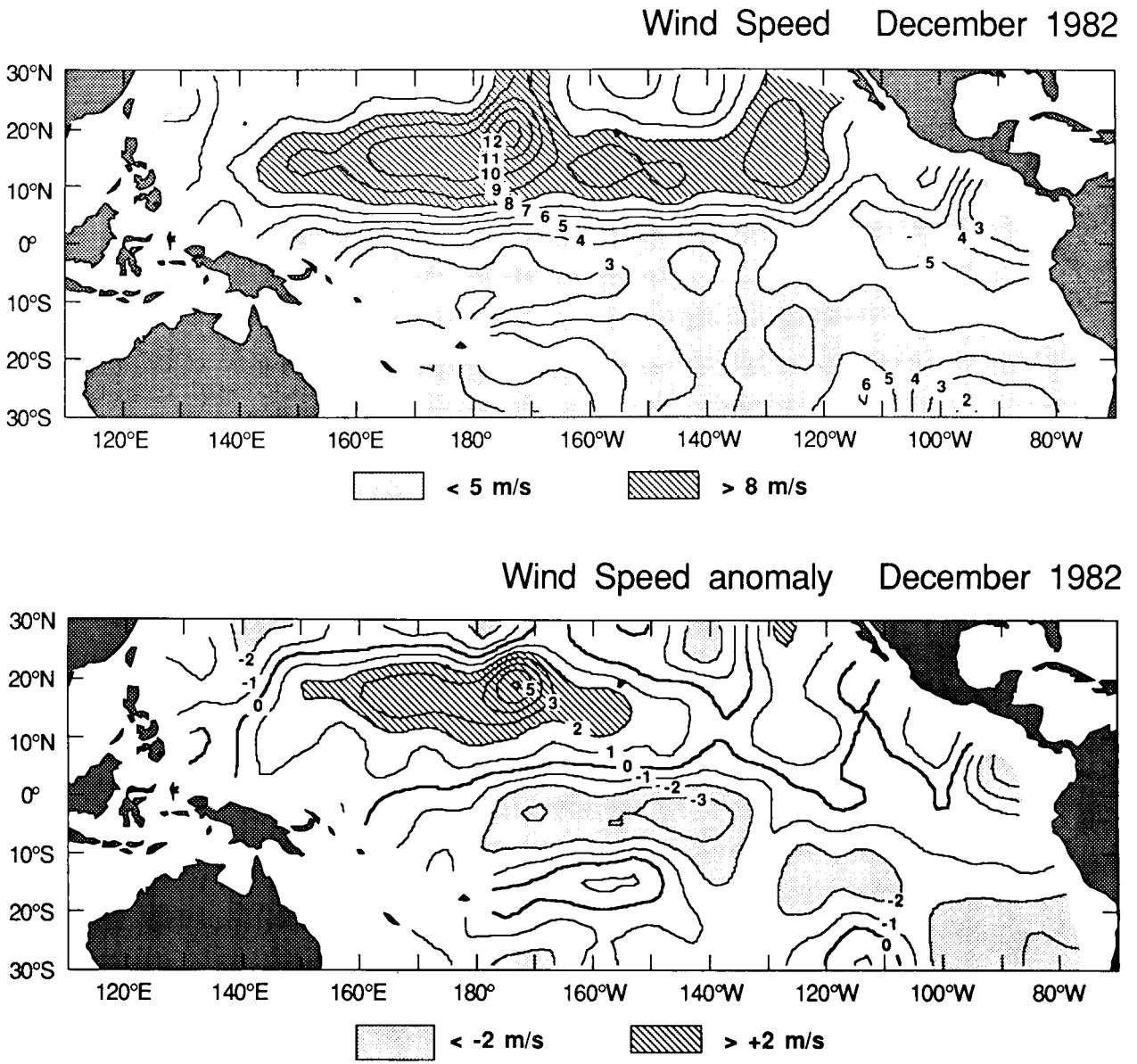

Fig. 50. Same as Fig. 44, except for December 1982

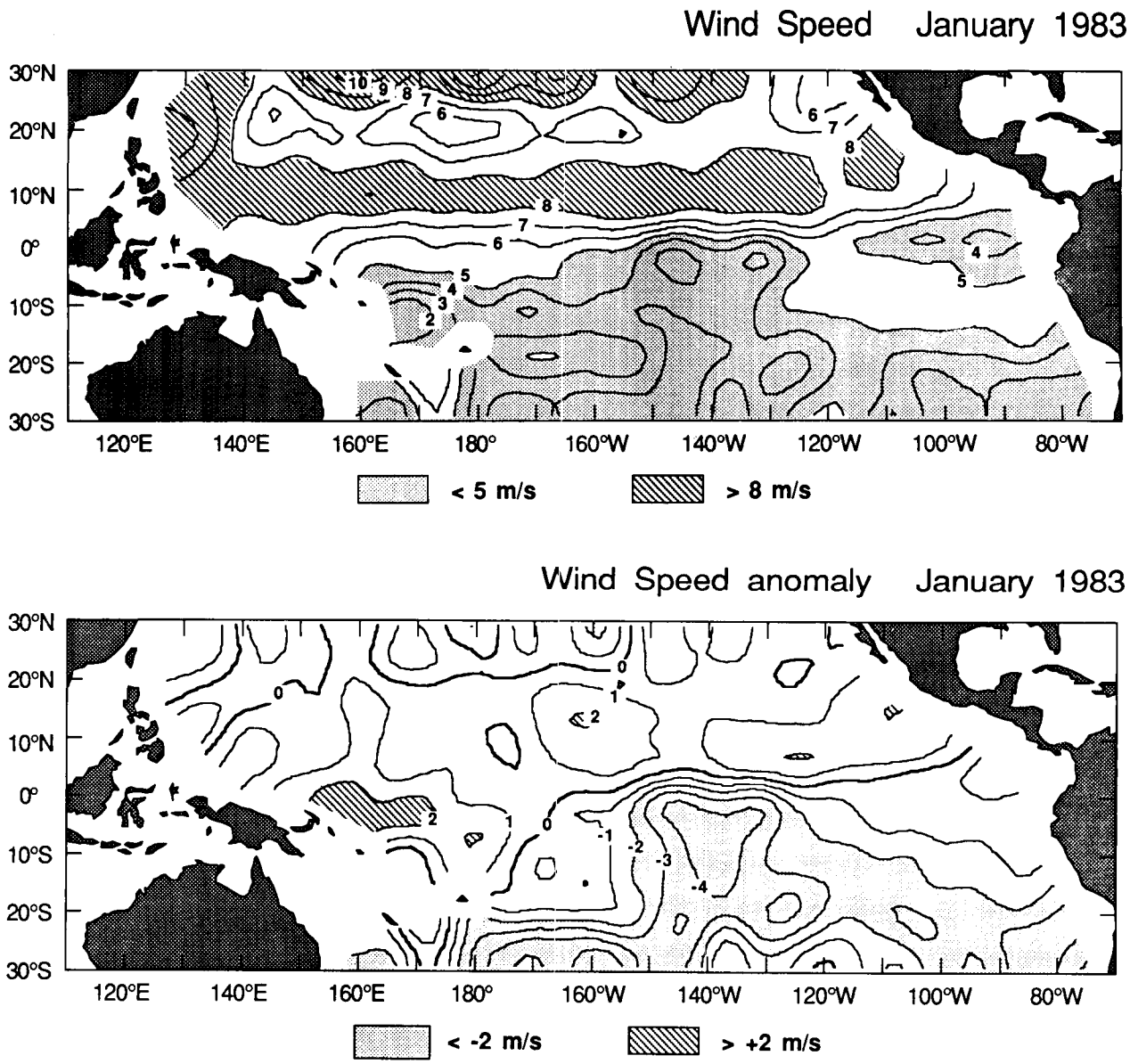

Fig. 51. Same as Fig. 44, except for January 1983

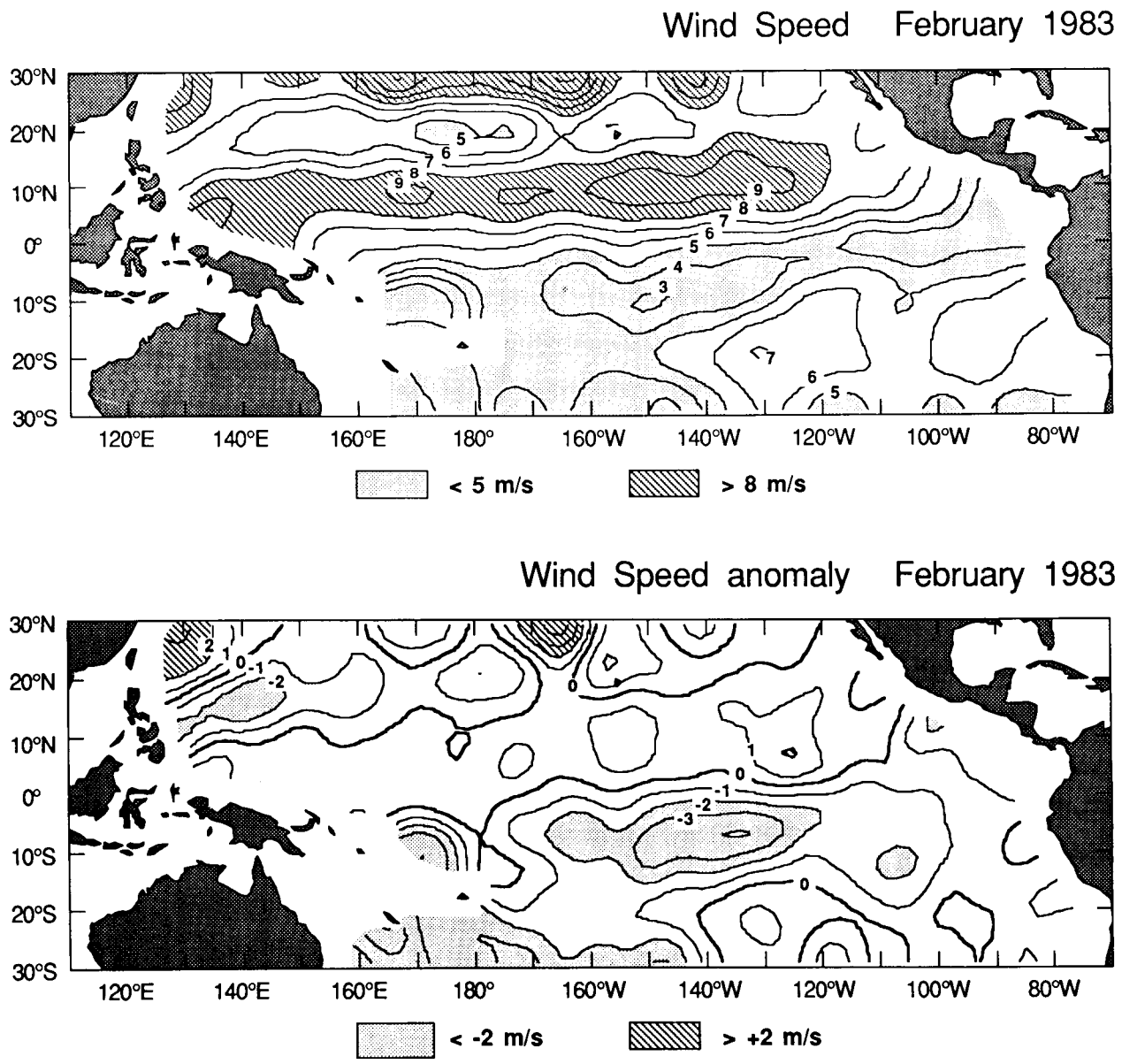

Fig. 52. Same as Fig. 44, except for February 1983

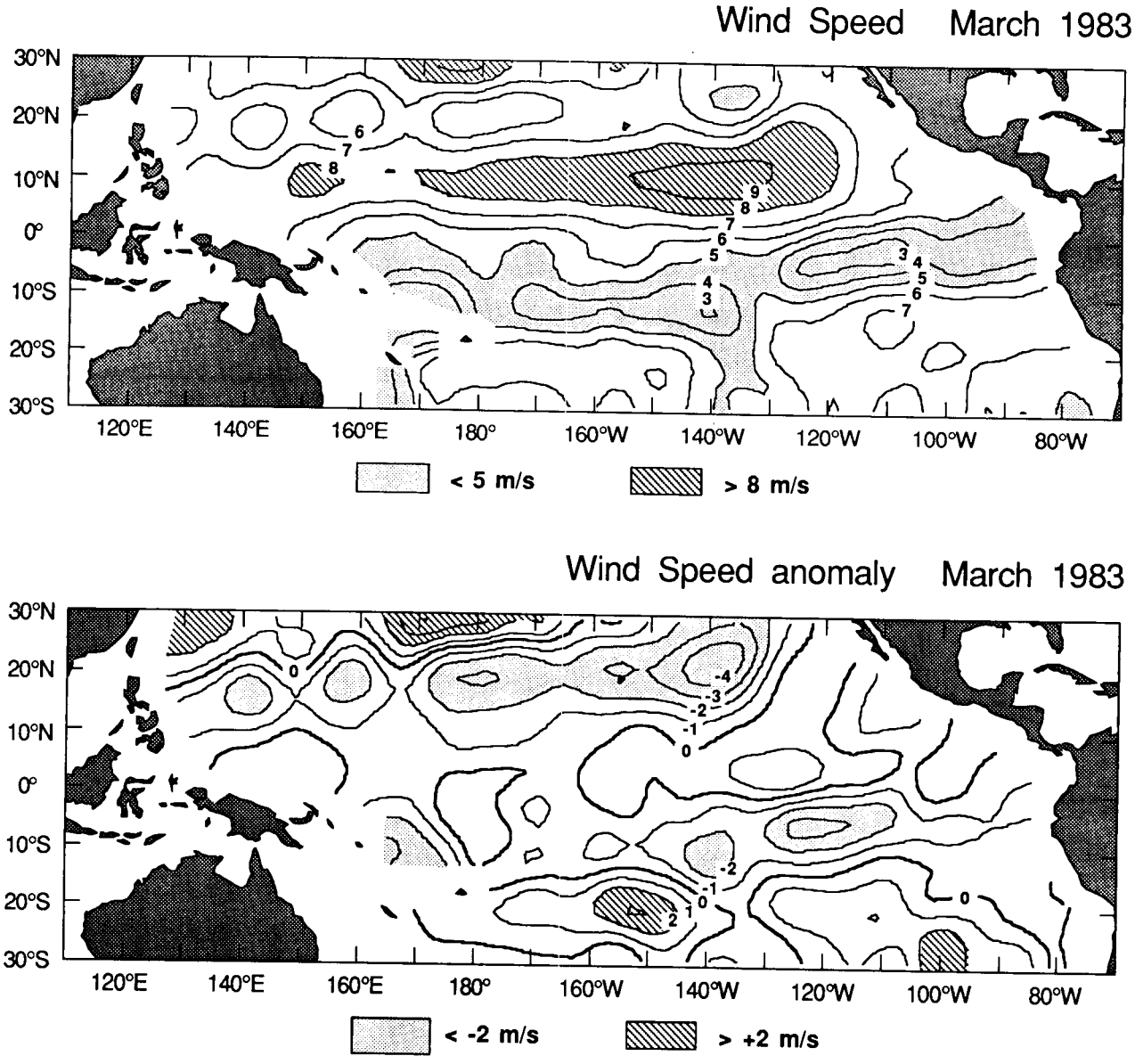

Fig. 53. Same as Fig. 44, except for March 1983

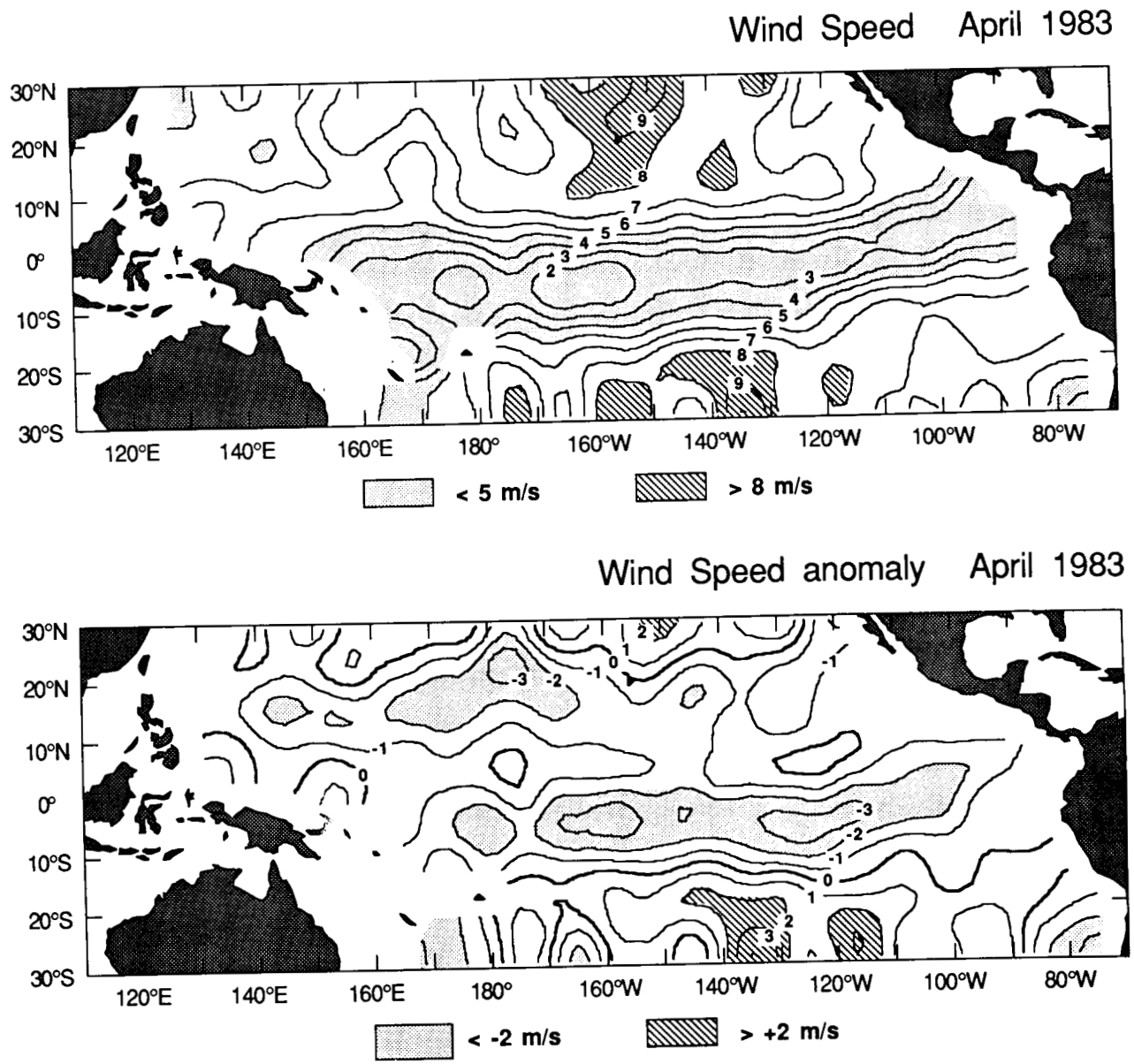

Fig. 54. Same as Fig. 44, except for April 1983

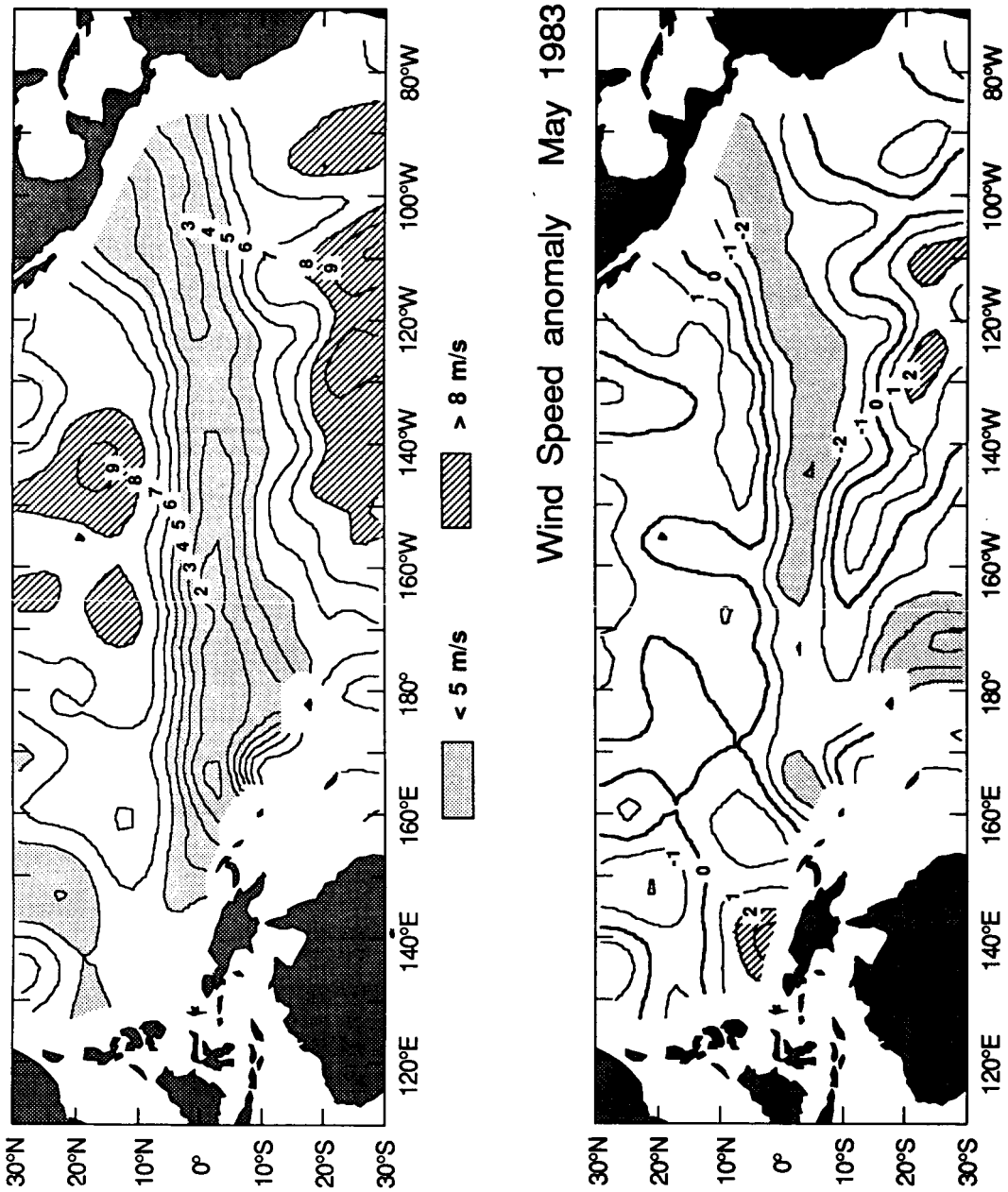

Fig. 55. Same as Fig. 44, except for May 1983

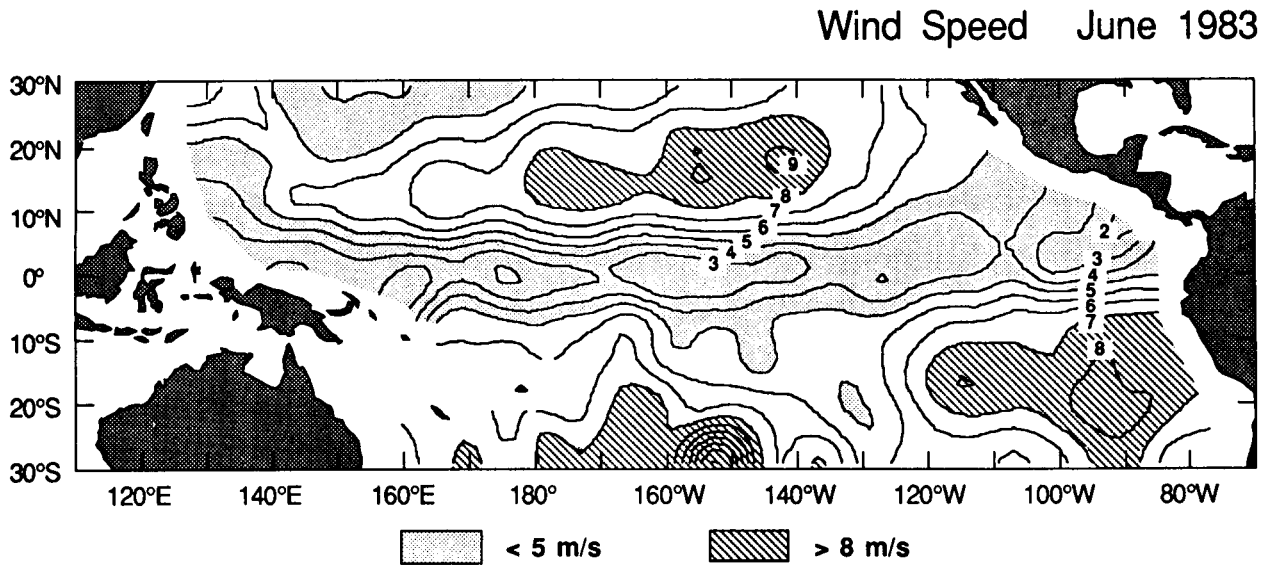

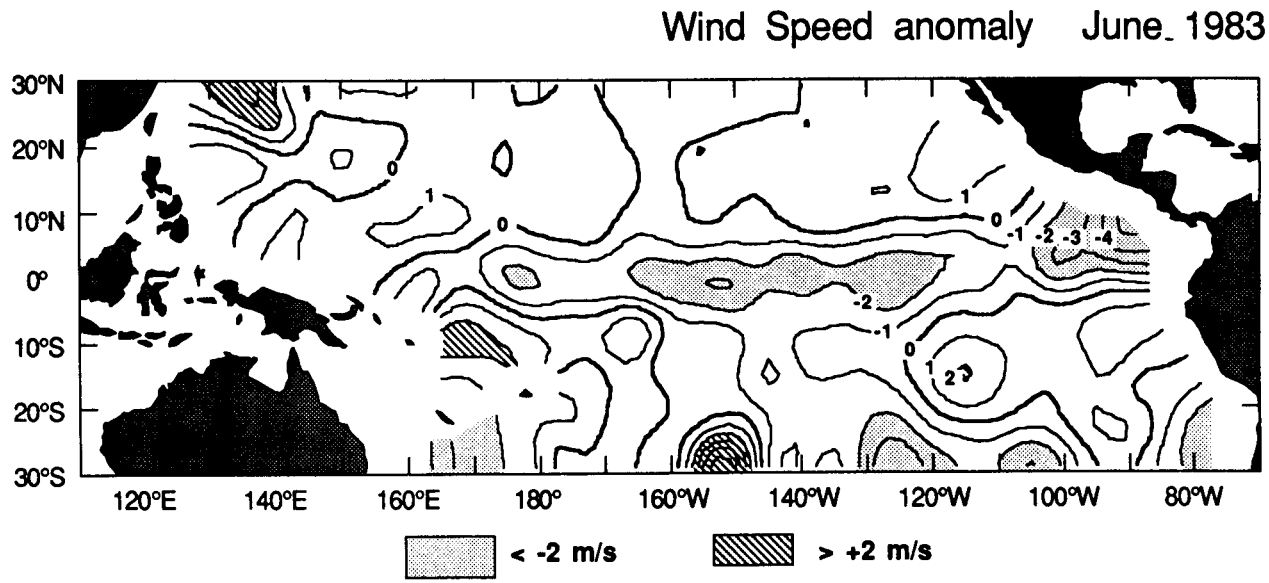

Fig. 56. Same as Fig. 44, except for June 1983

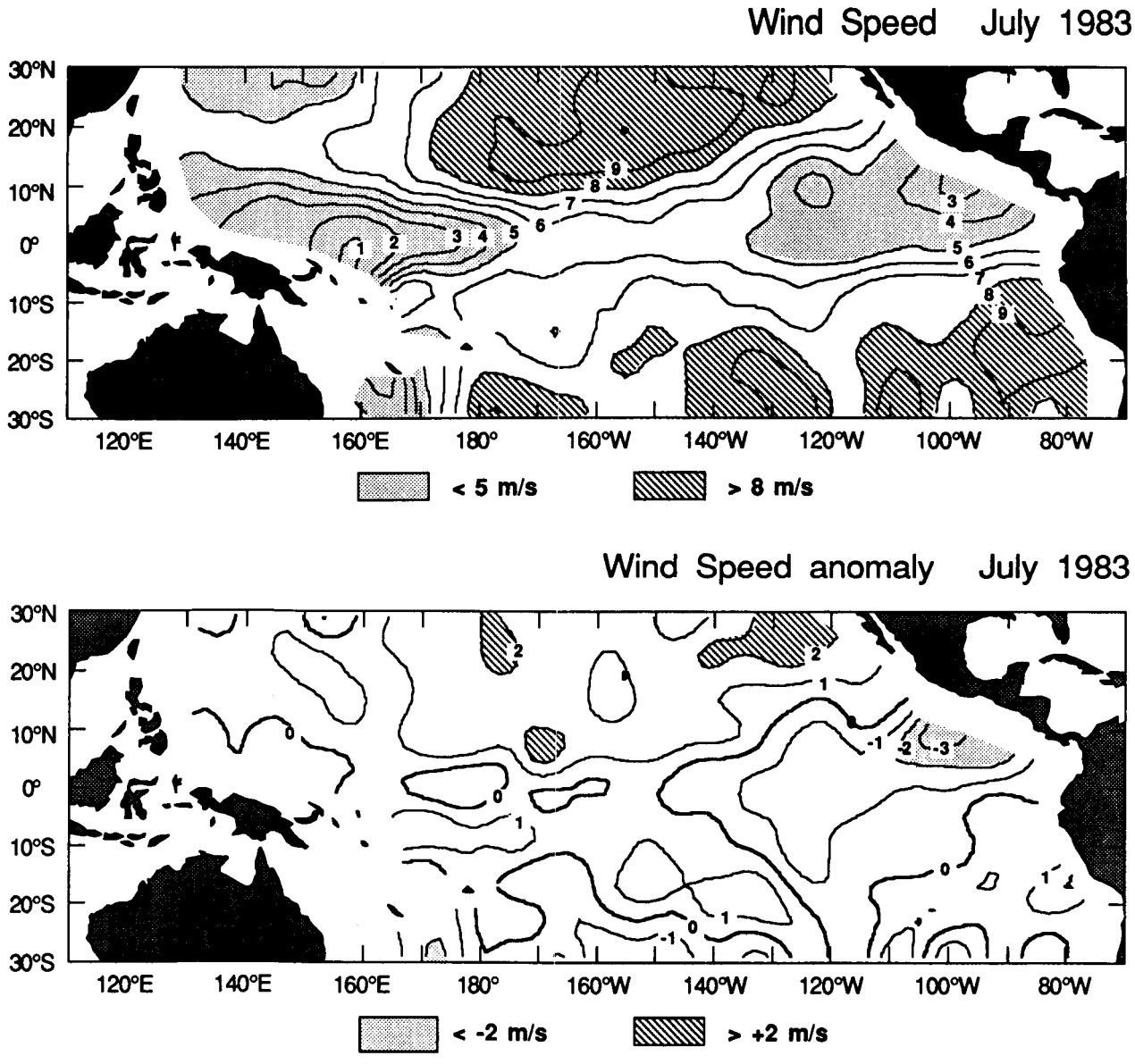

Fig. 57. Same as Fig. 44, except for July 1983

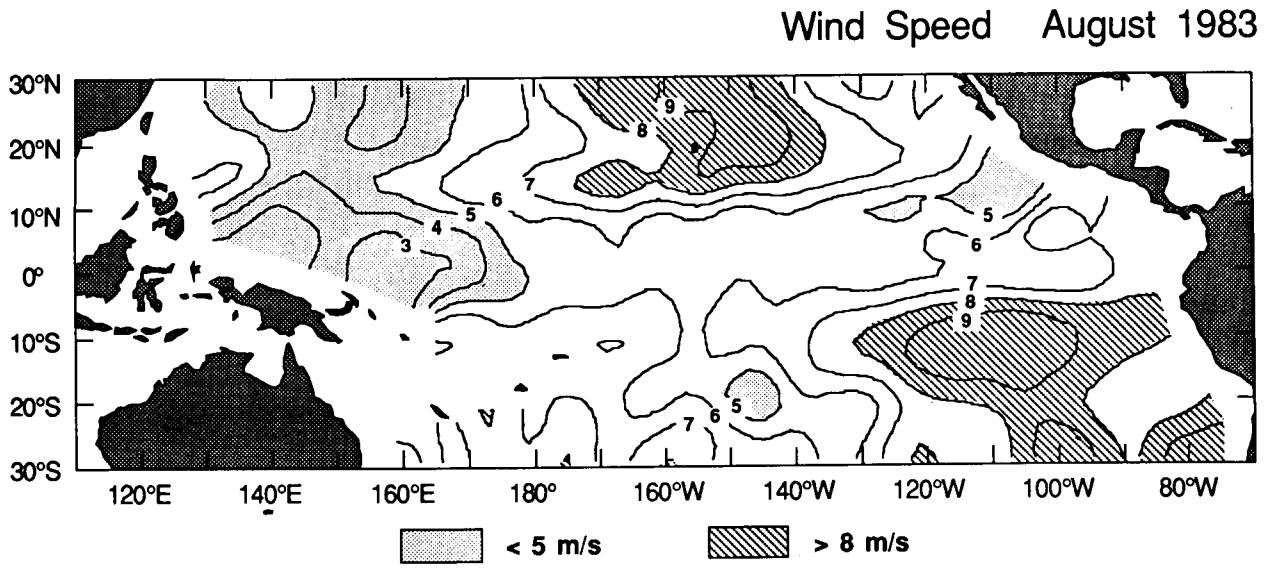

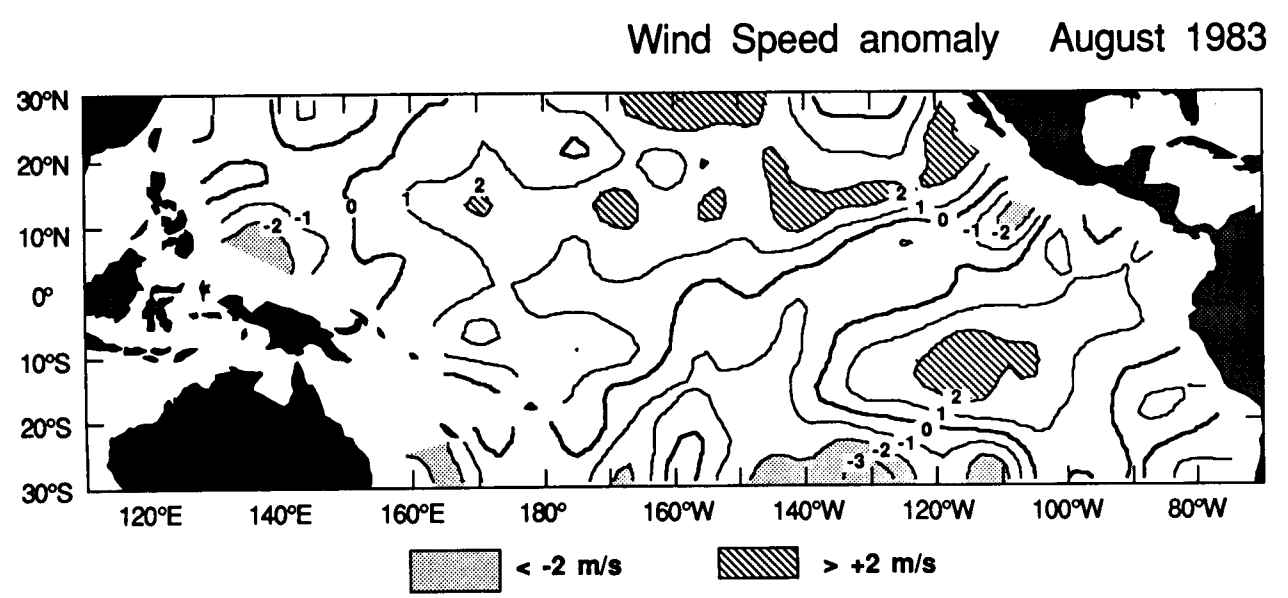

Fig. 58. Same as Fig. 44, except for August 1983

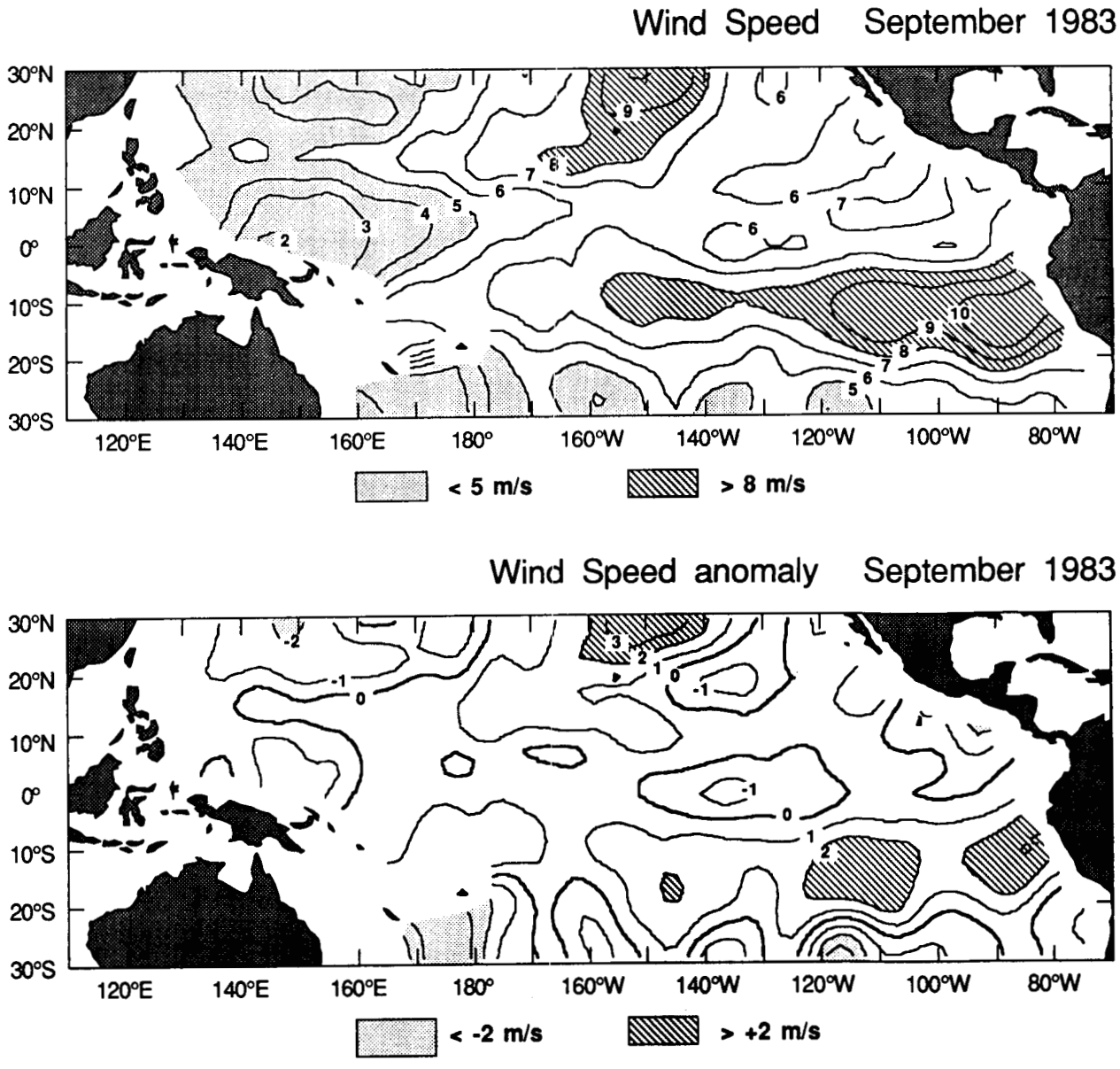

Fig. 59. Same as Fig. 44, except for September 1983

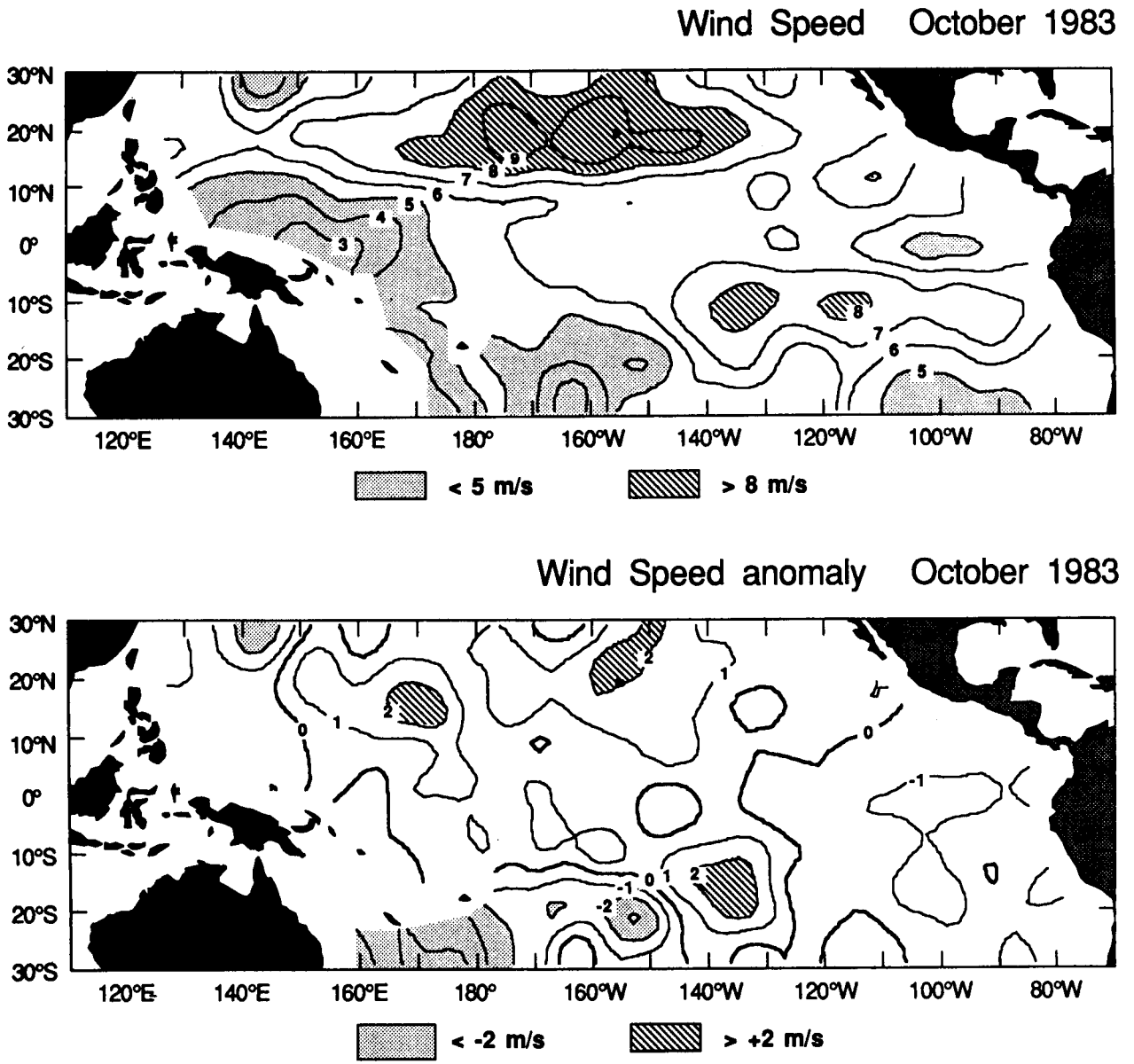

Fig. 60. Same as Fig. 44, except for October 1983